AD-A070 232 UNIVERSITY OF SOUTHERN CALIFORNIA LOS ANGELES DEPT O--ETC F/G 20/4
THE OBLIQUE WING AS A LIFTING-LINE PROBLEM IN TRANSONIC FLOW.(U)
MAY 79 H K CHENG, S Y MENG N00014-75-C-0520
UNCLASSIFIED USCAE-53-4514-1541 NL

1 OF 2
AD A070232

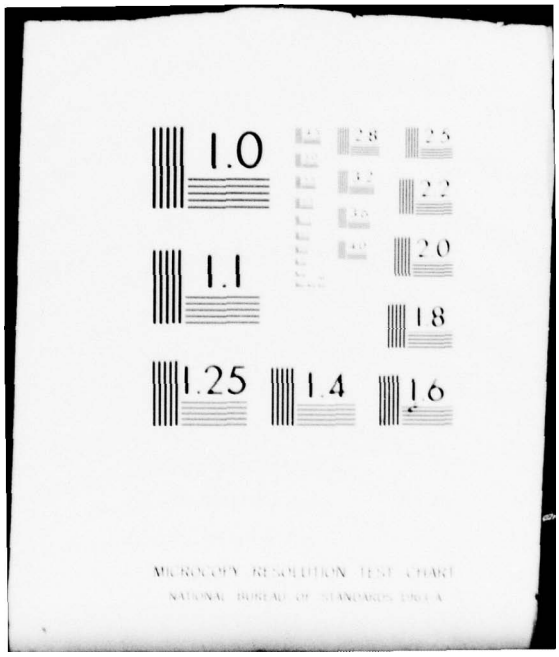
1.0
1.1
1.25
1.4
1.6
2.0
2.2
MICROCOPY RESOLUTION TEST CHART
NATIONAL BUREAU OF STANDARDS 1963-A

LEVEL

USCAE 136
May 1979

912

UNIVERSITY OF SOUTHERN CALIFORNIA

SCHOOL OF ENGINEERING

THE OBLIQUE WING AS A LIFTING-LINE PROBLEM IN TRANSONIC FLOW

H.K. Cheng and S.Y. Meng

See 1473 in back

Office of Naval Research
Contract No. N00014-75-C-0520
Identification Number NR 061-192

DEPARTMENT OF AEROSPACE ENGINEERING

USC

Engineering

THE OBLIQUE WING AS A LIFTING-LINE PROBLEM IN TRANSONIC FLOW

H.K. Cheng and S.Y. Meng

SUMMARY

A transonic-flow theory of thin oblique wing of high aspect ratio is presented, which permits a delineation of the influence of wing sweep, center-line curvature, and other three-dimensional (3-D) effects on the nonlinear mixed flow in the framework of an asymptotic theory. The component flow near the wing section is basically plane (two-dimensional) but nonlinear and mixed, being governed by equations consistent with the transonic small-disturbance approximation. The work analyzes 3-D corrections to this nonlinear problem and matching its solutions to that of an outer flow. In the (parameter) domain of interest, the outer solutions correspond to a high subsonic, or a linear sonic, outer flow, representable by a Prandtl-Glauert solution involving a swept (or curved) lifting line in the leading approximation.

Among the 3-D effects is one arising from the compressibility correction to the velocity divergence, absent in classical works. More important are the upwash corrections which include the influence of both the near and far wakes, as well as the local curvature of the center line. For straight oblique wings, local similarities exist in the 3-D flow structure, permitting the reduced equations to be solved once for all stations. An analogy also exists between the oblique-wing problem and that of a 2-D transonic flow which is weakly time-dependent; this provides an alternative method of solving numerically the inner airfoil problem. Of theoretical interest is the uncovering of a compressibility correction to the outer flow in the form of a line source and a nonuniformity of the perturbation solutions at a shock root (and its treatment).

A procedure based on a line relaxation method for solving numerically the reduced inner problem is described; solutions with high subcritical, as well as slightly supercritical, component flows are demonstrated. Comparison with corresponding numerical solutions based on full-potential equations for oblique elliptic wing shows encouraging agreement.

1. INTRODUCTION

Use of wing sweep to control the compressibility effect has long been a practice in aircraft design (see Busemann 1935, Jones 1946, Jones & Cohen 1957, Küchermann 1965). Consider a high-aspect-ratio wing in a supersonic or transonic flow; there is generally a range of wing-sweep angle (for each wing section), in which the velocity component normal to the center line is sufficiently low to permit a shock-free (or nearly shock-free) component flow, yet is close enough to the sonic speed for the maintenance of a high lift coefficient. In this sweep range lies the potentiality for applying the well documented supercritical airfoil data (see Bauer et al. 1974, Boerstoel 1974, Kacprzynski et al. 1971, and Whitcomb 1974) to aircraft design. The flow field, in this case, is necessarily nonlinear and admits features characterizing the mixed (elliptic-hyperbolic) flow. In the present work, we study the three-dimensional (3-D) structure of this nonlinear mixed flow by solving a perturbation problem and determining its solution through matching with a lifting-line solution to an outer problem.

The approach taken is that of an asymptotic theory for high-aspect-ratio planar wings, and, therefore, shares a common base with Prandtl's (1918) lifting-line theory, as well as the more systematic development of Van Dyke (1964) and Ashley & Landahl (1965). Apart from the nonlinear mixed flow and other compressibility effects, the following development takes into account the influence of the wing sweep, as well as the curvature of the planform's centerline, absent in the classical work. The analysis was motivated, in part, by Jones' (1971, 1977) works on the straight oblique wing, which offers an ideal opportunity for extending the lifting-line concept and naturally becomes the focus of the present investigation.

Similar extensions have been made earlier by the first author in the context of unsteady incompressible flow for a curved center-line (Cheng 1976) and of steady incompressible flow for an oblique wing (Cheng 1978a and b).[+] In the latter work, agreement of the lifting-line results with

[+] Cheng's work involving a curved center line in the steady incompressible case has not, as yet, been published.

those from the numerical, wing-panel and other solutions obtained for high aspect-ratio wings are found to be consistently good. The present study is carried out in a framework equivalent to the transonic small-disturbance approximation for a potential flow with an aim of bringing about a greater simplicity in the problem analysis, which will greatly reduce computation works and shed light on the 3-D structure of the transonic mixed flow. For straight oblique wings, the theory yields an analogy with the unsteady flow of a two-dimensional thin airfoil in the nonlinear transonic regime; the formulation also admits a local similarity in the 3-D structure, providing a further reduction of the computation work for a rather useful class of oblique-wing geometry.

An outline of the analysis concerning the similarity solutions of the oblique wings has been sketched in a greatly condensed note (Cheng & Meng 1979). This report presents the theory in a fuller context; apart from the crucial details in the theoretical development, the work presents several comparisons of the analysis with computer solutions based on full-potential equations for oblique wings at high-subcritical, as well as slightly-supercritical, component flows.[+] The theory developed is valid also for a curved centerline (see requirements below) and is expected to hold in the case of a conventional symmetric swept wing, although without further treatment, the solution is not applicable to the vicinity of the wing apex.

For a straight unswept wing, the 3-D effect would appear mainly as a local upwash correction; more specifically, the local flow field next to the wing section can be taken as being <u>planar</u> as in Prandtl's original theory. Cook and Cole (1978) have given a rather complete elucidation of this problem; Cook (1978) has also studied the uniqueness of the solution to the reduced problem. With the wing sweep, two important features emerge. One is a pronounced <u>upwash</u> induced by the near-wake vorticities, which is

[+] The report is an expanded version of an earlier draft entitled, and referred to in Cheng & Meng (1979) as, "Transonic Lifting-Line Theory of Oblique Wings and Other High-Aspect-Ratio Planforms".

responsible for the pronounced rolling moment characteristic of an untwisted oblique wing (see Jones 1977, also Cheng 1978a); the other is an additional compressibility correction arising from the spanwise density variation (§2.1). On account of the latter feature, the flow field next to each wing section can no longer be treated as being planar. At a subsonic Mach number, there is a local spanwise component of the near-wake vorticity, which is not negligibly small and must be accounted for in formulating the reduced inner problem. This feature does not appear however in the present analysis owing to the relatively small sweep angle required by the nonlinear domain (lest the inner problem becomes linear).+

An interesting development in the present asymptotic theory is the uncovering of a line source in the higher-order lifting-line theory, unsuspected in previous work. The effect in question arises from the spanwise compressibility correction mentioned and depends on the sectional lift (nonlinearly), as well as the spanwise and chordwise distributions of the wing thickness (Appendix III). Its appearance reminisces the nonlinear-lift influence on the transonic equivalence rule (Cheng & Hafez 1975) but plays a lesser role. Nevertheless, this source term is found to be useful in providing a description at the far boundary, needed in subsequent computations (§5). In passing, we observe that similar source effects should also arise in a linear problem, although the lift distributions of interest will not be affected (to the order of $\mathcal{R}_1^{-1}$) in such a case.

The theory admits shock waves and takes into account the perturbations in their strengths and locations. As well known from Oswatitsch & Zierep's (1960) work, there is a weak singularity at the juncture of the shock and the curved portion of an impermeable surface, where the flow will undergo a reexpansion. In the perturbation part of the solution, this singularity manifests to a logarithmic singularity in the pressure distribution behind the shock root. Although the validity of the perturbed solution in regions removed from the shock root could be defended, the breakdown in question raises doubts on the ability of such a solution procedure for computing

---

+ This fact, and the two features mentioned above, have been noted earlier by Cheng & Hafez (1973).

correctly the shock-excursion distance (displacement). Essentially the same problem (of nonuniformity) undermines the shock analysis in the context of an unsteady transonic plane flow (§ 4.1) where the difficulty is compounded by other complexities in computations and has not been fully recognized. This problem with the reexpansion singularity is treated in § 2.6.

In the following, 2b denotes the wing span (measured perpendicularly to the main flow direction) and c_0 the root chord (measured perpendicularly to the centerline). Refer to Figure 1. The aspect ratio is defined as $AR \equiv 2b/c_0$. We use α to characterize the wing camber and the angle of attack (measured from the zero-lift angle), and will assume that the wing-thickness ratio is also comparable to α. The local swept angle is Λ; the free-stream Mach number is M_∞, and the Mach number of the free-stream component flow is $M_n \equiv M_\infty \cos\Lambda$. Three parameters will control the reduced problems

$$K_n \equiv (1-M_n^2)/\alpha^{2/3} M_n, \qquad \textcircled{H} \equiv \Lambda/\alpha^{1/3}, \qquad \epsilon \equiv 1/\alpha^{1/3} AR \qquad (1)$$

where ϵ may be regarded as the reciprocal of a reduced aspect ratio, and $\textcircled{H}$ is a rescaled (typical) sweep angle. The parameter K_n is essentially the transonic similarity parameter written for the component flow, with the factor in the denominator taken as the <u>first</u> power of M_n, as in Murman & Krupp (1971); the theoretical reason supporting this preference is given in § 2. The flow field next to the wing section and that removed from it are analyzed as two asymptotically distinct (inner and outer) regions for $\epsilon \to 0$ with fixed K_n, $\textcircled{H}$, and $\alpha^{1/3}/\epsilon$. The last quotient is fixed in order to simplify the remainder estimate. As will become apparent later in § 3, the relative magnitude of $\textcircled{H}^2$ and K_n will also determine whether the outer flow is (high) subsonic, (near) sonic, or (low) supersonic. Only the domain in which $K_n > 0$ and $K_0 \equiv K_n - \textcircled{H}^2 \geq 0$, corresponding to a high subsonic, or a linear sonic, outer flow is considered.[+] Since

[+] Other regimes with $K_n < 0$, as well $K_0 < 0$ implies a much stronger shock extending far out into the outer flow, and perhaps are less attractive for aerodynamic applications.

the theory permits a curved center line, a smooth spanwise variation in K_n and Θ are also allowed. The result for an unyawed straight wing in a high subsonic flow is recovered in the special limit $\Theta \to 0$.[+]

In the next section, we formulate the perturbation problem for the inner region next to the wing section and analyze the far-field behavior, the reexpansion singularities, and other solution properties. The solution in the outer region and its matching with the inner solution are presented in Section 3. The important properties of the straight oblique wings (the unsteady analogy, and the local similarity in the 3-D flow structure, in particular) are brought out in Section 4. The essential elements in our computational procedure are discussed in Section 5, where solutions for oblique wings with high-subcritical and slightly-supercritical component flows are demonstrated; encouraging comparisons with results from full potential 3-D solutions and from solutions via the unsteady analogy are also shown. Fuller descriptions of the computer work, with more extensive results involving higher supercritical component flows and shocks, are presented in separate works.

[+] A recent study by P. Cook presented at the 8th U.S. National Congress of Applied Mechanics, held in Los Angeles, June 26 - 30, 1978, also considers sweep effect in transonic flow corresponding to $\Theta \neq 0$. Cook's paper is not yet available for comparison.

2. THE INNER AIRFOIL PROBLEM

2.1 Governing equations

We consider a steady irrotational flow of a calorically perfect gas with a uniform freestream. The partial differential equation (PDE) for the perturbation velocity potential ϕ can be written in Cartesian coordinates (x,y,z) as

$$(1-M_\infty^2)\,\phi_{xx} + \phi_{yy} + \phi_{zz} = M_\infty^2 U_\infty^{-1} \frac{\partial}{\partial x}\left[\left(1-\tfrac{\gamma-1}{2}M_\infty^2\right)\phi_x^2 + \phi_y^2 + \phi_z^2\right] + \cdots \qquad (2.1)$$

where the remainder (...) consists of triple and quadruple products of ϕ, e.g. $U_\infty^2 \phi_x^2 \phi_{xx}$, etc., γ is the specific-heat ratio and subscripts x, y and z signify partial derivatives.

For the analysis of the flow field in the neighborhood of the wing section, referred to as the inner region hereafter, a right-handed curvilinear orthogonal coordinate system (x', y', z') will be used (ref. Fig. 2) in which x' and z' are distances from the center line (a reference curve) of the wing planform, with z' measured along a normal from the wing plane. The y'-coordinate is then a distance measured along the (curved) center line. Writing Λ as the local sweep angle of the center line, one observes the following identities

$$dx^2 + dy^2 + dz^2 = dx'^2 + h_s^2 dy'^2 + dz'^2, \qquad h_s = 1 - x'\frac{d\Lambda}{dy'} \qquad (2.2)$$

$$\frac{\partial}{\partial x} = \cos\Lambda \frac{\partial}{\partial x'} + \frac{\sin\Lambda}{h_s}\frac{\partial}{\partial y'}, \qquad \frac{\partial}{\partial y} = -\sin\Lambda \frac{\partial}{\partial x'} + \frac{\cos\Lambda}{h_s}\frac{\partial}{\partial y'} \qquad (2.3)$$

The PDE (2.1) may then be expressed in the curvilinear coordinates as

$$\begin{aligned}(1-M_n^2)\phi_{x'x'} + \phi_{z'z'} - 2M_n^2 \tan\Lambda\, h_s^{-1}\phi_{x'y'} - (1-M_n^2\tan^2\Lambda)\,h_s^{-1}\Lambda_{y'}\phi_{x'} + \\ + (1-M_n^2\tan^2\Lambda)\,\phi_{y'y'} - M_n^2\tan\Lambda\, h_s^{-1}\Lambda_{y'}\phi_{y'} = M_n^2 U^{-1}\Big(\frac{\partial}{\partial x'} + \\ + \tan\Lambda\, h_s^{-1}\frac{\partial}{\partial y'}\Big)\Big[\Big(1+\tfrac{\gamma-1}{2}M_n^2\Big)\phi_{x'}^2 + \phi_{z'}^2 + \tfrac{\gamma-1}{2}M_n^2\tan\Lambda\, h_s^{-1}\phi_{x'}\phi_{y'} + \\ + \Big(1+\tfrac{\gamma-1}{2}M_n^2\tan^2\Lambda\Big)\phi_{y'}^2\Big] + \cdots \qquad (2.4)\end{aligned}$$

where $U_n = U_\infty \cos\Lambda$ and $M_n = M_\infty \cos\Lambda$ may vary with y' and the remainder .... is of the same order as in (2.1).

In anticipation of a local component flow which will be nearly two-dimensional and transonic in the x'-z' plane, we employ the dimensionless variables

$$\hat{x} \equiv \frac{2x'}{c_0}, \qquad \hat{z} \equiv 2M_n\left(\frac{\alpha}{M_n}\right)^{1/3}\frac{z'}{c_0}, \qquad \hat{y} \equiv \frac{y'}{b}, \qquad \hat{\phi} \equiv \frac{2\phi}{\left(\frac{\alpha}{M_n}\right)^{2/3} U_n c_0}. \tag{2.5}$$

The variables $\hat{x}$, $\hat{z}$ and $\hat{\phi}$ are identical to those in the earlier works on the small-disturbance theory of plane transonic flow (Sprieter 1953; also see Ashley and Landahl 1965), except for the trivial differences of using a half chord $c_0/2$ instead of c_0, and omitting factors with $(1+1)$. Using these variables, and eliminating $(1-M_n^2)$, $\tan\Lambda$, and c_0/b through K_n, $\textcircled{M}$ and ϵ, (2.4) can be reduced to

$$\frac{\partial}{\partial\hat{x}}\left[K_n\,\hat{\phi}_{\hat{x}} - \frac{1+1}{2}\,\hat{\phi}_{\hat{x}}^2\right] + \hat{\phi}_{\hat{z}\hat{z}} = \epsilon\left[2\textcircled{M}\frac{2}{\partial\hat{y}} + \textcircled{M}'\right]\hat{\phi}_{\hat{x}} + \cdots \tag{2.6}$$

where $\textcircled{M}'$ is $d\textcircled{M}/d\hat{y}$; the terms omitted (....) belong to orders ϵ^2 and $\alpha^{2/3}$ under the stipulation of a finite K_n and $\textcircled{M}$, or simply to the order ϵ^2 for finite K_n, $\textcircled{M}$ and $\alpha^{1/3}/\epsilon$. The pressure perturbation can be computed from $\hat{\phi}_{\hat{x}}$ as

$$c_p' \equiv (p - p_\infty)\Big/\tfrac{1}{2}\rho_\infty U_n^2 = -2\left(\frac{\alpha}{M_n}\right)^{2/3}\hat{\phi}_{\hat{x}} + \cdots \tag{2.7}$$

subject to an error comparable to ϵ^4. The retention of the factor M_n in the definition of K_n, in scaling factors for $\hat{\phi}$ and $\hat{z}$, as well as the factor $\cos\Lambda$ in $U_n = U_\infty\cos\Lambda$ of (2.5) and (2.7), are not fundamental from the viewpoint of an asymptotic theory. Our preference for these choices will be explained later (Section 2.3).[+]

For the present study, we consider impermeable wing surfaces prescribed over the planform $\hat{a}(\hat{y}) < \hat{x} < \hat{b}(\hat{y})$ as

$$z' = \frac{c_0}{2}\left[\alpha\,\hat{Z}^{\pm}(\hat{x},\hat{y}) + \alpha^{1/3}\hat{Z}_\theta(\hat{y}) + \alpha\epsilon\,(\hat{x}-\hat{x}_0)\hat{I}(\hat{y})\right]. \tag{2.8}$$

[+] These factors M_n and $\cos\Lambda$ were not used in the definition of K_n, $\hat{\phi}$, and $\hat{z}$ in our earlier note (Cheng & Meng 1979).

where $\hat{a}$ and $\hat{b}$ locate the leading and trailing edge, respectively, the superscripts + and - refer to the upper and lower surfaces, respectively, and $\hat{Z}$, $\hat{Z}_\theta$ and $\hat{I}$ are all of unit order.[+] The functions $\hat{I}(\hat{y})$ and $\hat{Z}_\theta(\hat{y})$ signify, respectively, a twist and an upward deflection. The latter is referred to as "wing bend" by Jones (1971, 1977). Both $\hat{Z}_\theta$ and $\hat{I}$ have been scaled in a way to allow the control of the 3-D effects (see below). The boundary condition on the wing can be transferred to the wing plane ($z' = 0$) as

$$\left(\frac{\partial\hat{\phi}}{\partial\hat{z}}\right)_w = \frac{\partial}{\partial\hat{x}}\hat{Z}^{\pm} + \epsilon\,\textcircled{M}\,\hat{Z}'_\theta + \epsilon\,\hat{I} + \cdots \qquad (2.9)$$

where $\hat{Z}'_\theta$ is $d\hat{Z}_\theta/d\hat{y}$, and the subscript "w" refers to points on the wing plane bounded by $\hat{a} < \hat{x} < \hat{b}$. The remainder, $(\cdots)$ including errors from the boundary condition transfer, belong to orders $\alpha^{3/2}$ or ϵ^2, same as in (2.6). The pressure and the velocity component normal to the trailing-vortex sheet is required to be continuous across the sheet. These conditions are again transferred to $z' = 0$ to read, subject to error comparable to ϵ^2,

$$[\![\hat{\phi}_{\hat{x}}]\!]_{TV} = [\![\hat{\phi}_{\hat{z}}]\!]_{TV} = 0 \qquad (2.10)$$

where $[\![\ ]\!]$ signifies the difference across the surface in question, and the subscript "TV" refers to the portion of the wing plane at $z' = 0$ corresponding to the trailing-vortex (TV) sheet. The first of (2.10) confirms that the cross-stream vorticity of the near wake is unimportant. The streamwise vorticity component of the near wake is nevertheless very significant (see (3.12) later).

2.2 Characteristic and shock

The reduced PDE comprised of terms shown in (2.6) has the characteristic $\hat{x} = \hat{x}^c(\hat{y}, \hat{z})$ satisfying (Courant and Hilbert, 1965, pp. 551-556)

[+] We assume that, in approaching the leading edge, $\hat{Z}^{\pm} \sim \pm$ const. $(\hat{x}-\hat{a})^{\frac{1}{2}}$.

$$K_n - (1+1)\,\hat{\phi}_{\hat{x}} + 2\epsilon\textcircled{H}\frac{\partial \hat{x}^c}{\partial \hat{y}} = -\left(\frac{\partial \hat{x}^c}{\partial \hat{z}}\right)^2 \quad ; \tag{2.11}$$

its existence as a real surface requires

$$K_n - (1+1)\,\hat{\phi}_{\hat{x}} + 2\epsilon\textcircled{H}\frac{\partial \hat{x}^c}{\partial \hat{y}} \quad < \quad 0 . \tag{2.12}$$

The limit $\epsilon \to 0$ (with finite $\textcircled{H}$ and K_n) determines a critical value of the component-flow velocity with

$$\hat{\phi}_{\hat{x}} = K_n/(1+1) \equiv \hat{u}_* . \tag{2.13}$$

This identifies the transition boundary of the hyperbolic and the elliptic regions, and is also the locus where the component velocity reaches the sonic speed -- a fact familiar from the transonic small-disturbance theory for the plane flow. Condition (2.13), as well as its modification with the $0(\epsilon)$ correction in (2.12), differs from the critical condition for the fuller 3-D PDE (2.1) or its equivalence (2.4). The transition boundary for the fuller equation is simply the sonic condition for the resultant velocity in three dimensions,[+] which derives from the property of characteristic conoids generated from a point. Whereas the characteristic (2.11) represents a hyperbolic-wave surface generated by a line of disturbances along the wing span, approaching a cylindrical symmetry in the limit $\epsilon \to 0$.

PDE (2.6) and the equations expressing irrotationality admit weak solutions with surfaces of discontinuity in $\nabla\phi$, say $\hat{x} = \hat{x}^D(\hat{y}, \hat{z})$, identifiable with gasdynamic shock waves. The shock conditions admissible to the weak solution and consistent with Rankine-Hugonoit relations, can be written as, at $\hat{x} = \hat{x}^D(\hat{y}, \hat{z})$,

$$K_n - (1+1)\langle \hat{\phi}_{\hat{x}} \rangle + 2\epsilon\textcircled{H}\frac{\partial \hat{x}^D}{\partial \hat{y}} = -\left(\frac{\partial \hat{x}^D}{\partial \hat{y}}\right)^2 , \tag{2.14a}$$

[+] This critical condition is $\phi_x/U_\infty = (1-M_\infty^2)/(1+1)$, not reducible to (2.13), even in the limit $\epsilon \to 0$ with K_n and $\textcircled{H}$ fixed. Also note that, if the centerline were slightly shifted to become parallel to the characteristic surface, so that $K_n' = K_n + 2\epsilon\textcircled{H}\partial\hat{x}^c/d\hat{y}$, (2.11) and (2.12) would be geometrically invarient.

$$[\![\,\hat{\Phi}\,]\!] = 0, \tag{2.14b}$$

where, as before, $\langle\ \rangle$ and $[\![\ ]\!]$ stands for the arithmetical mean and the jump of the quantity across the surface in question, respectively. The continuity of $\hat{\Phi}$ (2.14b), implies the continuity of the tangential velocities,

$$[\![\,\hat{\Phi}_{\hat{x}}\,]\!] : [\![\,\hat{\Phi}_{\hat{z}}\,]\!] : [\![\,\hat{\Phi}_{\hat{y}}\,]\!] = -1 : \frac{\partial \hat{x}^{D}}{\partial \hat{z}} : \frac{\partial \hat{x}^{D}}{\partial \hat{y}}. \tag{2.15}$$

2.3 On choosing the form for K_n and retaining $\cos\Lambda$ in U_n.

The use of $K_n \equiv (1-M_\infty^2)/\alpha^{4/3}M_\infty$ for the 2-D transonic small-disturbance solution has been proposed by Murman and Cole (1971), also Murman and Krupp (1971), which yields consistently good agreement with exact solutions for transonic flows past shock-free supercritical airfoils (Korn 1969).[+] Apart from practical considerations, the very similar parameter K_n in the present paper with, $M_n \equiv M_\infty \cos\Lambda$ replacing M_∞ is adopted, however, for additional theoretical reasons.

We observe that terms deleted from the coefficient of $\hat{\Phi}_{\hat{x}}\hat{\Phi}_{\hat{x}\hat{x}}$ in (2.6) will give an incorrect description of characteristic slopes near the transition boundary and may lead to a nonuniformity of the inner solution (at some stage of the higher-order expansion).[++] This deficiency can be improved through a correction to the critical speed for the component flow, hence, to the K_n in (2.6). The latter can be explicitly determined independently of the solution (Appendix I). The result takes the form of a slightly modified definition for the similarity parameter, namely

$$K_n' \equiv (1-M_n^2)/\alpha^{2/3}M_n^{\omega}, \qquad \omega=(\gamma+1)/3(\gamma+1). \tag{2.16}$$

[+] See Bailey & Ballhaus (1973) for similar consideration in 3-D cases.

[++] Among those deleted from the coefficient the major terms are

$$(\alpha/M_n)^{4/3}\left[(\gamma-1)K_n\hat{\Phi}_{\hat{x}} - \frac{\gamma+1}{2}(2\gamma-1)\hat{\Phi}_{\hat{x}}^2\right].$$

The value of ω ranges from 5/6 to 23/24 for $\gamma = 1$ to 5/3, and, therefore has been taken as unity in our definition of K_n.

A similar transonic parameter, though in a more complicated form, has been pointed out by Sirovich and Ho (1978), who considered simple-wave solutions in a purely supercritical case, for which a nonuniformity at the transition boundary can be readily identified. In a study by Klunker and Newman (1974), a term $-\frac{|t|}{2} M_\infty^2 \phi_x^2$ is added to the coefficient of ϕ_{xx} of PDE (2.1) with an aim to better approximate the critical speed, the result may be shown to be equivalent to a modification of the similarity parameter in the manner of (2.16) for a straight unyawed wing.

The component of the free-stream velocity $U_n = U_\infty \cos\Lambda$ which appears in (2.5) and (2.7) defining $\hat{\phi}$ and C_p' could be replaced simply by U_∞ causing errors no larger than $0(\epsilon^2)$ or $0(\alpha^{2/3})$, since $\Lambda = \mathcal{M}\alpha^{1/3} = 0(\alpha^{1/3})$ has been assumed. However, its retention in the inner solution has a definite advantage for enlarging (slightly) the applicability range of the sweep angle. This follows from an examination of terms associated with Λ in the remainder of (2.6) - (2.10), comparing them to the 3-D effects of interest. The latter belong to $0(\epsilon\mathcal{M})$. The errors resulting from replacing U_n with U_∞ in (2.5) and (2.7) are proportional to Λ^2. The remainders related to Λ in PDE (2.6) and in (2.7), as well as (2.10), fall into two types, one is $0(\epsilon\mathcal{M}\Lambda^2)$ and the other $0(\Lambda/R_1)$. The relative magnitude of the four groups in question are, therefore, in the proportion:

$$\epsilon\mathcal{M} : \Lambda^2 : \epsilon\mathcal{M}\Lambda^2 : \Lambda R_1^{-1} = 1 : \epsilon\mathcal{M} : \epsilon^2\mathcal{M}^2 : \epsilon , \qquad (2.17)$$

where the assumption of $\epsilon = 0(\alpha^{1/3})$ is made as before and the order of magnitude symbols have been omitted. From (2.17), it is clear that if U_n were replaced by U_∞, errors in the solution would be of an order ϵ higher than the 3-D effects analyzed only when $\mathcal{M} = 0(1)$. Now, the retention of the $\cos\Lambda$ factor in the definition of $\hat{\phi}$ and C_p' eliminates the need of considering the second group. Therefore, the error of the solution can remain an order ϵ higher than the 3-D effects analyzed as long as

$$\mathcal{M} = O(\epsilon^{-1/2}) = O(\alpha^{-1/6}). \qquad (2.18)$$

or smaller, according to (2.17).[+]

2.4 Perturbation of the component flow

Equations (2.6), (2.9) and (2.10) permit an expansion of $\hat{\phi}$ in ϵ

$$\hat{\phi} = \hat{\phi}_0 + \epsilon \hat{\phi}_1 + \cdots \tag{2.19}$$

where a weak (logarithmic) dependence of $\hat{\phi}_0$, on ϵ is anticipated. The leading term $\hat{\phi}_0$ is a 2-D solution to the component flow at the span station $\hat{y}$ satisfying the PDE

$$\left[K_n - (\gamma+1)\frac{\partial}{\partial \hat{x}}\hat{\phi}_0\right]\frac{\partial^2}{\partial \hat{x}^2}\hat{\phi}_0 + \frac{\partial^2}{\partial \hat{z}^2}\hat{\phi}_0 = 0 \tag{2.20}$$

and the conditions on the x-axis

$$\left(\frac{\partial}{\partial \hat{z}}\hat{\phi}_0\right)_w = \frac{d}{d\hat{y}}\hat{Z}^{\pm} \quad ; \quad \left[\!\left[\frac{\partial}{\partial \hat{x}}\hat{\phi}_0\right]\!\right]_{TV} = \left[\!\left[\frac{\partial}{\partial \hat{z}}\hat{\phi}_0\right]\!\right]_{TV} = 0, \tag{2.21}$$

where the subscripts "w" and "TV" carry some meanings as before. The coefficient $\hat{\phi}_1$ is governed by the linear nonhomogeneous PDE in variables $\hat{x}$ and $\hat{z}$ (obtained after equating terms proportional to the first power of ϵ)

$$\left[K_n - (\gamma+1)\frac{\partial}{\partial \hat{x}}\hat{\phi}_0\right]\frac{\partial^2}{\partial \hat{x}^2}\hat{\phi}_1 + \frac{\partial^2}{\partial \hat{z}^2}\hat{\phi}_1 - (\gamma+1)\frac{\partial^2}{\partial \hat{x}^2}\hat{\phi}_0 \cdot \frac{\partial}{\partial \hat{x}}\hat{\phi}_1 = \left[2\Theta\frac{\partial}{\partial y} + \Theta'\right]\frac{\partial}{\partial \hat{x}}\hat{\phi}_0 \tag{2.22}$$

and the conditions on the $\hat{x}$-axis (obtained in a similar manner)

$$\left(\frac{\partial}{\partial \hat{z}}\hat{\phi}_1\right)_w = \Theta\frac{d}{d\hat{y}}\hat{Z}_B \quad ; \quad \left[\!\left[\frac{\partial}{\partial \hat{x}}\hat{\phi}_1\right]\!\right]_{TV} = \left[\!\left[\frac{\partial}{\partial \hat{z}}\hat{\phi}_1\right]\!\right]_{TV} = 0, \tag{2.23}$$

where $\hat{y}$ appears essentially as a parameter. We note also that the

---

[+] It is rather well known that the PDE governing the transonic component flow around a thin yawed wing of infinite aspect ratio cannot be recovered completely from PDE (2.1) without either retaining ϕ_y^2 or invoking the approximation $\cos\Lambda \approx 1$. We, therefore, may expect the present work to be slightly more accurate than those based on the standard 3-D transonic small-disturbance equation.

solutions $\hat{\phi}_1$ and $\hat{\phi}_0$ share the same characteristics system $\hat{x} = \hat{x}_0^c(\hat{y},\hat{z})$ given by

$$K_n - (1+1)\frac{\partial}{\partial \hat{x}}\hat{\phi}_0 = -\left(\frac{\partial \hat{x}_0^c}{\partial \hat{z}}\right)^2 . \tag{2.24}$$

Thus, the transition boundary separating the elliptic and hyperbolic regions is $K_n - (1+1)\frac{\partial}{\partial \hat{x}}\hat{\phi}_0 = 0$ for both $\hat{\phi}_0$ and $\hat{\phi}_1$.

The equation describing the shock is expanded as

$$\hat{x} = \hat{x}^D(\hat{y},\hat{z}) = \hat{x}_0^D(\hat{y},\hat{z}) + \epsilon\, \hat{x}_1^D(\hat{y},\hat{z}) + \cdots , \tag{2.25}$$

allowing again a weak (logarithmic) dependence of $\hat{x}_1^D$ on ϵ . The Hugoniot relations (2.14) can be transferred from $\hat{x} = \hat{x}^D$ to $\hat{x} = \hat{x}_0^D$, yielding, after equating terms of equal algebraic powers of ϵ ,

$$K_n - (1+1)\left\langle \frac{\partial}{\partial \hat{x}}\hat{\phi}_0 \right\rangle = -\left(\frac{\partial \hat{x}_0^D}{\partial \hat{z}}\right)^2 , \quad [\![\, \hat{\phi}_0 \,]\!] = 0 ; \tag{2.26}$$

$$\left.\begin{aligned} 2\textcircled{M}\frac{\partial \hat{x}_0^D}{\partial \hat{y}} - (1+1)\left\langle \frac{\partial}{\partial \hat{x}}\hat{\phi}_1 + \hat{x}_1\frac{\partial^2}{\partial \hat{x}^2}\hat{\phi}_0 \right\rangle &= -2\,\frac{\partial \hat{x}_0^D}{\partial \hat{z}}\cdot\frac{\partial \hat{x}_1^D}{\partial \hat{z}}, \\ [\![\, \hat{\phi}_1 + \hat{x}_1\frac{\partial}{\partial \hat{x}}\hat{\phi}_0 \,]\!] &= 0 . \end{aligned}\right\} \tag{2.27}^{+}$$

As noted earlier, the subcritical flow right behind the shock root over a curved (wing) surface has a weak singularity in the surface value of $(\hat{\phi}_0)_{\hat{x}}$, like $(\hat{x}-\hat{x}_0^D)\ln|\hat{x}-\hat{x}_0^D|$, this will then give a logarithmic singularity in $\hat{\phi}_{1\hat{x}}$, in view of the shock condition (2.27). This nonuniformity is treated in § 2.6.

+ For flow-field computation, it may be more convenient to apply the first of (2.26) and (2.27) with $(\hat{x}_0^D)_{\hat{z}}$, $(\hat{x}_1^D)_{\hat{z}}$ and $(\hat{x}_0^D)_{\hat{z}}$ eliminated through the second of (2.26) and (2.27), e.g. $[\![\, (\hat{\phi}_0)_{\hat{z}} + (\hat{x}_0^D)_{\hat{z}}(\hat{\phi}_0)_{\hat{x}} \,]\!] = 0$.

2.5 Behavior at large distance

Since $\partial\hat{\Phi}_0/\partial\hat{x}$ vanishes as $|\hat{\zeta}| \equiv \sqrt{\hat{x}^2 + K_n\hat{z}^2} \to \infty$, PDE (2.20) approaches the Laplace equation in $\hat{x}$ and $\hat{\eta} \equiv \sqrt{K_n}\,\hat{z}$; the leading term in an asymptotic expansion for $\hat{\Phi}_0$ at large $|\hat{\zeta}|$ may therefore be represented by a vortex potential in the variable $\hat{\zeta} \equiv \hat{x} + i\hat{\eta}$. This and the successive terms in the development of $\hat{\Phi}_0$ for $|\hat{\zeta}| \gg 1$ can be inferred from PDE (2.20) under the requirement that $(\hat{\Phi}_0)_{\hat{x}}$ and $(\hat{\Phi}_0)_{\hat{\eta}}$ are continuous everywhere including the $\hat{x}$ - axis (removed from the wing section)

$$\hat{\Phi}_0 \sim \frac{\hat{\Pi}_0}{2\pi}\left[\tan^{-1}\left(\frac{\hat{x}}{\sqrt{K_n}\hat{z}}\right) + \frac{\pi}{2}\,Sgn(\hat{z})\right] + \frac{1+1}{4K_n}\left(\frac{\hat{\Pi}_0}{2\pi}\right)^2\left[\ln|\hat{\zeta}| + K_n\frac{\hat{z}^2}{|\hat{\zeta}|^2}\right]\frac{\hat{x}}{|\hat{\zeta}|^2} +$$

$$+\left[\hat{D}_0^r\,\hat{x} + \hat{D}_0^i\sqrt{K_n}\,\hat{z}\right]\frac{1}{|\hat{\zeta}|^2} + \cdots \qquad (2.28)$$

where $\hat{\Pi}_0 \equiv [\![\hat{\Phi}_0]\!]_{TE}$ is the circulation determined by the potential jump at the trailing edge(TE); the remainder (...) is at most of the order $(\ln|\hat{\zeta}|)^2|\hat{\zeta}|^{-2}$. The coefficients $\hat{D}_0^r$ and $\hat{D}_0^i$ may be taken as the real and imaginary parts of a complex doublet strength $\hat{D}_0 = \hat{D}_0^r + i\hat{D}_0^i$; they are functional of $[\![(\hat{\Phi}_0)_{\hat{x}}]\!]_{\sim}$, $[\![\hat{Z}]\!]_{\sim}$ and $(\hat{\Phi}_{\hat{x}})^2$, and can be explicitly computed in the forms of line and area integrals, unaffected by the presence of an imbedded shock (Appendix II). A form comparable to (2.28) has been given earlier by Cole (1975).[+] For numerical analysis, these explicit forms for the doublet strengths are unnecessary, since they can be determined along with solutions at and near the far boundary, with the help of a least-square method (§ 5), as has been in Hafez & Cheng (1977a & b).

The PDE (2.22) governing $\hat{\Phi}_1$ approaches a Poisson equation at large $|\hat{\zeta}|$, which gives the two leading terms in the expansion of $\hat{\Phi}_1$. These and the successive terms fulfilling the continuity requirements on $\hat{\Phi}_{\hat{x}}$ and $\hat{\Phi}_{\hat{z}}$ can be determined, for $|\hat{\zeta}| >> 1$, as

---

[+] The term proportional to $\hat{\Pi}_0^2$ in Eq. (2.28) differs from that given by Cole (1975). The angle of the arc tangent is restricted to the range $[-\pi/2\,,\,\pi/2]$.

$$\hat{\phi}_1 \sim \frac{\Theta\hat{z}}{\sqrt{K_n}}\left[\left(\frac{d}{d\hat{y}}+\frac{1}{2}\frac{K_0}{K_n}\frac{\Theta'}{\Theta}\right)\frac{\hat{\Pi}_0}{2\pi}\ln|\hat{\zeta}| + \frac{\Theta\Theta'}{2}\frac{\hat{\Pi}_0}{2\pi}\frac{\hat{z}^2}{|\hat{\zeta}|^2}\right] -$$

$$- \hat{C}_1^i\sqrt{K_n}\,\hat{z} + \hat{C}_1^r\,\hat{x} + \hat{N}_1 + \frac{\hat{Q}_1}{2\pi}\ln|\hat{\zeta}| +$$

$$+\frac{\Theta}{\sqrt{K_n}}\frac{\hat{z}}{|\hat{\zeta}|^2}\left[\hat{x}\left(\frac{d}{d\hat{y}}+\frac{1}{2}\frac{K_0}{K_n}\frac{\Theta'}{\Theta}\right)\hat{D}_0^i - \sqrt{K_n}\,\hat{z}\left(\frac{d}{d\hat{y}}+\frac{1}{2}\frac{K_0}{K_n}\frac{\Theta'}{\Theta}\right)\hat{D}_0^r\right] +$$

$$+\frac{\Theta\Theta'}{2K_n}\frac{\hat{z}^2}{|\hat{\zeta}|^4}\left[\hat{D}_0^r(\hat{x}^2-K_n\hat{z}^2)+2\sqrt{K_n}\,\hat{D}_0^i\,\hat{x}\,\hat{z}\right] +$$

$$+\frac{\hat{\Pi}_1}{2\pi}\left[\tan^{-1}\left(\frac{\hat{x}}{\sqrt{K_n}\,\hat{z}}\right)+\frac{\pi}{2}\,\mathrm{sgn}\,\hat{z}\right] + \hat{F}(\hat{y}) + \cdots \qquad (2.29)$$

where $\hat{\Pi}_1$ is $[\![\hat{\phi}_1]\!]_{TE}$; $\hat{C}_1^i$ and $\hat{C}_1^r$ correspond, respectively, to the induced upwash and a component-Mach-number correction to be determined later through matching; the parameter $K_0 \equiv K_n - \Theta^2$ can be identified as the transonic similarity parameter at zero sweep $(1-M_\infty^2)/\alpha_1^{2/3}M_\infty$. The remainder (...) vanishes as $|\hat{\zeta}| \to \infty$,[+] and the symbol $\hat{N}_1$ designates terms arising from nonlinear corrections in the far field of orders $(\ln|\hat{\zeta}|)^2$ $\ln|\hat{\zeta}|$ and unity

$$\hat{N}_1 \sim \frac{\gamma+1}{32}\frac{\Theta}{K_n^2}\frac{\hat{\Pi}_0}{2\pi}\left(\frac{d}{d\hat{y}}+\frac{1}{2}\frac{\Theta'}{\Theta}\right)\hat{\Pi}_0\left[2(\ln|\hat{\rho}|)^2+2\left(\frac{2\hat{x}^2}{|\hat{\zeta}|^2}-1\right)\cdot\left(\ln|\hat{\rho}|+\frac{1}{2}\right)-\right.$$

$$\left.-\frac{1}{2}\left(1-8K_n\frac{\hat{z}^2\hat{x}^2}{|\hat{\zeta}|^4}\right)\right] + \frac{\gamma+1}{16}\frac{\Theta^2\Theta'}{K_n^3}\left(\frac{\hat{\Pi}_0}{2\pi}\right)^2\left\{-20\left(\ln|\hat{\zeta}|\right)^2+\right.$$

$$+\left[\left(\frac{\hat{\zeta}}{\hat{\zeta}_*}\right)^2+\left(\frac{\hat{\zeta}_*}{\hat{\zeta}}\right)^2-12\left(\frac{\hat{\zeta}}{\hat{\zeta}_*}\right)-12\left(\frac{\hat{\zeta}_*}{\hat{\zeta}}\right)\right]\ln|\hat{\rho}| -$$

$$\left.-\frac{1}{3}\left(\frac{\hat{\zeta}}{\hat{\zeta}_*}\right)^3-\frac{1}{3}\left(\frac{\hat{\zeta}_*}{\hat{\zeta}}\right)^3+\frac{5}{4}\left(\frac{\hat{\zeta}}{\hat{\zeta}_*}\right)^2+\frac{5}{4}\left(\frac{\hat{\zeta}_*}{\hat{\zeta}}\right)^2+\frac{\hat{\zeta}}{\hat{\zeta}_*}+\frac{\hat{\zeta}_*}{\hat{\zeta}}\right\} \qquad (2.30)$$

where $\hat{\zeta} \equiv \hat{x}+i\sqrt{K_n}\,\hat{z}$ and $\hat{\zeta}_* \equiv \hat{x}-i\sqrt{K_n}\,\hat{z}$. The appearance of the source term in the far field with a strength $\hat{Q}_1 \neq 0$ should not be too surprising, since

---

[+] Among the remainders are terms of order $(\ln|\hat{\zeta}|/|\hat{\zeta}|)^2$ and $(\ln|\hat{\zeta}|)^4/|\hat{\zeta}|$.

(2.22), cast into a Poisson equation

$$4\frac{\partial^2}{\partial\hat{\xi}\partial\hat{\xi}_0}\hat{\Phi}_1 = \left[2\textcircled{M}\frac{\partial}{\partial\hat{y}} + \textcircled{M}'\right]\frac{\partial}{\partial\hat{x}}\hat{\Phi}_0 + (1+1)\frac{\partial}{\partial\hat{x}}\left[(\hat{\Phi}_0)_{\hat{x}}\cdot(\hat{\Phi}_1)_{\hat{x}}\right], \quad (2.31)$$

indicates clearly a source distribution which gives a nonvanishing total <u>volume</u> flux to the <u>component</u> flow.

The influence of this term on the outer flow is quite similar to the one in the transonic equivalence rule involving lift (Cheng & Hafez, 1973) although the line-source effect has a considerably greater influence therein. The source strength $\hat{Q}_1$ is completely determined by the far-field property of $\hat{\Phi}_0$, more specifically, $\hat{D}_0'$ and $(\hat{\Gamma}_0)^2$. In cases where $(\hat{\Gamma}_0)^2$ can be neglected, the area integral of the RHS (2.31) over $\hat{x}$ and $\hat{\eta}$ can be correctly equated to the total volume flux and determined as

$$\begin{aligned}\hat{Q} &= \frac{2\textcircled{M}}{K_n}\iint\left(\frac{\partial}{\partial\hat{y}} + \frac{\textcircled{M}'}{2\textcircled{M}} + \frac{\textcircled{M}\textcircled{M}'}{K_n}\hat{\eta}\frac{\partial}{\partial\hat{x}}\right)\frac{\partial}{\partial\hat{x}}\hat{\Phi}_0\, d\hat{x}\, d\hat{\eta} \\ &= \frac{2\textcircled{M}}{K_n}\lim_{|\hat{\xi}|\to\infty}\oint\left(\frac{\partial}{\partial\hat{y}} + \frac{\textcircled{M}'}{2\textcircled{M}} + \frac{\textcircled{M}\textcircled{M}'}{K_n}\hat{\eta}\frac{\partial}{\partial\hat{\eta}}\right)\hat{\Phi}_0\, d\hat{\eta} \\ &= \frac{2\textcircled{M}}{K_n}\left[\frac{\partial}{\partial\hat{y}} + \frac{1}{2}\frac{K_0}{K_n}\frac{\textcircled{M}'}{\textcircled{M}}\right]\pi\hat{D}_0', \end{aligned} \quad (2.32)$$

confirming the existence of a $\hat{Q}_1 \neq 0$ (unless $\hat{D}_0'$ or the wing thickness vanishes). For $\hat{\Gamma}_0 \neq 0$, (2.29) shows that $|\hat{\Phi}_1| \gg \ln|\hat{\xi}|$ and $\hat{Q}_1$, in this case cannot be evaluated simply from the area integral of RHS (2.22), which may be unbounded; the quantity of interest may nevertheless be determined by constructing first functions $\hat{\Phi}_{0c}$ and $\hat{\Phi}_{1c}$ which satisfy two Poisson equations and agree with $\hat{\Phi}_0$ and $\hat{\Phi}_1$, respectively, in the far field in accordance with (2.28) and (2.29); applying next a result of Green's theorem to the difference of $(\hat{\Phi}_0 + \epsilon\hat{\Phi}_1)$ and $(\hat{\Phi}_{0c} + \epsilon\hat{\Phi}_{1c})$. Using (2.14), the result can be shown to be unaffected by the presence of shocks. The explicit relation connecting $\hat{Q}_1$ to $\hat{D}_0'$ and $(\hat{\Gamma}_0)^2$ will be given later in §4 in the case of oblique wings under local similarity; its derivation is described in Appendix III.

The demonstration in (2.32) indicates that similar line-source effect will arise in the corresponding lifting-line theory in a linear subsonic flow, although the lifting and the thickness problems in this case can be

separately analyzed on account of the linearity.

It is assumed that the solutions $\hat{\phi}_0$ and $\hat{\phi}_1$ are uniquely determined after fulfilling the Kutta condition at the trailing edge, the conditions (2.21), (2.24), (2.27), and the far-field behavior represented by the leading groups of terms on RHS (2.28) and RHS (2.29). The latter is

$$\left.\begin{aligned} \hat{\phi}_0 &\sim \frac{\hat{\Pi}_0}{2\pi}\left[\tan^{-1}\left(\frac{\hat{x}}{\sqrt{K_n}\,\hat{z}}\right) + \frac{\pi}{2}\,\mathrm{Sgn}\,\hat{z}\right] ; \\ \hat{\phi}_1 &\sim \frac{\Theta\,\hat{z}}{\sqrt{K_n}}\left[\left(\frac{d}{d\varphi} + \frac{1}{2}\,\frac{K_a}{K_n}\,\frac{\Theta'}{\Theta}\right)\frac{\hat{\Pi}_0}{2\pi}\,\ln|\hat{\zeta}| + \frac{\Theta\Theta'}{2}\,\frac{\hat{\Pi}_0}{2\pi}\,\frac{\hat{z}^2}{|\hat{\zeta}|^2} - \right. \\ &\qquad \left. - \hat{C}_1^{i}\sqrt{K_n}\,\hat{z} + \hat{C}_1^{r}\,\hat{x}\right. . \end{aligned}\right\} \qquad (2.33)$$

The first of (2.33) is equivalent to the vanishing of the gradient of $\hat{\phi}_0$ and the second requires specifications of the upwash and component Mach-number corrections.

2.6 Treatment of the nonuniformity at the shock root

Recall that the logarithmic singularity in $(\hat{\phi}_0)_{\hat{x}}$ is a result of the breakdown of the analytic continuation of $\langle(\hat{\phi}_1)_{\hat{x}}\rangle$ from the perturbed to the unperturbed shock boundaries, cf. (2.27). It is apparent that terms like $\frac{1}{2}(\hat{x}_1^D)^2\langle\hat{\phi}_{0\hat{x}\hat{x}\hat{x}}\rangle$ and $\hat{x}_2^D\langle\hat{\phi}_{1\hat{x}\hat{x}}\rangle$ will arise in the corresponding shock relations in the next order. This and similar reasons lead to the expectation that $(\hat{\phi}_2)_{\hat{x}}$ is singular like $1/\hat{x}'$ with $\hat{x}' \equiv \hat{x} - \hat{x}_0^D$, and $(\hat{\phi}_3)_{\hat{x}}$ like $1/\hat{x}'^2$. Thus, a nonuniformity of the expansion (2.19) is identified at $\hat{x} - \hat{x}_0^D = O(\epsilon)$.

Instead of carrying through the formalism of expansion in a new inner variable for this (inner of the inner) region, we treat the nonuniformity directly in the framework of the composite system (2.6), (2.9), (2.10) and (2.14a & b). We shall first establish below that the reexpansion singularity in $(\hat{\phi})_{\hat{x}}$, written in coordinates fixed to the shock root is unaffected by the 3-D corrections. Using this as a valid flow description near the shock root, it becomes possible to determine the 3-D corrections to the shock jump, the shock-excursion distance, as well as another parameter of the reexpansion singularity, from matching the perturbation of this solution with the logarithmically singular field of $(\hat{\phi}_1)_{\hat{x}}$.

For this purpose, we identify the location of the shock root by $\hat{x} = \hat{x}_{sr}$; we will use the subscript "sr" to denote values at $\hat{x} = \hat{x}_{sr}$ on the wing, and the superscripts "-" and "+" to denote the pre-shock and post-shock condition, respectively. For convenience, we introduce

$$\left.\begin{aligned} \xi_1 &\equiv \hat{x} - \hat{x}_{sr}\,, \qquad \eta_1 \equiv \beta_1 \hat{z}\;;\quad \zeta_1 \equiv \xi_1 + i\eta_1 \\ \beta_1 &\equiv \left| K_n - (\gamma+1)\,\hat{u}^{+}_{sr} \right|^{1/2} \end{aligned}\right\} \tag{2.34}$$

where $\hat{u}^{+}_{sr}$ is the post-shock value of $\hat{\phi}_{\hat{x}}$ at the shock root.† In addition, we let

$$\left.\begin{aligned} D &\equiv \epsilon\left[\textcircled{M}\frac{\partial}{\partial \hat{y}} + \textcircled{M}'\right], \\ Z'_w &\equiv \frac{\partial}{\partial \hat{x}}\hat{Z}^{t} + \epsilon\textcircled{M}\hat{Z}'_{B} + \epsilon\hat{I}\,. \end{aligned}\right\} \tag{2.35}$$

PDE (2.6) admits a development near the shock root (on the subcritical, downstream side) consistent with the impermeable wing condition (2.9),

$$\left.\begin{aligned} \hat{\phi} = \hat{\phi}_{sr} &+ \hat{u}^{+}_{sr}\cdot\xi_1 + (Z'_w)_{sr}\,\beta_1^{-1}\eta_1 + \\ &+ \text{R.P.}\left[A\zeta_1^2 \ln\zeta_1 + B\zeta_1^2\right] + C|\zeta_1|^2 + \cdots, \\ C &\equiv D\,\hat{u}^{+}_{sr}/2\beta_1 \end{aligned}\right\} \tag{2.36}$$

where "R.P." stands for the real part, and the remainder (...) is comparable to $O(|\zeta_1|^3)$. The latter corresponds to a relative error comparable to $O(\epsilon)$ in the inner region $\zeta_1 = O(\epsilon)$. The wing boundary condition also requires that

$$\text{I.P.}(A) = 0\,, \qquad \text{I.P.}(B) = -(Z''_w)_{sr}/2\beta_1\,, \tag{2.37}$$

where "I.P." refers to the imaginary part, and Z''_w stands for $\frac{\partial}{\partial \hat{x}} Z'_w$. The real parts of A together with the shock geometry near the root $\xi_1 = \xi_1^{D}(\eta_1)$ can be determined consistently from the two Hugoniot relations (2.14a & b) and a regular upstream supercritical solution for small ξ_1 and η_1. The

---

† Note that

$$K_n - (\gamma+1)\,\hat{u}^{+}_{sr} = (\gamma+1)\,\hat{u}^{-}_{sr} - K_n = \frac{\gamma+1}{2}\left(\hat{u}^{-}_{sr} - \hat{u}^{+}_{sr}\right) = -\frac{\gamma+1}{2}\left[\!\left[\hat{\phi}_{\hat{x}}\right]\!\right]_{sr}.$$

final result for A is

$$A \equiv \frac{\varepsilon}{\pi}\left(Z_w''\right)_{sr} / \beta_1 . \tag{2.38}$$

The real part of B can be determined only through matching with the solution in the region removed from the shock root. The 3-D effects can enter (2.36) only through R.P. (B) and through the known constant C. Whereas the description (2.36) differ from the original (Oswatitsch & Zierep 1960) form in the addition of a nonanalytic term proportional to $|\zeta_1|^2$, the field of the pressure perturbation, or $\hat{\Phi}_{\hat{x}}$, is nevertheless analytic and of the same original form. The result can be expressed, writing $\hat{\Phi}_{\hat{x}}$ as $\hat{u}$, as

$$\frac{\hat{u} - \hat{u}^{+}_{sr}}{\mathbb{I}\hat{u}\mathbb{I}_{sr}} \sim R.P.\left[\frac{4}{\pi}\zeta \ln\left(\frac{\zeta}{\kappa_1}\right) - i\zeta\right] , \tag{2.39a}$$

$$\zeta \equiv \xi + i\eta \; ; \quad \xi \equiv \frac{\left(Z_w''\right)_{sr}\left(\hat{x} - \hat{x}^{0}_{sr}\right)}{\sqrt{\frac{\gamma+1}{2}}\cdot\left|\mathbb{I}\hat{u}\mathbb{I}_{sr}\right|^{3/2}} \; , \quad \eta \equiv \frac{\left(Z_w''\right)_{sr}\hat{z}}{\left|\mathbb{I}\hat{u}\mathbb{I}_{sr}\right|} . \tag{2.39b}$$

The parameter κ_1 is an arbitrary constant containing the undetermined R.P. (B) as well as a contribution from $D\hat{u}^{+}_{sr}$. The corresponding form of the shock boundary is

$$\xi^{D} \sim \eta^2\left[\frac{2}{\pi}\ln\left(\frac{\eta}{\kappa_1}\right) + \mu\right] , \tag{2.40a}$$

$$\mu \equiv -\frac{1}{\pi} + \frac{1}{2}\left|\frac{\gamma+1}{2}\mathbb{I}\hat{u}\mathbb{I}_{sr}\right|^{1/2}\cdot\left(Z_w''\right)^{-1}_{sr}\cdot\left[\left(\hat{\Phi}_{\hat{x}\hat{x}}\right)^{-}_{sr} + D\left(\hat{u}^{-}_{sr}\right)\cdot\left|\frac{\gamma+1}{2}\mathbb{I}\hat{u}\mathbb{I}_{sr}\right|^{-1}\right] . \tag{2.40b}$$

The above description confirms that the analytic form of the pressure perturbation on $\hat{\Phi}_{\hat{x}\hat{x}}$ near the shock root is unaffected by the 3-D effects. As a matter of fact, this conclusion holds even if the 3-D effect through $D\hat{u}^{+}_{sr}$ was of order unity (cf. (2.35)). This observation will have relevance in the analagous problem of unsteady transonic problems (see § 4.1 below).

The result (2.39) indicates that any 3-D influence on this (inner) structure can result only through changes in the three parameters: $\mathbb{I}\hat{u}\mathbb{I}_{sr}$, $\hat{x}_{sr}$, and κ_1. Conversely, the structure determined through matching with

the perturbed solution in region exterior to this neighborhood should yield knowledge on the 3-D corrections to $[\![\hat{\phi}_{\hat{x}}]\!]_{sr}$, $\hat{x}^D_{sr}$, and κ_1.

Introduce

$$\delta\hat{u} \equiv \hat{u} - \hat{u}_o\,, \qquad \delta\hat{x}^D_{sr} \equiv \hat{x}^D_{sr} - (\hat{x}^D_o)_{sr}, \quad \delta\kappa_1 \equiv \kappa_1 - (\kappa_1)_o\,. \tag{2.41}$$

The subscript "$_o$" refers to values based on $\hat{\phi}_o$. At sufficiently large $|\xi|$, we can expand (2.39) for small $\delta\hat{u}$, $\delta\hat{x}^D_{sr}$ and $\delta\kappa_1$, taking into account of their effects on ξ and η. The final result yields a logarithmically singular behavior for the correction to $\hat{u} \equiv \hat{\phi}_{\hat{x}}$

$$\frac{\delta\hat{u}}{|[\![\hat{u}_o]\!]_{sr}|} \sim \mathcal{D}\ln|\xi| + d + d_1\xi\ln|\xi| + d_2\eta\arg(\xi) + e\xi + e_1\eta + \cdots\,, \tag{2.42}$$

with

$$\mathcal{D} = -\frac{4}{\pi}\left(\hat{Z}''_w\right)_{sr}\left(\frac{\gamma+1}{2}\right)^{-1/2}\left|[\![\hat{u}_o]\!]_{sr}\right|^{-3/2}\delta\hat{x}^D_{sr}\,,$$

$$d = -\frac{1}{2}\frac{\delta[\![\hat{u}]\!]_{sr}}{[\![\hat{u}_o]\!]_{sr}} + (1-\ln\kappa_1)\mathcal{D}\,,$$

$$d_1 = d_2 - \frac{2}{\pi}\delta[\![\hat{u}]\!]_{sr}/[\![\hat{u}_o]\!]_{sr}\,, \qquad d_2 = \frac{4}{\pi}\left[\frac{\partial}{\partial\hat{x}}\ln\hat{Z}''_w\right]_{sr}\delta\hat{x}^D_{sr}\,,$$

$$e = -\frac{4}{\pi}\frac{\delta\kappa_1}{\kappa_1} - \frac{4}{\pi}\ln\kappa_1\,\delta[\![\hat{u}]\!]_{sr}/[\![\hat{u}_o]\!]_{sr} + (1-\ln\kappa_1)\left[d_2 - \frac{6}{\pi}\delta[\![\hat{u}]\!]_{sr}/[\![\hat{u}_o]\!]_{sr}\right],$$

$$e_1 = d_2 - \frac{4}{\pi}\delta[\![\hat{u}]\!]_{sr}/[\![\hat{u}_o]\!]_{sr}\,.$$

The result (2.42) corresponds to the inner solution (2.39) in the outer limit, and should match with the logarithmically singular behavior of the $\hat{\phi}_1$ solution near $\hat{x} = \hat{x}^D_o$, $\hat{z} = 0$. Since the coefficients $\mathcal{D}$, etc. are completely determined once the exterior $\hat{\phi}_o$ and $\hat{\phi}_1$ problems (posed in §§ 2.4 and 2.5) are solved, the matching then will determine the 3-D corrections to the shock-root location from $\mathcal{D}$, the velocity jump at the root from d, and the parameter κ_1 from e. The matching of the coefficients

d_1 and d_2 furnishes additional checks on the theory's internal consistency.[+]

In passing, we point out that the singularities at the leading and trailing edges, and the related problems of nonuniformity, have not been considered. It is well known that for a $\hat{Z}^{\pm} \sim \text{const.}\ (\hat{x}-\hat{a})^{1/2}$, the 2-D surface pressure is singular like $(\hat{x}-\hat{a})^{-1/3}$, according to the transonic small-disturbance theory (Nonweiler 1958, Cole 1975). Keyfitz, Melnik and Grossman (1978) are able to show that as long as α does not far exceed the thickness ratio τ, i.e. $\alpha/\tau = O(1)$, the symmetric behavior, with the $-1/3$ exponent, remains to dominate the surface pressure near such a leading edge. One may then argue that nonuniformity <u>cannot</u> arise from 3-D corrections, because the flow asymmetry will not alter the $-1/3$ exponent, and also because the spanwise compressibility correction in the right of PDE (2.22) is, at worst, comparable to $(\hat{\Phi}_0)_{\hat{x}\hat{x}}$ which can be no more singular than terms on the left of (2.22) involving $\frac{\partial}{\partial \hat{x}}(\hat{\Phi}_0)_{\hat{x}}(\hat{\Phi}_1)_{\hat{x}}$.

[+] Preliminary computational results based on a shock-fitting procedure to determine $\hat{\Phi}_0$ and $\hat{\Phi}_1$ in a supercritical case indicates that such a procedure for determining the corrections for $[\![\hat{u}]\!]_{sr}$, $\hat{x}^D_{sr}$ and κ_1 is feasible.

3. OUTER SOLUTION AND MATCHING

3.1 The outer solution

In the flow domain of interest ($K_n > 0$, $K_0 \equiv K_n - \Theta^2 \geq 0$) the basic outer flow is described by the linear, elliptic Prandtl-Glauert equation. For subsequent analysis, we shall employ a set of dimensionless variables

$$\bar{x} \equiv x/Bb, \quad \bar{y} \equiv y/b, \quad \bar{z} \equiv z/b; \quad \bar{\phi} \equiv \phi/\alpha_1^{4/3} U_\infty c_0, \tag{3.1}$$

with

$$B \equiv \sqrt{1-M_\infty^2}, \qquad \alpha_1 \equiv \alpha/M_\infty,$$

and assume an expansion for a dimensionless perturbation potential

$$\bar{\phi} = \bar{\phi}_0 + \epsilon \bar{\phi}_1 + \cdots \tag{3.2}$$

where a weak (logarithmic) dependence of ϕ_1 on ϵ is anticipated. The term $\epsilon\bar{\phi}_1$ accounts for the higher aspect-ratio effect as well as the nonlinear correction to the outer solution. PDE (2.1) yields equations governing $\bar{\phi}_0$ and $\bar{\phi}_1$

$$\left(\frac{\partial^2}{\partial \bar{x}^2} + \frac{\partial^2}{\partial \bar{y}^2} + \frac{\partial^2}{\partial \bar{z}^2}\right)\bar{\phi}_0 = 0,$$

$$\left(\frac{\partial^2}{\partial \bar{x}^2} + \frac{\partial^2}{\partial \bar{y}^2} + \frac{\partial^2}{\partial \bar{z}^2}\right)\bar{\phi}_1 = \frac{\gamma+1}{2K_0^{3/2}}\frac{\partial}{\partial \bar{x}}\left(\bar{\phi}_{0\bar{x}}\right)^2. \tag{3.3}$$

In the far field, the gradients of $\bar{\phi}_0$ and $\bar{\phi}_1$ are required to vanish, and on the wing trace behind the center line, the continuity of the pressure and normal velocity across the trailing-vortex sheet dictates that the partial $\bar{x}$ and $\bar{z}$ derivatives of $\bar{\phi}_0$ and $\bar{\phi}_1$ be continuous there.

The $\bar{\phi}_0$ is the velocity potential of a lifting line, representing the bound and trailing vortex system associated with the center line $x = x_c(y)$ [+]

$$\bar{\phi}_0 = \frac{\bar{z}}{4\pi}\int_{-1}^{1} \frac{\bar{\Gamma}_0(\bar{y}_1)}{(\bar{y}-\bar{y}_1)^2 + \bar{z}^2}\cdot\left[1 + \frac{\bar{x} - \bar{x}_c(\bar{y}_1)}{R_1}\right] d\bar{y}_1, \tag{3.4}$$

where $R_1 \equiv \left[(\bar{x}-\bar{x}_c(\bar{y}_1))^2 + (\bar{y}-\bar{y}_1)^2 + \bar{z}^2\right]^{1/2}$.

[+] The factor $\bar{z}$ in (3.4) was left out in Eq. (14) of Cheng 1978a, in Eq. (5.1) of Cheng 1978b, as well as in Eq. (12), Cheng & Meng 1979 — an unforgivable transcribing error called to our attention by Dr. T. Evans.

3.2 The lifting-line solution in the inner limit

In approaching the center line, i.e. $\bar{\xi} \equiv \bar{x} - \bar{x}_c(\bar{y}) \to 0$, $\varepsilon \to 0$, the integrand shown in (3.3) becomes nonintegrable at $\bar{y}_1 = \bar{y}$. By subtracting a suitable function, say g, from the integrand, the resultant integral may yield a limit as $\bar{\xi}$ and $\bar{z}$ vanish. This, together with the quadrature of g, then gives the behavior of $\bar{\phi}_o$ in the inner limit sought. This procedure has been used in the analysis for straight oblique wings (Cheng 1978a & b). Among the indefinite integrals in the quadrature mentioned, the following two are basic †

$$\int \frac{du}{(u-i\bar{z})R} = \frac{1}{\sqrt{\bar{c}_o}} \ln\left(\frac{\chi}{u-i\bar{z}}\right), \qquad \int \frac{du}{R} = \ln\left|R+u+\bar{b}_o\right|, \tag{3.5}$$

where $\bar{b}_o$, $\bar{c}_o$, $\sqrt{\bar{c}_o}$, R and χ are

$$\left.\begin{aligned} \bar{b}_o &\equiv -\bar{m}\bar{\xi}/(1+\bar{m}^2), \qquad \bar{c}_o \equiv (\bar{\xi}^2+\bar{z}^2)/(1+\bar{m}^2), \\ \sqrt{\bar{c}_o} &\equiv (\bar{\xi} - i\bar{m}\bar{z})/\sqrt{1+\bar{m}^2}, \end{aligned}\right\} \tag{3.6a}$$

---

† Among the typical definite integrals resulting from the quadrature are (omitting all the bars):

$$\int_{-1-y}^{1-y} z\,(u^2+z^2)^{-1}\left[1+(\xi-mu)/\sqrt{1+m^2}\,R^{-1}\right]du = \arg\chi\Big|_{-1-y}^{1-y} \sim 2\left[\tan^{-1}\left(\xi/\sqrt{1+m^2}\,z\right)+\right.$$

$$\left.+\frac{\pi}{2}\,\mathrm{sgn}\,z\right] - z\,(1+m^2)^{-1/2}\left[\left(\sqrt{1+m^2}-m\right)|1-y|^{-1}+\left(\sqrt{1+m^2}+m\right)|1+y|^{-1}\right].$$

$$\int_{-1-y}^{1-y} u^2\,(u^2+z^2)^{-1}R^{-1}\,du = \sqrt{1+m^2}\,\left(\xi^2-m^2z^2\right)^{-1}\left[\xi\ln\left(\chi/(u-iz)\right) - mz\arg\left(\chi/(u-iz)\right)\right]\Big|_{-1-y}^{1-y} \sim$$

$$\sim \ln\left|4(1+m^2)^2(1-y^2)/\left[\xi^2+(1+m^2)z^2\right]\right| - z\sqrt{1+m^2}\left(\xi^2+m^2z^2\right)^{-1}\left\{-\right.$$

$$-2mz\arg\left(e+i\sqrt{1+m^2}\,z\right) + mz\left[\tan^{-1}\left(z/(1-y)\right)+\tan^{-1}\left(z/(1+y)\right)\right] +$$

$$\left.+mz\ln\left|\left(\sqrt{1+m^2}+m\right)/\left(\sqrt{1+m^2}-m\right)\right|\right\}.$$

$$R \equiv \sqrt{u^2 + 2\bar{b}_0 u + \bar{c}_0}, \qquad \mathcal{F} \equiv P + iQ \tag{3.6b}$$

with

$$P \equiv \bar{c}_0 + \bar{b}_0 u - R.P.\sqrt{\xi_0}\cdot R, \quad Q \equiv \bar{z}(\bar{b}_0 + u) - I.P.\sqrt{\xi_0}\cdot R \tag{3.6c}$$

The equation $\bar{x} = \bar{x}_c(\bar{y})$ defines the centerline in the Prandit-Glauert variables.

To arrive at a suitable form for matching with the inner solution, the result for small $\bar{\xi} = \bar{x} - \bar{x}_c(\bar{y})$ and $\bar{z}$ is first transformed to a system of curvillinear orthogonal coordinates $(\bar{x}', \bar{y}', \bar{z}')$, with $\bar{z}' = \bar{z}$, and the curved $\bar{y}'$-axis identified with $\bar{x} = \bar{x}_c(\bar{y})$, also

$$d\bar{x}^2 + d\bar{y}^2 = d\bar{x}'^2 + \left(1 - \bar{x}'\frac{d\bar{\Lambda}}{d\bar{y}'}\right)^2 d\bar{y}'^2, \qquad \frac{d\bar{\Lambda}}{d\bar{y}'} = \frac{\bar{m}''(y)}{(1+\bar{m}^2)^{3/2}} \tag{3.7}$$

This is followed by a transformation to the inner variables $\hat{x}$, $\hat{z}$ and $\hat{y}$, , observing that[+]

$$\cos\bar{\Lambda} = \frac{B\cos\Lambda}{\sqrt{1-M_n^2}} = \sqrt{\frac{K_e}{K_n}}, \qquad \sin\bar{\Lambda} = \frac{\sin\Lambda}{\sqrt{1-M_n^2}} = \frac{\Theta}{\sqrt{K_n}} \tag{3.8a}$$

$$\tan\bar{\Lambda} = \frac{\tan\Lambda}{B}, \qquad \frac{d\bar{\Lambda}}{d\bar{y}'} = \frac{B^2}{(1-M_n^2)^{3/2}}\alpha_1^{1/3}\frac{d\Theta}{d\hat{y}} = K_0 K_n^{-3/2}\Theta'$$

and that, near the inner limit,

$$\bar{x}' = \frac{1}{\sqrt{1-M_n^2}}\frac{\hat{x}}{AR_1} - \frac{M_n^2\tan^2\Lambda}{2(1-M_n^2)^{5/2}}\frac{d\Lambda}{d\hat{y}}\frac{\hat{x}^2}{AR_1^2} + \cdots$$

$$\bar{y}' = \int_0 B^{-1}\sqrt{1-M_n^2}\,d\hat{y} + \frac{M_n^2\tan\Lambda}{B\sqrt{1-M_n^2}}\frac{\hat{x}}{AR_1} + \cdots \tag{3.8b}$$

The final result for $\bar{\phi}_0$ in the inner limit is

$$\bar{\phi}_0 \sim \frac{\bar{\Gamma}_0((\hat{y}))}{2\pi}\left[\tan^{-1}\left(\frac{\hat{x}}{\sqrt{K_n}\hat{z}}\right) + \frac{\pi}{2}\operatorname{Sgn}\hat{z}\right] + \epsilon\frac{\Theta}{\sqrt{K_n}}\left(\frac{d}{d\hat{y}} + \frac{1}{2}\frac{K_0}{K_n}\frac{\Theta'}{\Theta}\right)\frac{\bar{\Gamma}_0}{2\pi}\hat{z}\left(\ln|\hat{\zeta}| - \right.$$

$$\left. - \ln 2\right) + \epsilon\frac{\Theta^2\Theta'}{2\sqrt{K_n}}\frac{\bar{\Gamma}_0}{2\pi}\frac{\hat{z}^3}{|\hat{\zeta}|^2} + \epsilon\,\bar{V}_1^{\infty}\hat{z} + \cdots \tag{3.9a}$$

[+] Note that the linear sonic outer flow corresponds to $\sin\bar{\Lambda} \approx 1$, which also gives $\cos\bar{\Lambda} \ll 1$, $|\tan\bar{\Lambda}| \gg 1$, $|K_0| \ll 1$, as well as $d\bar{\Lambda}/d\bar{y}' \ll 1$.

where the remainder is comparable to $\epsilon|\hat{\xi}|^2$, $\bar{\Gamma}_0((\hat{y}))=\bar{\Gamma}_0(\bar{y}')=\bar{\Gamma}_0(\bar{y})$, and

$$4\pi\bar{V}_1^{\infty} \equiv -\frac{\textcircled{W}^2\textcircled{H}'}{K_n^{3/2}}\bar{\Gamma}_0(\bar{y}) - \frac{1}{2\bar{\Gamma}_0(\bar{y})}\frac{d}{d\bar{y}}\left(\sin\bar{\Lambda}\,\bar{\Gamma}_0^2\right)\left[\ln\left|\frac{K_n}{\epsilon^2}\right| + \right.$$
$$\left. + \ln\left|\frac{1-\bar{y}^2}{\cos^2\bar{\Lambda}}\right| + 2\right] + 2\bar{\Gamma}_0\frac{d\bar{\Lambda}}{d\bar{y}'} + \frac{d\bar{\Gamma}_0}{d\bar{y}}\ln\left|\frac{1-\bar{y}}{1+\bar{y}}\frac{1+\sin\bar{\Lambda}}{1-\sin\bar{\Lambda}}\right| +$$
$$+\int_{-1}^{1}\frac{\bar{\Gamma}_0'(\bar{y}_1)-\bar{\Gamma}_0'(\bar{y})}{\bar{y}_1-\bar{y}}\left[1-\sin\bar{\Lambda}\,\mathrm{Sgn}(\bar{y}_1-\bar{y})\right]d\bar{y}_1 -$$
$$-\int_{-1}^{1}\frac{1}{(\bar{y}_1-\bar{y})^2}\left\{\bar{\Gamma}_0(\bar{y}_1)\left[\frac{\bar{x}_c(\bar{y}_1)-\bar{x}_c(\bar{y})}{\sqrt{(\bar{x}_c(\bar{y}_1)-\bar{x}_c(\bar{y}))^2+(\bar{y}_1-\bar{y})^2}}-\right.\right.$$
$$\left.\left.-\sin\bar{\Lambda}\,\mathrm{Sgn}(\bar{y}_1-\bar{y})\right] - \frac{1}{2}\frac{d\bar{\Lambda}}{d\bar{y}_1}\bar{\Gamma}_0(\bar{y})\cdot|\bar{y}_1-\bar{y}|\right\}d\bar{y}_1 \qquad (3.9b)$$

noting that $d\bar{y}'/d\bar{y} = \sec\bar{\Lambda}$, $K_0 = K_n - \textcircled{W}^2$, and that we have replaced $\cos\Lambda$ (not $\cos\bar{\Lambda}$) by unity and $\bar{y}'$ by $\bar{y}$, throughout (3.9) except in the leading term (cf. § 2.3).+

The outer expansion of the inner solution ($\hat{\phi}_0 + \epsilon\hat{\phi}_1 + \cdots$), according to (2.28) and (2.29), share a domain of validity with the inner expansion of the outer solution ($\bar{\phi}_0 + \cdots$) in $1 \ll |\hat{\xi}| \ll \epsilon^{-1}$ where matching is achieved after identifying

$$\left.\begin{aligned}\bar{\Gamma}_0(\bar{y}) \equiv \bar{\Gamma}_0((\hat{y})) &= \cos\Lambda\;\hat{\Gamma}_0(\hat{y}); \quad \hat{C}_0^{r}(\hat{y}) = 0,\\ \hat{C}_1^{i}(\hat{y}) &= -(K_n)^{-1/2}\left[\bar{V}_1^{\infty} - (8\pi\bar{\Gamma}_0)^{-1}\ln 4\,\frac{d}{d\bar{y}}\left(\sin\bar{\Lambda}\,\bar{\Gamma}_0^2\right)\right].\end{aligned}\right\} \qquad (3.10)$$

The induced upwash and, hence, the inner solution is completely determined. Terms in $(\hat{\phi}_0+\epsilon\hat{\phi}_1)$ not matched at this stage are those from the inner solutions belonging to order

$$|\hat{\xi}|^{-1}|\ln\hat{\xi}|, \quad |\hat{\xi}|^{-2}, \quad \epsilon|\ln\hat{\xi}|^2, \quad \epsilon|\ln\hat{\xi}|, \quad \epsilon. \qquad (3.11)$$

These should find their counterparts in $\bar{\phi}_1$ which includes the nonlinear corrections to the outer solution.

+ For straight oblique wings, $\bar{V}_1^{\infty}$ is precisely the $\bar{\Sigma}$ in Cheng and Meng (1979).

The upwash function V_1^∞ is dominated by

$$-\frac{1}{8\pi\bar{\Gamma}_0}\cdot\frac{d}{d\bar{y}}\left(\sin\bar{\Lambda}\,\bar{\Gamma}_0^2\right)\ln\left|\frac{K_0}{\epsilon^2}\right| = \frac{1}{4\pi}\left[\sin\bar{\Lambda}\,\frac{d\bar{\Gamma}_0}{d\bar{y}} + \frac{1}{2}\cos\bar{\Lambda}\,\frac{d\bar{\Lambda}}{d\bar{y}}\bar{\Gamma}_0\right]\ln\left|\frac{K_0}{\epsilon^2}\right|, \tag{3.12}$$

the part proportioned to $d\bar{\Gamma}_0/d\bar{y}$ represents the important influence of the near wake, the part proportioned to $\bar{\Gamma}_0$ represents the downwash induced by the bound vorticities. Those together with other competing contributions, lead generally to a maximum induced upwash near the wing tip on the aft wing panel of an oblique wing, and a maximum induced downwash near the tip on a swept-forward panel, as noted earlier by Cheng (1978b, p.17).+

In the very special limit corresponding to an upyawed straight wing ($\textcircled{M}\to 0$), the upwash correction determined from (3.9) and (3.10) agrees with the linear subsonic results of Jones & Cohen (1957). Interestingly, for a symmetric swept wing, i.e. $\bar{x}_c(\bar{y}) = \bar{m}|\bar{y}|$, the last integral of $\bar{V}_1^\infty$ diverges in approaching the wing apex like

$$\bar{V}_1^\infty \sim -\bar{\Gamma}_0(0)\,\frac{\sin\bar{\Lambda}}{4\pi\,\bar{y}}\ . \tag{3.13a}$$

This agrees with the downwash induced by the bound vortices on the opposite wing panel computed according to the Biot-Savart law. It exhibits clearly the extent of nonuniformity at the apex

$$\bar{y} = O\left(\textcircled{M}\,K_n^{-1/3}\,\epsilon\right). \tag{3.13b}$$

The remainders in the matching listed in (3.11) contains contributions from the source terms as well as nonlinear corrections, which are of theoretical interest. To ascertain more clearly their influence on the outer flow, we shall investigate in the following the correction to the lifting-line solution $\bar{\Phi}_1$, and examine its matching with the inner solution. To avoid tedious details, only the case with a straight center line will be considered.

+ Same can be said of the upwash field near the tip of a symmetric swept wing. With a suitably chosen distribution of the center-line curvature $d\bar{\Lambda}/d\bar{y}'$, such an upwash effect can be mitigated (Cheng 1976).

3.3 Higher-order outer solution and matching

The second PDE of (3.3) governing $\bar{\Phi}_1$ is a 3-D Poisson equation. In the curvilinear coordinates ($\bar{x}'$, $\bar{y}'$ and $\bar{z}'$) of (3.7), this equation becomes (with $\bar{h}_2 = 1 - \bar{x}'\, d\bar{\Lambda}/d\bar{y}'$)

$$\left(\frac{\partial^2}{\partial \bar{x}'^2} + \frac{\partial^2}{\partial \bar{z}'^2} + \frac{\partial^2}{\partial \bar{y}'^2}\right)\bar{\Phi}_1 - \frac{1}{\bar{h}_2}\frac{d\bar{\Lambda}}{d\bar{y}'}\frac{\partial}{\partial \bar{x}'}\bar{\Phi}_1 = \frac{(\gamma+1)}{2K_0^{3/2}}\frac{\partial}{\partial \bar{x}}\left(\frac{\partial \bar{\Phi}_0}{\partial \bar{x}}\right)^2 . \tag{3.14}$$

We shall confine the analysis to the case $\bar{M}' \equiv 0$ (the swept wings with a straight center line) for which the term with $d\bar{\Lambda}/d\bar{y}'$ on the LHS (3.14) is absent. Writing

$$\zeta' \equiv \bar{x}' + i\bar{z}', \qquad \zeta'_* \equiv \bar{x}' - i\bar{z}' \tag{3.15}$$

(3.9) gives, for small $|\zeta'|$,

$$\frac{\partial}{\partial x}\bar{\Phi}_0 \sim \left(\cos\bar{\Lambda}\frac{\partial}{\partial \bar{x}'} + \sin\bar{\Lambda}\frac{\partial}{\partial \bar{y}'}\right)\bar{\Phi}_0 \sim \frac{1}{2}\cos\bar{\Lambda}\,\frac{i\bar{\Gamma}_0}{2\pi}\left(\frac{1}{\zeta'} - \frac{1}{\zeta'_*}\right) + \cdots$$

with the remainder $(\cdots)$ vanishing as $|\zeta'| \to \infty$. Thus (3.14) may take the form for small $|\zeta'|$ as

$$\frac{\partial^2}{\partial\zeta'\partial\zeta'_*}\bar{\Phi}_1 \sim \frac{\gamma+1}{2K_0^{3/2}}\left[\frac{1}{8}\cos^3\bar{\Lambda}\left(\frac{\bar{\Gamma}_0}{2\pi}\right)^2\left(\frac{1}{\zeta'^3} + \frac{1}{\zeta'^3_*} - \frac{1}{\zeta'^2\zeta'_*} - \frac{1}{\zeta'\zeta'^2_*}\right) - \right.$$
$$\left. - \frac{1}{32}\sin\bar{\Lambda}\cos^2\bar{\Lambda}\,\pi^{-2}\bar{\Gamma}_0\, d\bar{\Gamma}_0/d\bar{y}'\left(\frac{1}{\zeta'^2} + \frac{1}{\zeta'^2_*} - \frac{2}{\zeta'\zeta'_*}\right)\right] + \cdots \tag{3.16}$$

where the remainder $(\cdots)$ includes contribution from $\partial^2\bar{\Phi}_1/\partial\bar{y}'^2$. Integrating with respect to ζ' and ζ'_*, (3.16) yields the asymptotic behavior of the particular solution for $\bar{\Phi}_1$ as $|\zeta'| \to 0$. Adding the homogeneous part, the solution $\bar{\Phi}_1$ in the inner limit, which will permit matching with the inner solution, is

$$\bar{\Phi}_1 \sim \frac{\gamma+1}{K_0^{3/2}}\,\frac{\cos^3\bar{\Lambda}}{16}\left(\frac{\bar{\Gamma}_0}{2\pi}\right)^2\left[\frac{\bar{x}'}{|\zeta'|^2}\ln|\zeta'| + \frac{\bar{x}'\bar{z}'^2}{|\zeta'|^4}\right] +$$
$$+ \frac{\gamma+1}{K_0^{5/2}}\,\frac{\sin\bar{\Lambda}\cos^2\bar{\Lambda}}{16\pi^2}\,\bar{\Gamma}_0\frac{d\bar{\Gamma}_0}{d\bar{y}'}\left[(\ln|\zeta'|)^2 - \frac{\bar{z}'^2}{|\zeta'|^2}\right] +$$
$$+ \text{R.P.}\left(\frac{\bar{D}_1}{\zeta'}\right) + \frac{\bar{Q}_1}{2\pi}\ln|\zeta'| + \frac{\bar{\Gamma}_1}{2\pi}(\pi - \arg.\zeta') + \bar{F}_1(y') \tag{3.17}$$

This can be expressed in terms of the inner variables $\hat{x}$, $\hat{z}$, and $\hat{y}$,

cf. (3.8b), to yield finally

$$\epsilon\Phi_1 \sim \frac{1+1}{4K_n}\left(\frac{\bar\Gamma_0(\hat y)}{2\pi}\right)^2\left[\ln\left|\frac{\epsilon}{\sqrt{K_n}}\hat\zeta\right| + \frac{K_n\hat z^2}{|\hat\zeta|^2}\right]\frac{\hat x}{|\hat\zeta|^2} + \frac{\hat x\sqrt{K_n}\,\bar D_1^r + \sqrt{K_n}\,\hat z\sqrt{K_n}\,\bar D_1^i}{|\hat\zeta|^2} +$$

$$+ \frac{\epsilon\textcircled{M}}{K_n}\left[\hat x\frac{d}{d\hat y}\left(\sqrt{K_n}\,\bar D_1^r\right) + \sqrt{K_n}\,\hat z\frac{d}{d\hat y}\left(\sqrt{K_n}\,\bar D_1^i\right)\right]\frac{\hat x}{|\hat\zeta|^2} +$$

$$+ \frac{\epsilon\textcircled{M}}{8K_n^2}\frac{\bar\Gamma_0}{\pi^2}\frac{d\bar\Gamma_0}{d\hat y}\left[\ln\left|\frac{\epsilon}{\sqrt{K_n}}\hat\zeta\right| + \frac{K_n\hat z^2}{|\hat\zeta|^2}\right]\frac{\hat x^2}{|\hat\zeta|^2} +$$

$$+ \frac{\epsilon\textcircled{M}(1+1)}{16K_n^2}\frac{\bar\Gamma_0}{\pi^2}\frac{d\bar\Gamma_0}{d\hat y}\left[(\ln|\hat\zeta|)^2 + 2\ln\left(\frac{\epsilon}{\sqrt{K_n}}\right)\ln|\hat\zeta| + \frac{\hat x^2}{|\hat\zeta|^2}\right] +$$

$$+ \frac{\bar Q_1}{2\pi}\ln\left|\frac{\epsilon}{\sqrt{K_n}}\hat\zeta\right| + \frac{\bar\Gamma_1}{2\pi}(\pi - \arg\hat\zeta) + F_1(\hat y), \tag{3.18}$$

where the first two terms proportional to $\epsilon\textcircled{M}$ results from expansions of the coordinates $\bar x'$ and $\bar y'$, cf. (3.8b).

Adding the result of (3.18) to (3.9) gives $(\bar\Phi_0 + \epsilon\bar\Phi_1)$ in the inner limit. Comparing this with $(\hat\Phi_0 + \epsilon\hat\Phi_1)$ from (2.28) and (2.29), indicates that, except for $F_1(\hat y)$ which does not affect the pressure and the $\hat\Phi_{\hat x}$ and $\hat\Phi_{\hat z}$, the outer expansion of $\bar\Phi$ and the inner expansion of $\cos\Lambda\,\hat\Phi$ do match, including <u>all</u> terms exhibited in (2.28), (2.29), (3.9) and (3.18), after determining $\bar\Gamma_0$, $\hat C_1^r$ and $\hat C_1^i$ according to (3.10) and choosing the doublet, source and the vortex strengths

$$\bar D_1^i(\bar y) \equiv \bar D_1^i(\bar y') = (K_n)^{-1/2}\hat D_0^i(\hat y),$$

$$\bar D_1^r(\bar y) \equiv \bar D_1^r(\bar y') = (K_n)^{-1/2}\hat D_0^r(\hat y) + (1+1)2^{-5}K_n^{-3/2}\pi^{-2}\bar\Gamma_0^2\ln\left|\frac{K_n}{\epsilon^2}\right|,$$

$$\bar Q_1(\bar y) \equiv \bar Q_1(\bar y') = \hat Q_1(\hat y) + (1+1)8^{-1}K_n^{-2}\pi^{-1}\hat\Pi_0\,d\hat\Pi/d\hat y\left[\ln\left|\frac{K_n}{\epsilon^2}\right| - 1\right],$$

$$\bar\Gamma_1(\bar y) \equiv \bar\Gamma_0(\bar y') = \hat\Pi_1(\hat y). \tag{3.19}$$

Except in the relation $\bar\Gamma_0(\bar y) = \cos\Lambda\,\hat\Pi_0(\hat y)$, $\bar y$ and $\hat y$ in above, as well as in (3.10), are interchangeable without altering the order of the error (even for $\textcircled{M} = O(\epsilon^{-1/2})$, cf. §2.3). Apart from the line doublet associated

with the lift in Van Dyke's (1964) "third-order theory", the corresponding solution in the present theory has a line source and a line doublet associated with the local $\bar{x}'$-direction. In addition to the $\hat{Q}_1$ and $\hat{D}_1^r$ determined from the inner solution, there is a dominant part in $\bar{Q}_1$ and $\bar{D}_1^r$ contributed by the nonlinear lift effect proportional to $\hat{\pi}^2 \ln|K_n/\epsilon^4|$.

4. STRAIGHT OBLIQUE WINGS

For applications to the type of oblique wings considered by Jones (1971 , 1977), the center line can be assumed to be straight, i.e. $\textcircled{M}' \equiv 0$, or $|\textcircled{M}'| \ll 1$, and PDE (2.6) reduces to

$$\frac{\partial}{\partial \hat{x}}\left[K_* \hat{\phi}_{\hat{x}} - \frac{\gamma+1}{2}\hat{\phi}_{\hat{x}}^2\right] + \hat{\phi}_{\hat{z}\hat{z}} = 2\epsilon \textcircled{M} \hat{\phi}_{\hat{x}\hat{y}} + \cdots \qquad (4.1)$$

subject to errors of $O(\epsilon^2)$. If the variable $\hat{y}$ is taken as a normalized time variable, (4.1) can be interpreted as one governing a 2-D transonic small-disturbance flow near the quasi-steady limit, in which the RHS represents an unsteady correction. The perturbed solution $\hat{\phi}_0 + \epsilon\hat{\phi}_1 + \cdots$ under $\textcircled{M}' \equiv 0$ also admits a local-similarity in $\hat{\phi}_0$ and in $\hat{\phi}_1$, applicable to a rather useful class of wing geometry; the reduced problems in this case can be solved once for all span stations. These will be discussed in §§ 4.1 and 4.2 below.

4.1 An unsteady analogy with a 2-D transonic flow

To bring out more precisely the nature of the analogy in question, we introduce

$$\varphi \equiv \hat{\phi} + \epsilon\sqrt{K_*}\,\hat{C}_1'\,\hat{z} \;, \qquad \hat{t} \equiv \hat{y}/\epsilon\textcircled{M}. \qquad (4.2)$$

PDE (4.1) takes the form

$$\frac{\partial}{\partial \hat{x}}\left[K_* \varphi_{\hat{x}} - \frac{\gamma+1}{2}\varphi_{\hat{x}}^2\right] + \varphi_{\hat{z}\hat{z}} = 2\varphi_{\hat{x}\hat{t}} \;, \qquad (4.3)$$

familiar in most nonlinear analysis of unsteady transonic flows (Landahl 1962, Oswatitsch 1962, Timman 1962). The equations for the characteristics and the shock relations, (2.11) and (2.14), also go over correctly, upon substituting (4.2), to the unsteady transonic system in question, and the continuity requirements on $\hat{\phi}_{\hat{x}}$ and $\hat{\phi}_{\hat{z}}$, (2.10), remain unchanged. The wing boundary condition (2.9) becomes

$$\left(\frac{\partial\varphi}{\partial\hat{z}}\right)_w \equiv \frac{\partial}{\partial\hat{x}}\hat{Z}^* + \frac{\partial}{\partial\hat{t}}\hat{Z}_0 + \epsilon\left(\hat{I} + \sqrt{K_*}\,\hat{C}_1'\right). \qquad (4.4)$$

The far-field description for $\varphi = \hat{\phi}_0 + \epsilon\hat{\phi}_1 + \epsilon\sqrt{K_*}\hat{C}_1'\hat{z}$ based on the expressions for $\hat{\phi}_0$ and $\hat{\phi}_1$ of (2.28) and (2.29), with $\partial/\partial\hat{t}$ replacing $\epsilon\textcircled{M}\partial/\partial\hat{y}$ and $\textcircled{M}' \equiv 0$ is precisely that describing the solution to (4.3) at large $|\hat{\zeta}|$ near the quasi-steady limit. One must note that the induced-upwash term $\epsilon\sqrt{K_*}\hat{C}_1'\hat{z}$ in φ ,

(4.2), cancels out the corresponding term in $\epsilon\hat{\phi}_1$ from (2.29), and therefore, the resultant far-field description for φ is independent of the influence of the wake vorticity. Hence, our inner airfoil problem is mathematically equivalent to that of a (special) unsteady transonic airfoil pertaining to the nonlinear (lower-frequency) domain governed by PDE (4.3) near the quasi-steady limit, with a wing-surface condition (4.4), and time-dependent locations of the leading and trailing edges. The wake influence of the oblique-wing, as well as the wing bend and wing twist, thus, appear as additional incidence corrections in the equivalent unsteady problem.

The foregoing examination indicates that the solution to the oblique-wing problem can be generated from an unsteady 2-D calculation based on (4.3) for which existing numerical procedures, e.g. those using alternating direction implicit algorithms similar to Ballhaus & Goorjiian (1977), can be quite readily adopted. The crucial input to such an application lies, of course, in the incidence correction, and, to fully utilize the (available) computer storage and time for this purpose, the description for φ based on (2.28) and (2.29) should be used at the far boundary. (The values of $\hat{\Gamma}_0$, $\hat{D}_0^i$ and $\hat{D}_0^r$ in (2.29) can be taken from those determined from the previous time step.)

The approach via this unsteady analogy promises an alternative solution procedure without the requirement for the local similarity (cf. (4.5) below), as well as providing a method for capturing shock waves on oblique wings without the difficulty associated with the reexpansion singularity discussed earlier (§ 2.6).[+] Sample calculations via the unsteady analogy and their comparison with the perturbation solutions are given at the end of § 5 for a subcritical case. From the viewpoint of unsteady transonic-flow analysis, it is of interest to point out that putting $D = \epsilon\mathcal{M}^2\partial/\partial\hat{y} = \partial/\partial\hat{t}$ in (2.35),

[+] With the inclusion of $\epsilon\mathcal{M}'\varphi_{\hat{x}}$ on the RHS of (4.3), the unsteady analogy can be used as a procedure for solving PDE (2.6) with a nonvanishing center-line curvature.

the treatment of the nonuniformity at the shock root presented in § 2.6 applies equally well to the corresponding problem arising from the unsteady perturbation considered by Ehler (1974), Traci, Albano & Farr (1976), Hafez, Rizk & Murman (1977), Ballhaus & Goorjian (1978), Fung, Yu & Seebass (1978), also Nixon (1978).+

4.2 Local similarities

Owing to the linearity, the 3-D correction to $\hat{\phi}$, $\epsilon\hat{\phi}_1$, can be decomposed into suitably scaled separate parts. For a certain class of oblique-wing geometry, these separate parts have similarity solutions independent of $\hat{y}$, as does the basic solution $\hat{\phi}_0$. This wing class requires, in addition to $\textcircled{M}' \equiv 0$, or a small $\textcircled{M}'$, that the basic wing section at each span station be generated from a single airfoil shape of the same thickness at a fixed incidence. More specifically, it requires a form of wing coordinates

$$z' = \frac{c_0}{2}\hat{C}(\hat{y})\left[\alpha\tilde{Z}^{\frac{1}{2}}\left(\frac{\hat{x}}{\hat{c}}\right) + \alpha^{1/3}\hat{Z}_0(\hat{y}) + \alpha\epsilon\frac{\hat{x}}{\hat{c}}\cdot\hat{I}(\hat{y})\right] \qquad (4.5)$$

where $\hat{C}(\hat{y})$ is the ratio of the local wing chord $C(\hat{y})$ to the root chord c_0. Implicit is that $\hat{x}=0$ is a straight axis on the wing; the planform, as well as the functions $\hat{Z}_0(\hat{y})$ and $I(\hat{y})$, are otherwise quite arbitrary.

For this case, we introduce the variables (with $b' = \sec\Lambda\, b$)

$$\tilde{x} \equiv \hat{x}/\hat{c} = 2x/C(\hat{y}), \quad \tilde{z} \equiv \hat{z}/\hat{c} = 2\alpha^{1/3}z/C(\hat{y}), \quad \tilde{y} \cos\Lambda\, \hat{y} = y'/b', \qquad (4.6)$$

and assume

$$\hat{\phi}/\hat{c} = \tilde{\phi}_0 + \epsilon\textcircled{M}\hat{c}'\tilde{\phi}_1 + \epsilon\left[\sqrt{K_n}\,\hat{C}_1^{1/2}(\hat{y}) + \hat{I}(\hat{y}) + \textcircled{M}\hat{Z}_0'(\hat{y})\right]\tilde{\phi}_2 - \epsilon\sqrt{K_n}\,\hat{C}_0^{1/2}\tilde{z} + \cdots \qquad (4.7)$$

where $\tilde{\phi}_0$, $\tilde{\phi}_1$, and $\tilde{\phi}_2$ are independent of $\tilde{y}$, and $\hat{c}' \equiv d\hat{c}/d\hat{y}$. The separation into $\tilde{\phi}_1$ and $\tilde{\phi}_2$ allows the induced-upwash effect to be treated independently of the spanwise-compressibility correction. The PDE (2.20) and (2.22)

+ In the last two works cited, the reexpansion singularity and the resulting anomaly does not appear, its absence is presumably a consequence of the assumption of a plane, normal shock stipulated therein.

become in this case

$$\frac{\partial}{\partial \tilde{x}}\left[K_n \tilde{\Phi}_{0\tilde{x}} - \frac{\gamma+1}{2}\left(\tilde{\Phi}_{0\tilde{x}}\right)^2\right] + \frac{\partial^2}{\partial \tilde{z}^2}\tilde{\Phi}_0 = 0, \tag{4.8a}$$

$$\left\{\left[K_n - (\gamma+1)\tilde{\Phi}_{0\tilde{x}}\right]\frac{\partial^2}{\partial \tilde{x}^2} + \frac{\partial^2}{\partial \tilde{z}^2} - (\gamma+1)\tilde{\Phi}_{0\tilde{x}\tilde{x}}\frac{\partial}{\partial \tilde{x}}\right\}\tilde{\Phi}_1 = -$$

$$-2\left(\tilde{x}\frac{\partial}{\partial \tilde{x}} + \tilde{z}\frac{\partial}{\partial \tilde{z}}\right)\tilde{\Phi}_{0\tilde{x}}, \tag{4.8b}$$

$$\left\{\left[K_n - (\gamma+1)\tilde{\Phi}_{0\tilde{x}}\right]\frac{\partial^2}{\partial \tilde{x}^2} + \frac{\partial^2}{\partial \tilde{z}^2} - (\gamma+1)\tilde{\Phi}_{0\tilde{x}\tilde{x}}\frac{\partial}{\partial \tilde{x}}\right\}\tilde{\Phi}_2 = 0. \tag{4.8c}$$

The right-hand member of (4.8b) arises from $\partial/\partial\hat{y} = \partial/\partial\tilde{y} - (\hat{c}'/\hat{c})(\tilde{x}\,\partial/\partial\tilde{x} + \tilde{z}\,\partial/\partial\tilde{z})$.
The conditions on wing surfaces and the wake, (2.21) and (2.23), give

$$\left(\frac{\partial}{\partial \tilde{z}}\tilde{\Phi}_0\right)_{\sim} = \frac{\partial}{\partial \tilde{x}}\tilde{Z}^{\pm}, \quad \left(\frac{\partial}{\partial \tilde{z}}\tilde{\Phi}_1\right)_{\sim} = 0, \quad \left(\frac{\partial}{\partial \tilde{z}}\tilde{\Phi}_2\right)_{\sim} = 1; \tag{4.9a,b,c}$$

and

$$[\![\tilde{\Phi}_{0\tilde{x}}]\!]_{TV} = [\![\tilde{\Phi}_{0\tilde{z}}]\!]_{TV} = 0, \quad [\![\tilde{\Phi}_{1\tilde{x}}]\!]_{TV} = [\![\tilde{\Phi}_{1\tilde{z}}]\!]_{TV} = 0, \quad [\![\tilde{\Phi}_{2\tilde{x}}]\!]_{TV} = [\![\tilde{\Phi}_{2\tilde{z}}]\!]_{TV} = 0. \tag{4.10a,b,c}$$

Consistent with the similarity structure of $\hat{\phi}/\hat{c}$, (4.7), the equation of the shock boundary (2.25) takes the form

$$\hat{x}/\hat{c} = \hat{x}_0^D(\tilde{z}) + \epsilon \circledast \hat{c}'(\hat{y})\hat{x}_1^D(\tilde{z}) + \epsilon\left[\sqrt{K_n}\,\hat{C}_1^{\pm}(\hat{y}) + \hat{I}(\hat{y}) + \circledast \hat{Z}_B'\right]\hat{x}_2^D(\tilde{z}). \tag{4.11}$$

The Rankine-Hugoniot relations transferred to the unperturbed shock boundary, i.e. (2.26) and (2.27), now read as at $\tilde{x} = \tilde{x}_0^D(\tilde{z})$.[+]

$$K_n - (\gamma+1)\left\langle \tilde{\Phi}_{0\tilde{x}} \right\rangle = -\left(\partial\tilde{x}_0^D/\partial\tilde{z}\right)^2, \tag{4.12a}$$

$$2\tilde{x}_0^D - (\gamma+1)\left\langle \tilde{\Phi}_{1\tilde{x}} + \tilde{x}_1^D\,\tilde{\Phi}_{0\tilde{x}\tilde{x}} \right\rangle = -2\left(\partial\tilde{x}_0^D/\partial\tilde{z}\right)\left(\partial\tilde{x}_1^D/\partial\tilde{z}\right), \tag{4.12b}$$

$$-(\gamma+1)\left\langle \tilde{\Phi}_{2\tilde{x}} + \tilde{x}_2^D\,\tilde{\Phi}_{0\tilde{x}\tilde{x}} \right\rangle = -2\left(\partial\tilde{x}_0^D/\partial\tilde{z}\right)\left(\partial\tilde{x}_2^D/\partial\tilde{z}\right), \tag{4.12c}$$

[+] These jump conditions for $\tilde{\Phi}_1$ and $\tilde{\Phi}_2$ are not the same as those for the (formal) weak solutions of PHE (4.8b) and (4.8c).

and

$$[\![\, \tilde{\Phi}_0 \,]\!] = [\![\, \tilde{\Phi}_1 + \tilde{x}_1^D \tilde{\Phi}_{0\tilde{x}} \,]\!] = [\![\, \tilde{\Phi}_2 + \tilde{x}_2^D \tilde{\Phi}_{0\tilde{x}} \,]\!] = 0 \,. \qquad (4.13a,b,c)$$

Approaching the outer limit, $|\tilde{\xi}| = |\hat{\xi}/\hat{\epsilon}| \to \infty$, PDE (4.8a,b) admits the developments

$$\tilde{\Phi}_0 \sim \frac{\tilde{\Pi}_0}{2\pi}\left[\tan^{-1}\left(\frac{\tilde{x}}{\sqrt{K_n}\,\tilde{z}}\right) + \frac{\pi}{2}\,\mathrm{Sgn}\,\tilde{z}\right] + (\tilde{D}_0^r \tilde{x} + \tilde{D}_0^i \sqrt{K_n}\,\tilde{z})/|\tilde{\xi}|^2 +$$

$$+ \frac{1+1}{4K_n}\left(\frac{\tilde{\Pi}_0}{2\pi}\right)^2 \left[\ln|\tilde{\xi}| + K_n \tilde{z}^2/|\tilde{\xi}|^2\right] \tilde{x}/|\tilde{\xi}|^2 + \cdots \qquad (4.14a)$$

$$\tilde{\Phi}_1 \sim \frac{\tilde{x}}{\sqrt{K_n}} \frac{\tilde{\Pi}_0}{2\pi} \ln|\tilde{\xi}| + \frac{1+1}{32 K_n^2}\left(\frac{\tilde{\Pi}_0}{\pi}\right)^2 \left\{ 2(\ln|\tilde{\xi}|)^2 + 2\,\frac{\tilde{x}^2 - K_n \tilde{z}^2}{|\tilde{\xi}|^2} \ln|\tilde{\xi}| - \right.$$

$$\left. - \frac{1}{2}\left[(\tilde{x}^2 - K_n \tilde{z}^2)^2 - 4 K_n \tilde{z}^2 \tilde{x}^2\right]/|\tilde{\xi}|^4 \right\} +$$

$$+ \frac{\tilde{Q}_1}{2\pi} \ln|\tilde{\xi}| + \frac{\tilde{\Pi}_1}{2\pi}\left[\tan^{-1}\left(\frac{\tilde{x}}{\sqrt{K_n}\,\tilde{z}}\right) + \frac{\pi}{2}\,\mathrm{Sgn}\,\tilde{z}\right] +$$

$$+ \frac{2}{\sqrt{K_n}}\left(\tilde{D}_0^i \tilde{x} - \tilde{D}_0^r \sqrt{K_n}\,\tilde{z}\right) \tilde{z}/|\tilde{\xi}|^2 + \cdots \qquad (4.14b)$$

$$\tilde{\Phi}_2 \sim \frac{\tilde{\Pi}_2}{2\pi}\left[\tan^{-1}\left(\frac{\tilde{x}}{\sqrt{K_n}\,\tilde{z}}\right) + \frac{\pi}{2}\,\mathrm{Sgn}\,\tilde{z}\right] +$$

$$+ (1+1)\,8^{-1}\pi^{-2} K_n^{-2}\, \tilde{\Pi}_0 \tilde{\Pi}_2 \left[\ln|\tilde{\xi}| + K_n \tilde{z}^2/|\tilde{\xi}|^2\right] \tilde{x}/|\tilde{\xi}|^2 +$$

$$+ \left(\tilde{D}_2^r \tilde{x} + \tilde{D}_2^i \tilde{z}\right)/|\tilde{\xi}|^2 + \cdots \qquad (4.14c)$$

These results are recoverable (completely) from the far-field expansion for $\hat{\Phi} = \hat{\Phi}_0 + \epsilon\,\hat{\Phi}_1 + \cdots$ in the more general case, (2.28) and (2.29), through transformations (4.6) and (4.7) and the relations for the coefficients

$$\tilde{\Pi}_0 = \hat{\Pi}_0/\hat{c}\,, \quad \tilde{D}_0^i = \hat{D}_0^i/\hat{c}^2\,, \quad \tilde{D}_0^r = \hat{D}_0^r + \frac{1+1}{16 K_n}\left(\frac{\hat{\Pi}_0}{\pi \hat{c}}\right)^2 \ln \hat{c}\,; \qquad (4.15)$$

$$\tilde{C}_1^i = \hat{C}_1^i - \frac{\Theta}{2K_n}\left(\frac{\hat{\Pi}_0}{\pi \hat{c}}\right) \hat{c}' \ln \hat{c}\,, \qquad (4.16a)$$

$$\tilde{Q}_1 = \frac{\hat{Q}_1}{\Theta \hat{c}\,\hat{c}'} + \frac{1+1}{4\pi K_n^2}\left(\frac{\hat{\Pi}_0}{\hat{c}}\right)^2 \ln \hat{c}\,, \qquad (4.16b)$$

$$\tilde{\Pi}_1 = \Theta \hat{c}\,\hat{c}'\,\tilde{\Pi}_1 + \left[\sqrt{K_n}\,\tilde{C}_1^i + \hat{I} + \Theta \hat{Z}_B'\right] \tilde{\Pi}_2 \,. \qquad (4.16c)$$

We note that, according to the last of (4.15),

$$\frac{1}{2\hat{\epsilon}\hat{\epsilon}'}\frac{d}{d\hat{y}}\hat{D}_0^r = \hat{D}_0^r - \frac{\gamma+1}{16K_n}\left(\frac{\hat{\Pi}_0^r}{\pi}\right)^2\left(\ln\hat{c}+\frac{1}{2}\right).$$

The $\frac{1}{2}$ in $\left(\ln\hat{c}+\frac{1}{2}\right)$ above explains the formal difference of $\left(\ln|\hat{\xi}|+\frac{1}{2}\right)$ in (2.30) and $\ln|\hat{\xi}|$ in the second term inside the curly bracket in (4.14b).

The source strength $\tilde{Q}_1$ can be explicitly evaluated in terms of $\tilde{D}_0^r$ and $\tilde{\Pi}_0^2$ in this case with the help of the Green theorem, unaffected by the presence of imbedded shocks (Appendix III),

$$\tilde{Q}_1 = \frac{4\pi}{K_n}\tilde{D}_0^r + \frac{\gamma+1}{8\pi K_n^2}\left(\tilde{\Pi}_0^r\right)^2\cdot\left[3+\hat{a}+(\hat{a}+\hat{b})^2\right], \qquad (4.17)$$

where $\tilde{a}=\hat{a}/\epsilon$ and $\tilde{b}=\hat{b}/\epsilon = 2+\tilde{a}$ are the leading and trailing-edge locations in $\tilde{x}$, respectively.

With $\tilde{C}_1^i$ known, ways to control the induced upwash by wing twist and wing bend through (4.7) are evident. From the form of solution (4.7), the similitude of the 3-D flow structure is also apparent. In flow regions removed from shocks, the local pressure coefficient $C_p' \equiv 2(p-p_\infty)/\rho_\infty U_n^2$ can be correlated as

$$\left(C_p' - C_{p_{2\text{-}D}}''\right)/\epsilon^{(4)} = f\left(\frac{x'}{c}, \alpha^{1/3}\frac{y'}{c}; K_n\right), \qquad (4.18a)$$

independent of $\hat{y}$, where $C_{p_{2\text{-}D}}''$ is the local value of C_p' computed according to the 2-D theory after an incidence correction

$$\Delta\alpha_i = \alpha_1\epsilon\sqrt{K_n}\,\tilde{C}_1^i. \qquad (4.18b)$$

The 3-D effects on the field near the shock and the shock boundary itself may also be correlated through (4.11) - (4.13), excluding the vicinity of the shock root. In the latter, the pressure field should be correlated in the original form of the Oswatitsch & Zierep (1960), shown in (2.39).

5. COMPUTATION METHODS AND EXAMPLE: STRAIGHT OBLIQUE WINGS

5.1 Remarks on examples and comparison

Demonstration of solutions to the reduced problems of the theory is an essential part of the present study. This is so, not only because it affords an opportunity for assessing the adequacy of the present approach as an aerodynamic-analysis method, but because the existence and uniqueness of the solutions to the reduced problems have not been thoroughly investigated. This demonstration is given below for the class of straight oblique wings, for which similarity solutions exist , thus the sweep and other 3-D effects can be more clearly delineated with the least geometrical complexity. In the following, the computation procedure is described (§ 5.2), shock-free examples (including two with slightly supercritical component flows) are presented (§ 5.3). Comparisons with corresponding solutions from 3-D, full potential computer programs (the Jameson FLO 22) will be discussed in § 5.4. A comparison with solutions obtained via the unsteady analogy is also shown in § 5.5. Numerical solutions involving imbedded shocks, which require treatment of the logarithmic singularity at the shock root, are the subject of a separate paper.

The present theory is limited by the assumptions of a high aspect ratio and of the small disturbance; it is uncertain without a demonstration that the solutions may adequately predict the (inviscid) aerodynamic characteristics to a degree enjoyed by the classical lifting-line theory. In addition, the possibility of committing algebraic errors is not low. This, together with the two limitations mentioned, makes direct comparison with more exact (3-D full potential) solutions essential.

The limitation on the computer storage available to the current 3-D flow-field computation programs is well known. With this limitation, it is not clear whether the grid distributions in these programs are sufficiently refined for the purpose of describing the induced up-wash of the trailing vorticities of the far wake, so crucial to a high aspect-ratio wing. This uncertainty is erased, however, by the consistently good

comparisons shown below.+

5.2 Computation procedures

Line-relaxation methods are used to solve the algebraic systems of the difference equations for the similarity solutions $\tilde{\phi}_0$, $\tilde{\phi}_1$, and $\tilde{\phi}_2$; the methods employ Murman's type-sensitive difference operators, including a shock-point operator (Murman & Cole 1971, Murman 1974). The basic computer code for $\tilde{\phi}_0$ is adopted from one used earilier in Hafez & Cheng's (1977a & b) studies, improved in the far-field description with (4.14a) and in the use of a higher-order convergence acceleration scheme (Meng & Cheng 1977). The doublet strength $\tilde{D}_0^r$ and $\tilde{D}_0^i$ in (4.14a) are determined by a least-square fit of data near and at the far boundary. The inclusion of the doublets and the nonlinear terms shown in (4.14a) have improved substantially the accuracy and internal consistency of the numerical solutions at the far boundary; this results in a two to five percent (2-5%) change in the surface pressure. The basic program will also furnish input data for the relaxation solutions involving shock-fitting algorithms (Hafez & Cheng 1977b), the latter is not needed, however, in the shock-free examples considered below.

The procedures for $\tilde{\phi}_1$ and $\tilde{\phi}_2$ solving the linear PDE's, with conditions on the x-axis and the far-field description, (4.8)-(4.16), are similar to that for $\tilde{\phi}_0$. The programs are simpler in that the transition boundary is fixed to the sonic boundary of $\tilde{\phi}_0$, but it requires a larger storage for the inclusion of $\tilde{\phi}_0$, in addition to the $\tilde{\phi}_1$'s obtained in previous iterations. The same grid with nonuniform mesh is employed for $\tilde{\phi}_0$, $\tilde{\phi}_1$, and $\tilde{\phi}_2$, covering a region $|\tilde{x}| \lesssim 5, |\tilde{r}| \lesssim 6$, with a total of 81 x 65 grid points. The leading edge is made to locate at $\tilde{x} = -1$, and the trailing edge at $\tilde{x} = 1$ (i.e. $\tilde{a} = -1, \tilde{b} = 1$), any departure of $\tilde{a}$ from unity is accounted for by

---

+ Unpublished studies by Ronald C. Smith at NASA Ames Research Center appears to have raised doubts on certain earlier results from the 3-D, full potential program (FLO 22) used for oblique-wing analyses. We also point out that currently available 3-D computer programs based on the transonic small-disturbance equation (e.g. Bailey & Ballhaus 1972) are inapplicable to wings without bi-lateral symmetry. Therefore, comparisons with 3-D small-disturbance computer solutions have not been made.

changing $\tilde{x}$ into $[\tilde{x}+(1-\hat{a})]$ in (4.8) through (4.16). The case $|\hat{x}|=1$ corresponds to an oblique-wing planform with fore-and-aft symmetry about the (straight) center line. The Kutta condition is implicit in the programs in requiring the continuity of $\tilde{\Phi}_{0\tilde{x}}$, $\tilde{\Phi}_{1\tilde{x}}$ and $\tilde{\Phi}_{2\tilde{x}}$ at the trailing edge.

The iterative solutions use a relaxation factor 1.8 in the elliptic region and 0.8 in the hyperbolic region; typically, 200 line-sweeps are needed for the convergence of the circulations to within 10^{-5}. The calculation for $\tilde{\Phi}_1$ involves more work, and requires twenty-five (25) minutes on an IBM 370/158 Version III, using double-precision arithmetics.+

5.3 Examples of solutions

As examples, we apply the solution procedure to oblique wings with the section function $\tilde{Z}^{\pm}(\tilde{x})$ generated from the NASA 3612-02,40 airfoil, scaled to an arbitrary thickness. This airfoil has been used in various wind-tunnel and preliminary-design studies of oblique wing at Mach number between 0.60 and 1.4 (Black, Beamish & Alexander, 1975; Jones 1977). For the present purpose, we assume that the straight axis ($\tilde{x}=0$) to coincide with the mid chord of each wing section; the spanwise distribution of the wing chord, is, however, left arbitrary. In this application, it suffices to set the ratio of the thickness and camber parameters τ/α equal to unity, replacing all α by τ in scales entering the definitions of $\tilde{z}$ and $\tilde{\Phi}$, as well as K_n, M and ϵ. The determination of $\tilde{\Phi}_0$, $\tilde{\Phi}_1$, and $\tilde{\Phi}_2$ requires the specification of the component similarity parameter K_n.

Three sets of results for wing-surface distribution of $(\tilde{\Phi}_0)_{\tilde{x}}$, $(\tilde{\Phi}_1)_{\tilde{x}}$, and $(\tilde{\Phi}_2)_{\tilde{x}}$ are presented in Figs. 3 and 4. The first set (Fig. 3) is computed for $K_n=3.6$ with $\tilde{Z}^{\pm}(\tilde{x})$ taken from the rescaled coordinates of NASA 3612-02, 40 at zero incidence.++ The second and the third sets

---

+ A computer program similar to that for $\tilde{\Phi}_2$ has been considered in the context of a straight unyawed wing by Small (1978).

++ The coordinates of the airfoil section NASA 3612-02,40 may be expressed as, with $\xi' \equiv (x'-x'_{LE})/C(y')$,

$$z'/10\tau C(y') = (0.078/1.20)\,\xi'(1-\xi'^2) \pm \left\{0.20\sqrt{\xi'} + \xi'\left[-0.3087 + \xi'\left(0.5638 + \xi'(-0.8236 + 0.3704\,\xi')\right)\right]\right\}.$$

(Figs. 4a, b & c) are computed for a lower similarity parameter, $K_n = 3.45$, which gives a slightly supercritical 2-D component flow in $\tilde{\phi}_0$; the airfoil section and incidence in the second set (solid curves) is the same as in the first; the third set (dash curves) differs from the second only because a nonzero incidence $\Delta\alpha = 0.0582\tau$ (radian) is added to dz_w'/dx'.† From these results, the pressure coefficient $C_p \equiv (p - p_\infty)/\frac{1}{2}\rho_\infty U_\infty^2$ on the wing surfaces is calculated from

$$C_p = \cos^2\Lambda\, C_p' = -2\cos^2\Lambda\left(\frac{\alpha}{M_n}\right)^{2/3}\left\{(\tilde{\phi}_0)_{\tilde{x}} + \right.$$

$$\left. + \epsilon\textcircled{M}\frac{d\hat{c}}{d\hat{y}}(\tilde{\phi}_1)_{\tilde{x}} + \epsilon\left[\sqrt{K_n}\,\tilde{C}_1^{i\prime}(\tilde{y}) + \tilde{I} + \textcircled{M}\tilde{Z}_\beta'\right](\tilde{\phi}_2)_{\tilde{x}}\right\} \qquad (5.1)$$

In Fig. 3, the computed surface distribution of $(\tilde{\phi}_0)_{\tilde{x}}$, $(\tilde{\phi}_1)_{\tilde{x}}$, and $(\tilde{\phi}_2)_{\tilde{x}}$ are presented as thin solid curves, heavy solid curves, and dash curves, respectively, with the italic "u" and "l" referring to the upper and the lower surfaces. The peak of $(\tilde{\phi}_0)_{\tilde{x}}$ occurring near the mid-chord point lies slightly below the critical value $K_n/(1+\tau) = 1.50$. The surface values of $(\tilde{\phi}_1)_{\tilde{x}}$ which arises from the spanwise variation of the compressibility correction are seen to be numerically small as compared to $(\tilde{\phi}_2)_{\tilde{x}}$. The latter accounts for the incidence correction and includes the far-wake vorticity influence. The circulations given by the jump of $\tilde{\phi}_0$, $\tilde{\phi}_1$, and $\tilde{\phi}_2$ at the trailing edge are found to be $\tilde{\Gamma}_0 = 2.048$, $\tilde{\Gamma}_1 = -0.494$, and $\tilde{\Gamma}_2 = -2.667$, respectively. Their contributions to the potential $\hat{\phi}$ at the trailing edge, hence, the rolling moment about the wind axis, are weighted by $\hat{c}$, $\epsilon\textcircled{M}\hat{c}\frac{d\hat{c}}{d\hat{y}}$, and $\epsilon\hat{c}\left[\sqrt{K_n}\hat{C}_1^{i\prime} + \tilde{I} + \textcircled{M}\hat{Z}_\beta'\right]$, respectively. For a planform which is symmetrical with respect to $\tilde{y} = 0$ (not $y = 0$), $\tilde{\Gamma}_0$ is also symmetric. The induced upwash in this case is positive ($\tilde{C}_1^{i\prime} < 0$) on an aft panel and negative ($\tilde{C}_1^{i\prime} > 0$) on a fore panel, as noted earlier. Therefore, the last two of the three weighting factors mentioned are <u>both</u> negative on an aft panel and positive on a fore panel. It is, thus, seen from this example that, with the negative $\tilde{\Gamma}_1$ and $\tilde{\Gamma}_2$, the inviscid 3-D effects will give rise to an unbalanced rolling moment (as well as pitching

† For $\tau = 0.12$, this amount of $\Delta\alpha$ gives an incidence of 0.40 degree.

moment). The asymmetrical forces, if unchecked, will tend to raise the aft panel and lower the fore panel.

The least-square fit of the doublet strengths determined from the relaxation solution $\tilde{\Phi}_0$ of Fig. 3 are $\tilde{D}_0^r = 0.2472$ and $\tilde{D}_0^i = 0.0958$; with these and the value of $\tilde{\Pi}_0 = 2.048$, the source strength in the far field for $\tilde{\Phi}_1$ is determined from (4.17) as $\tilde{Q}_1 = 0.9270$. We note in passing that the program for computing $\tilde{\Phi}_2$ is relatively straightforward and the result can be reproduced quite well by computing $\tilde{\Phi}_0$ at a slightly different incidence, taking the difference of the two $\tilde{\Phi}_0$'s, and normalizing.

To assess the relative importance of these contributions, we apply the results of Fig. 3 to an elliptic planform with a major-to-minor axes ratio of 16.78 at 30° yaw. Assuming a 6% thickness ratio for each wing section, we have for this example $\epsilon = 0.1522$, $\textcircled{M} = 1.337$ (corresponding to $M_n = 0.7615$, and $M_\infty = 0.8793$ under $K_n = 3.6$). No wing-bend is considered, but a uniform $\tilde{I}(\tilde{y})$ corresponding to an (overall) incidence adjustment is chosen to eliminate 3-D effects on the total lift (this is possible owing to the pure antisymmetry of the 3-D effects in this special example). The resultant distribution of $\tilde{\Phi}_{\tilde{x}}$ on the upper surface at the span station $\tilde{y} = 0.80$ is shown as a dotted curve in Fig. 3. A small region of supercritical component flow is seen, which in this case is brought about mainly through the upwash induced by the wake vorticities.

The corresponding results for the other two sets shown in Figs. 4a, b and c are similar, with the noticeable difference being the appearance of supercritical regions on the upper surface in the leading approximation $(\tilde{\Phi}_0)_{\tilde{x}}$. The computation does not experience convergence difficulty and examination of the solution does not reveal evidence of shock waves in these cases. For the second set with $K_n = 3.45$ and $\Delta\alpha = 0$ (zero incidence), the solutions give $\tilde{\Pi}_0 = 2.0712$, $\tilde{\Pi}_1 = -0.5291$, $\tilde{\Pi}_2 = -2.6839$, $\tilde{D}_0^r = 0.2549$, $\tilde{D}_0^i = 0.0071$ and $\tilde{Q}_1 = 0.9530$; for the third set with $K_n = 3.45$ and an incidence of 0.4° corresponding to $\Delta\alpha/\tau = 0.0582$, the corresponding results are $\tilde{\Pi}_0 = 2.2828$, $\tilde{\Pi}_1 = -0.5427$, $\tilde{\Pi}_2 = -2.2118$, $\tilde{D}_0^r = 0.2614$, $\tilde{D}_0^i = 0.02578$, and $\tilde{Q}_1 = 0.9893$.

5.4 Comparison with full-potential, 3-D solutions

The similarity solutions $\tilde{\phi}_{0\tilde{x}}$, $\tilde{\phi}_{1\tilde{x}}$ and $\tilde{\phi}_{2\tilde{x}}$ shown in Figs. 3 and 4 can be applied to examples of transonic oblique wings of various combinations of M_∞, τ, Λ as long as the component similarity parameter K_n is unchanged. The wing aspect ratio and the spanwise distribution of the local wing chord can be quite arbitrary.

Surface distributions of C_p have been obtained in several cases for the purpose of comparison with solutions from a computer program based on a 3-D full-potential equation. In this connection it is essential to differentiate the significance of the critical pressure coefficient corresponding to a local sonic speed,

$$C_p^* = -\frac{2}{\gamma M_\infty^2}\left\{\left[\frac{(\gamma+1)/2}{1+\frac{\gamma-1}{2}M_\infty^2}\right]^{-\gamma/(\gamma-1)} - 1\right\}, \tag{5.2}$$

and that corresponding to the sonic condition in the component flow, namely,

$$C_p^{**} = -\frac{2}{\gamma M_n^2}\left\{\left[\frac{(\gamma+1)/2}{1+\frac{\gamma-1}{2}M_n^2}\right]^{-\gamma/(\gamma-1)} - 1\right\}\cos^2\Lambda \tag{5.3}$$

For the viewpoint of swept-wing aerodynamics, C_p^* is relatively trivial, inasmuch as a three-dimensional flow with $C_p < C_p^*$ can readily be rendered shock-free by providing a sufficiently large wing sweep. The value of C_p^{**} of (5.3) is very well approximated by that deduced from the present study

$$C_p^{**} = -2\left(\frac{\alpha}{M_n}\right)^{2/3}\cos^2\Lambda\,\frac{K_n}{(\gamma+1)}\,. \tag{5.4}$$

The difference between (5.4) and (5.3) apparently depends on $\frac{\gamma-1}{2}(1-M_n^2)$, which are found to be less than 2% for M_n as low as 0.65.

It may be pointed out that existing 3-D computer codes based on the full-potential equations do not account (correctly) for the departure of the trailing vortex sheet from a planar (flat) surface. Thus, its validity also requires the small-disturbance assumption, strictly speaking. The value of the program lies, of course, on its ability to describe the flow field around the leading edge and near the trailing edge, where the small-disturbance approximation breakdown or becomes less accurate, assuming

that problems of convergence with respect to mesh size, and to iteration, may not cause inaccuracy.

Numerical results comparable with our solutions are generated from one version of A. Jameson's 3-D full-potential computer codes "FLO 22" (c.f. Bauer, Garabedian, Jameson & Korn 1974, Jameson 1974), which is used with implementations for oblique-wing analyses at NASA Ames Research Center Aeronautics Division and at Grumman Aerospace Corporation Research Department.[+] The algorithms employed in FLO 22 are not fully conservative, but this may not be essential for shock-free solutions presented below. We point out that the FLO 22 data from Ames and from Grumman are not identical owing mainly to the use of different meshes. The availability of data from two sources is helpful in delineating the nature of discrepancy between our theory and the more exact 3-D program. Data from the latter is still influenced by the mesh size, spacing of the span stations, number of iterations, the detail of the leading-edge geometry description, which are different in Ames and Grumman runs.

A number of FLO 22 runs have been made with free-stream Mach number, swept angle, wing-thickness, etc. chosen to give either $K_n = 3.6$ or $K_n = 3.45$, employing the same basic airfoil section. An elliptic planform is used in each case; wing twist and wing bend are assumed to be zero. Comparisons are made in Fig. 5-7 for three cases and may be considered being typical among most runs.

The oblique elliptic wing considered in Fig. 5 has a 6% thickness ratio, with the major-to-minor axes ratio of 20, and a sweep angle of 22.5°. The free-stream Mach number is $M_\infty = 0.8242$ in this case. This makes the free-stream component Mach number $M_n = 0.7615$ and $K_n = 3.60$, $\textcircled{M} = 1.003$ and $\epsilon = 0.1277$ in our analysis. The pressure coefficient for the critical component flow in this case is $C_p^{**} = -0.470$. The surface C_p values at three span stations, $\tilde{y} = -0.69$, $\tilde{y} = 0$ and $\tilde{y} = 0.69$ are shown in Fig. 5a, Fig. 5b and Fig. 5c, respectively. The FLO 22 data from Ames (in small crosses and "$_V$" and from Grumman (in small open circles) are seen to be quite close

[+] The FLO 22 data generated at the NASA Ames Research Center were kindly provided by Mr. Ronald C. Smith, and the data from Grumman Aerospace Corporation were made available to us by Dr. Rueben Chow.

except near the leading edge.[+] Near the leading edge, the small-disturbance assumption of our theory also breaks down as noted earlier. The agreement of the FLO 22 data with our values computed on the basis of data from Fig. 3 (in solid curves) must be considered as being better than anticipated, inasmuch as the relative error in our theory is of an order determined by the larger of $\tau^{2/3}$ and ϵ^2 (to be precise). In the present case, $\tau^{2/3} = (0.06)^{2/3} = 0.153$!

Encouraging is that the degree of agreement with the FLO 22 data appear to deteriorate little with increasing wing-thickness ratio or reducing aspect ratio. Results of comparisons for elliptic wings with a 12% thick airfoil section and a major-to-minor axes ratio of 14 are shown in Figs. 6 and 7. The case considered in Fig. 6 has a free-stream Mach number 0.7549, a yaw angle 30°. This gives $M_n = 0.6538$, $K_n = 3.60$, $\epsilon = 0.1448$, and $\textcircled{M} = 1.062$; also $C_p^{**} = -0.727$. The C_p values (compted from the present theory, based again on data of Fig. 3) are presented for five span stations in heavy curves with open circles; the corresponding FLO 22 data (from NASA Ames) are presented as thin curves.[++] Agreement similar to that found in Fig. 5 is again found in Fig. 6 except at the stations $\tilde{y} = \pm 0.89$ which are rather close to the wing tip.

In Fig. 7, the thickness ratios and aspect ratio remain the same as in Fig. 6, but $M_\infty = 0.7677$ and $\Lambda = 30^{\circ}$. This gives $M_n = 0.6648$, $C_p^{**} = -0.689$, and $K_n = 3.45$. For this, the C_p value in the present theory is computed on the basis of our data from Fig. 4. The results are presented in Fig. 7 for seven span stations: $\tilde{y} = 0, \pm 0.20, \pm 0.59, \pm 0.79$. The degree of agreement with the FLO 22 data (from NASA Ames) is again similar in the preceding comparisons. In this case, a small supercritical region appear in the aft wing panel, as anticipated (there are at least three surface grid points in the supercritical region).

[+] The two sets of FLO 22 data also differ near the wing tips ($\tilde{y} = \pm 0.90$) not shown.

[++] Note that, there are considerably more data points than the numbers of the open circles shown.

The reader is called to the attention that the C_p distributions are not the same in different span stations, therefore, the comparisons made with the FLO 22 data have provided a meaningful test for the theory. One of the major contributions to the 3-D effects is the incidence correction which accounts for the upwash induced by the wake vorticities, computed from $\bar{V}_1^{\infty}$ of (3.9) via (3.10) and (4.16a). The adequacy of this upwash calculation has already been demonstrated in examples pertaining to the linearized problem (Cheng 1978a & b); therefore, the good agreement reported here should not be too surprising. Worthy of note in this connection is the use of the transonic similarity parameter $K_n = (1-M_n^2)/\alpha^{2/3} M_n$, and the retention of the $\cos\Lambda$ factor in computing $\tilde{\Phi}_0 \tilde{x}$ and C_p, which prove to be crucial in maintaining an accurate leading approximation, and is partly responsible for the good agreement achieved here.

5.5 Comparison with solutions via the unsteady analogy

To demonstrate the degree to which the unsteady transonic analogy can be utilized for the oblique-wing analysis, we include here a comparison of the local-similarity solutions for non-lifting oblique wings with the corresponding results generated by a numerical procedure using an ADI algorithms similar to those in Ballhaus & Goorjian (1977).[+] As pointed out in § 4.1, the case involving lift ($\Gamma_0' \neq 0$) requires an implementation at the far boundary for the unsteady analogy, not needed for the example considered here. The result is nevertheless of interest in that the 3-D correction, in this case, is given entirely by the compressibility effect resulting from spanwise density variation mentioned earlier. For this purpose, we consider oblique wings with a symmetric airfoil section, NACA 64006 at zero incidence, and compute $\tilde{\Phi}_0$ for $K_n = 2.50$; (cf. § 5.2) the result for the surface pressure coefficient $C_{p(0)}' = -2\left(\frac{\tau}{M_n}\right)^{2/3}\left(\tilde{\Phi}_0\right)_{\tilde{x}}$ was computed for $\tau = 0.06$ and $M_n = 0.827$

[+] The unsteady transonic code used in this study was made by Dr. Tom Evans during 1977 on leave from the University of East Anglia, Norwich, England.

and is shown in Fig. 8 as a heavy solid curve.[+] The basic component flow in this case has a $C_p^{**} = -0.3624$, very closely approached by the C_p minimum shown. The solutions to the reduced problem of the 3-D correction have been computed for three cases (cases A, B and C) corresponding to three different chord-wise locations of the straight axes (center line); the results for the $(\tilde{\Phi}_1)_{\tilde{x}}$ on the surface are shown as thin solid curves in Fig. 8 (the maximum value of $\tilde{\Phi}_{1\tilde{x}}$ in case C is finite but exceeds the boundary of the figure). The noticeable differences among cases A, B and C, confirms the expectation that increasing the (local) leading-edge swept angle reduces the maximum local Mach number, and decreasing the sweep increases it. This is because the contribution of $\tilde{\Phi}_{1\tilde{x}}$ to $\hat{\Phi}_{\hat{x}}$ is weighted by $\epsilon(M)\, d\hat{c}/d\hat{y}$, the latter is positive on the fore panel and negative on the aft panel. Thus, moving the straight axis to the leading edge (say, changing from case A to case B), the $\hat{\Phi}_{\hat{x}}$ maximum will increase in the aft panel and decrease in the fore panel, whereas, moving the straight axis to the trailing edge (say, changing from case A to case B), the $\hat{\Phi}_{\hat{x}}$ peak will decrease in the aft panel and will increase in the fore panel.

To test the unsteady analogy in these (nonlifting) cases, we consider high aspect-ratio oblique wings with the same component similarity parameter ($K_n = 2.50$), choosing an aspect ratio and sweep angle to correspond to $\epsilon(M) = 0.10$.[++] Surface pressure coefficients C_p' are computed from $\tilde{\Phi}_{0\tilde{x}}$ and $\tilde{\Phi}_{1\tilde{x}}$ of Fig. 8 for four different planforms (an ellipse, a lenticular shape, and two half-lenticular shapes), assuming $\tau = 0.06$ and $M_n = 0.827$ for convenience. Fig. 9 presents C_p' vs. $\hat{x}' \equiv (\hat{x} - \hat{a})/2$ on a yawed elliptic planform at three representative span stations $\tilde{y} = -0.50$, 0, and 0.50. The data computed from the present theory (in dots, crosses and triangles) compare well with the corresponding data computed from the unsteady transonic

---

[+] The more general result for $(\tilde{\Phi}_0)_{\tilde{x}}$, independent of τ and M_n, may nevertheless be recovered by interpreting $C_{p(0)}$ in Fig. 8 as $C'_{p(0)}/2(\tau/M_n)^{2/3}$.

[++] If $\tau = 0.06$ and $\Lambda = 22.5^\circ$, these values of $K_n = 2.50$ and $\epsilon(M) = 0.10$ will mean $M_n = 0.827$, $M_\infty = 0.895$ and $AR_1 = 22.57$; if $\tau = 0.12$, $\Lambda = 22.5^\circ$, then $K_n = 2.50$ and $\epsilon(M) = 0.10$ require $M_n = 0.741$, $M_\infty = 0.8025$ and $AR_1 = 16.14$. The factor 0.909 in the ordinates of Figs. 9 and 10 results from a peculiar factor introduced in the C_p of T. Evans' program.

code of T. Evans (in thin solid curves). In Evans' work, the variables $\hat{t}'$, $\hat{x}'$, $\hat{y}'$, $\hat{z}'$ and φ with

$$\hat{t}' = [1 + \hat{t}/\epsilon(M)]/2 = (1+\hat{y})/2 \; ; \quad \hat{x}' = (\hat{x} - \hat{a})/2 \, , \quad \hat{z}' = \hat{z}/2 ; \quad \varphi = \hat{\phi}/2 .$$

are used. Discrepancies are noticeable near the leading edge, but are attributable to the cruder mesh near the leading edge used in computing $\tilde{\phi}_{0\hat{x}}$ and $\tilde{\phi}_{1\hat{x}}$ of Fig. 8.

Similar comparison for a yawed lenticular planform are given in Fig. 10a for the aft panel at span stations $\tilde{y} = 0$, 0.5, and 0.8, and for the fore panel at span station $\tilde{y} = -0.20$ and -0.50 in Fig. 10b. Figs. 11a & b present corresponding results for a half-lenticular planform with a straight leading edge; Figs. 12a & b shows results for the half-lenticular planform with a straight trailing edge. The degree of agreement between our calculations based on the local similarity and the data from unsteady analogy shown in Figs. 9 through 12 are very consistent. The encouraging results appear to suggest that the analogy should hold even for values of $\epsilon(M)$ considerably greater than 0.10.

Comparisons with unsteady solutions involving circulations and imbedded shocks, as well as the extension of the analogy to allow for centerline curvature, remain to be considered in future works.

6. CONCLUDING REMARKS

In summary, we have presented a transonic-flow theory of thin wings of high (reduced) aspect ratio ($\epsilon \ll 1$) which permits delineation of the influence of wing sweep, center-line curvature, and other 3-D effects on the nonlinear flows more explicity than available methods. In the domain of K_n and $\mathcal{H}$ considered, the outer 3-D flow has a transonic free stream ($M_\infty \sim 1$), but the disturbance is weak enough, and the wing aspect-ratio high enough, to allow a lifting-line description in Prandtl-Glauert variables (as a leading approximation to ϕ). In the inner region next to the wing section, the (local) sweep is large enough to avoid strong shock losses but low enough to sustain a transonic, mixed component flow. The 3-D corrections to this nonlinear component flow is analyzed by solving a perturbation problem for $\epsilon \ll 1$, and matching the result to the outer solution.

The basic flow around each wing section is the 2-D component flow characterized by a similarity parameter K_n which is, in turn, controlled by the local wing sweep, Λ. For a given wing geometry, 3-D corrections for the domain analyzed come mainly from two sources: one arises from a 3-D compressibility correction to the PDE, absent in the classical theory, and is proportional to $\epsilon\mathcal{H}$; the other corresponds to the familiar induced upwash corrections, including the contribution from the near wake and the velocity induced by the curved lifting line itself. The upwash correction, explicitly determined as a functional of the circulation in (3.9b) and (3.10), consists of terms proportional to ϵ as well as $\mathcal{H}\epsilon \ln\epsilon$. On a straight oblique wing, corrections from both sources generally tend to make the flow more critical on the aft panel and less critical on the fore panel. Nevertheless, center-line curvature, as well as the local leading-edge swept angle, may be used to control this undesirable 3-D effect.

For oblique wings, of which the center line of the planform can be taken as being straight ($\mathcal{H}' \equiv 0$), the 3-D flow structure possesses similarities, permitting the reduced PDE systems to be solved <u>once</u> for <u>all</u> stations. This similitude has a requirement on the wing geometry, namely, the wing ordinates be generated from the same airfoil section with a fixed

thickness ratio and incidence, allowing, however, wing twist and wing bend in the manner indicated in (4.5). The origin of the wing-section coordinates in this similitude must coincide with the (straight) center line, the planeform is otherwise arbitrary. For straight oblique wings, an analogy also exists with a 2-D transonic flow under the influence of slow (unsteady) changes in airfoil geometry and in the condition at the far boundary. The analogy (demonstrated in the nonlifting cases in § 5.5) promises an alternative method for oblique-wing analysis, utilizing existing numerical procedures for unsteady 2-D transonic flows, without requiring the local similarity as well as treatment of the shock-root nonuniformity (§ 2.6). Such a procedure, with the upwash function $\hat{C}_1'(\hat{y})$ determined by (3.9b) and (3.10), may also be extended to the more general case with a curved center line.

Of interest is a source term appearing in the far-field expansion of the inner solution, resulting from the 3-D compressibility correction and the nonlinear lift effects, this gives rise to a line source in the second approximation to the perturbation potential in the outer flow. It is pointed out that, unless $M_\infty = 0$, a line source must similarly arise in a linear theory. The existence of the source term with a nonvanishing strength in the present theory is firmly established for oblique wings by: (i) demonstrating (in § 3.3) the matching of the inner and outer solutions to all terms larger and comparable to the source term in the overlapping region; (ii) use of the result of Green's theorem to show (in Appendix II.1) that the source strength $\tilde{Q}_1$, is the same as that for a Poisson solution; (iii) explicit evaluation of $\tilde{Q}_1$ for the Poisson solution (in Appendix III).

For flow involving imbedded shock, the formal perturbation analysis leads to a nonuniformity at the shock root, owing to the reexpansion singularity. A nonuniform problem of the same nature has been present also in a number of existing perturbation analyses in the context of unsteady transonic flow, as noted. In the treatment presented in § 2.6, it is shown that, in coordinates fixed to (and moving with) the shock root, the Oswatitsch-Zierep (1960) description for the behavior of pressure or tangential velocity (not the velocity potential) remains valid, irrespective of the perturbation. Thus the 3-D (as well as the analogous time dependent) effects can influence

the pressure behavior in question only through changes in the three parameters (local shock strength, shock-root position and another constant) which specify the Oswatitsch-Zierep singularity. These changes can be determined by matching with the solution removed from the shock root.

The procedures for solving the similarity solutions to the reduced problem have been described; solutions are demonstrated for oblique-wing geometries using a rescaled NASA 3612-02,40 airfoil section. The solutions give maximum flow speeds which are slightly below and above the critical values. The results on surface pressure have been applied to specific 3-D oblique wing with elliptical planforms pertaining to various combinations of free-stream Mach number, wing sweep, thickness-ratio and aspect-ratio, and compare (in § 5.4) with the corresponding data obtained from a full-potential, 3-D computer program (FLO 22). The discrepancies found are generally smaller than the expected errors from the small-disturbance approximation and the descretization in some instances, the discrepancies could be attributed to the convergence problem in the FLO 22 data The encouraging agreement, consistently found in most cases examined (including thickness ratios as large as 0.12 and aspect ratios down to 10) has confirmed our expectation from a similarly encouraging, previous comparison for the linear theory (Cheng 1978a & b). Essential in this regard is the retention of the $\cos\Lambda$ factor in U_n for the inner solution and in C_p, and the adaptation of an M_n^{-1} factor in the similarity parameter K_n to better approximate the critical speed (§ 2.3). As yet to be demonstrated are similarity solutions with a more extensive region of supercritical component flow, with or without an imbedded shock.

For numerical solutions involving shocks, the type-sensitive difference schemes are implemented by shock-fitting algorithm for $\tilde{\phi}_0$, and by corresponding algorithm for $\tilde{\phi}_1$ and $\tilde{\phi}_2$. The latters are supplemented with a treatment of the shock-root nonuniformity. Their comparison with the corresponding unsteady solutions through the analogy should furnish an opportunity to test the adequacy of the proposed method and the ADI procedure in describing shocks. In this connection, a solution via the unsteady analogy involving lift is yet to be carried out. These works are in progress.

In future work, utilization of the unsteady analogy should be explored further for its potentiality in solving swept-wing problems without the assumptions of local similarities and a straight center line. The relaxation of the small-disturbance assumption would appear to be a natural extension of the present work. It must be pointed out, however, that the PDE governing the perturbation velocity potential in such cases is not only more complicated, but does not readily yield a similarity solution as in the present theory. For practical consideration, one may, of course, replace $\hat{\phi}_0$ by the corresponding full-potential value, applying $\epsilon\hat{\phi}_1$ from our theory as a 3-D correction.

One drawback discourages applications of the present work to conventional swept wings is the nonuniformity near the apex (cf. (3.13b)), removal of which would call for the use of the nonlinear 3-D transonic small-disturbance equation therein. The present theory may still provide reasonable results in regions removed from the apex, and a direct comparison with more exact numerical solutions (Jameson & Caughey 1977, or Bailey or Ballhaus 1972) for symmetric swept wings should be made. The problem of a supersonic (or slightly supersonic) oblique or swept wing with a transonic component flow represents an obvious, and equally interesting area of extension; in this case, the problem of the apex nonuniformity may become more tractable.

ACKNOWLEDGEMENT

The study is supported by the Office of Naval Research under Contract N00014-75-C-0520. Drs. E. Albano and M.M. Hafez contributed to an earlier computer-program development, under partial support from NASA Ames Research Center Aeronautics Division through Agreements NCR-730-501 and NCA2-OR-730-601. The many sets of numerical (FLO 22) data shown in the comparison study were made available to us through Mr. Ronald C. Smith at NASA Ames Research Center and Dr. Rueben Chow at Grumman Aerospace Corporation. Much of the numerical data used in the study of unsteady analogy were generated from an unsteady transonic code by Dr. T. Evans, University of East Anglia, England. Professor B.A. Troesch has assisted the evaluation of some of the basic integrals. The senior author would like to thank Dr. R.T. Jones for several valuable discussions.

REFERENCES

Ashey, H. & Landahl, M. 1965 Aerodynamics of Wings & Bodies, 137-142, 227-244.

Bailey, F.R. & Ballhaus, W. 1972, Proc. 3rd Inter. Conf. Numerical Methods in Fluid Dynamics, Paris, July 1972, Lecture Notes in Physics, Vol. 19, Springer-Verlag 1972, 2-9.

Ballhaus, W.F. & Goorjian , P.M. 1977, AIAA J., Vol. 15, No. 12, 1728-1735.

Ballhaus, F.G. & Goorjian , P.M. 1978, AIAA J., Vol. 16, No. 2, 117-124.

Bauer, F., Garabedian, P., Korn, D. & Jameson, A. 1974, Supercritical Wing Section, II, Lecture Notes in Economics and Math. Systems, No. 108, Springer-Verlag, Berlin, Heidelberg and New York.

Black, R.L., Beamish, J.F. & Alexander, W.K. 1975, NASA CR-137697, HST-TR-344-0, July, 11.

Boerstoel, J.W. 1974 National Aerospace Laboratory Report NLRMP 74024 U, Amsterdam, Netherlands, September.

Busemann, A. 1935, Luftfahrtforschung Bd. 12, Nr. 6.

Cheng, H.K. 1976, Univ. So. Calif., School of Engineering, Department of Aerospace Engineering Report USCAE 133, January.

Cheng, H.K. 1978a, AIAA J., Vol. 16, No. 11, 1211-1213.

Cheng, H.K. 1978b, Univ. So. Calif., School of Engineering, Department of Aerosapce Engineering Report USCAE 135, August.

Cheng, H.K. & Hafez, M.M. 1973, Univ. So. Calif., School of Engineering, Department of Aerospace Engineering Report USCAE 124.

Cheng, H.K. & Hafez, M.M. 1975, J. Fluid Mechanics, Vol. 72, pp. 161-187.

Cheng, H.K. & Meng, S.Y. 1979, AIAA J., Vol. 17, No. 1, 121-124.

Cole, J.D. 1975, SIAM J. Appl. Math., Vol. 29, No. 4, 763-787.

Cook, P. 1978, Indiana Univ. Math. J., Vol. 27, No. 1.

Cook, P. & Cole, J.D. 1978. SIAM J. Appl. Math., Vol. 35, September, 209-224.

Courant, R. & Hilbert, D. 1965, Methods of Mathematical Physics, Vol. II, 551-556.

REFERENCES (Con't)

Ehler, F.E. 1974. NASA CR-2257.

Fung, K.Y., Yu, N.J. & Seebass, R. 1978. AIAA J., Vol. 16, No. 8, 815-822.

Hafez, M.M. & Cheng, H.K. 1977a. AIAA J., Vol. 15, No. 3, 329-331.

Hafez, M.M. & Cheng, H.K. 1977b. AIAA J., Vol. 5, No. 6, 786-793.

Hafez, M.M., Rizk, X. & Murman, E.M. 1977. Proc. AGARD Unsteady Transonic & Separated Flows, held at Lisbon, Portugal, July.

Jameson, A. 1974. Comm. Pure Appl. Math., Vol. 27, 283-309.

Jameson, A. & Caughey, D.A. 1977. New York Univ. ERDA Report COO 3077-140, May.

Jones, R.T. 1946. NACA Report No. 851.

Jones, R.T. 1971. AIAA J., Vol. 10, 171-176.

Jones, R.T. 1977. Acta Aeronautica, Vol. 4, January, 99-110.

Jones, R.T. & Cohen, D. 1957. "Aerodynamics of Wings at High Speed", in Aerodynamic Components of Aircraft at High Speed, ed. by D.F. Donovan & H.R. Lawrence, Princeton Univ. Press.

Kacprzynski, J.J., Ohman, L.H., Garabedian, P.R. & Korn, D.G. 1971. Aeronautical Report LR-554, National Research Council of Canada, Ottawa.

Keyfitz, B., Melnik, R. & Grossman, R. 1978. Quart. J. Mech. Appl. Math., Vol. 31, pt. 2, 137-155.

Klunker, E.B. & Newman, P.A. 1974, (AIAA) J. Aircraft, Vol. 11, No. 4, 254-256.

Korn, D.G. 1969. Courant Inst. Math. Sci. Report NYO-1480-125.

Kücherman, N.D. 1965. Progress in Aeronautical Sciences, Vol. 6.

Landahl, M. 1962. Symposium Transsonicum, 414-439.

Meng, S.Y. & Cheng, H.K. 1977 Proc. Appl. Computer Methods in Engineering, held at Univ. So. Calif., Los Angeles, ed. L.C. Wellford, 395-404.

Murman, E.M. 1974. AIAA J., Vol. 12, pp. 626-633.

Murman, E.M. & Cole, J.D. 1971. AIAA J., Vol. 9, No. 1, 114-121.

REFERENCES (Con't.)

Murman, E.M. & Krupp, J.A. 1971. Proc. 2nd International Conf. Numerical Methods in Fluid Dynamics, Lecture Notes in Physics, Springer-Verlag Berlin-Heidelberg, New York, 199-206.

Nixon, D. 1978. AIAA J., Vol. 16, No. 1, 47-52.

Nonweiler, T.R. 1958. J. Fluid Mech., Vol. 4, 140-

Oswatitsch, K. & Zierep, J. 1960. ZAMM, Vol. 40, Suppl., 143-144.

Oswatitsch, K. 1962. Symposium Transsonicum, 402-413.

Prandtl, L. 1918. Nachrichten d.k. Gesellschaft d. Wiss. zu Göttingen, Math-Phys. Klasse, pp. 451-477.

Sirovich, L. & Ho, C. 1976. AIAA J., Vol. 14, No. 8, 1125-1127.

Small, R.D. 1978. AIAA J., Vol. 16, No. 6, 632-634.

Sprieter, J.R. 1953. NACA Report 1153.

Timman, R. 1962. Symposium Transsonicum, 394-401.

Traci, R.M., Albano, E.D. & Farr, J.L. 1976. AIAA J., Vol. 4, No. 9, 1258-1265.

Van Dyke, M.D. 1964. Perturbation Methods in Fluid Mechanics, Academic Press, New York, 167-176.

Whitcomb, R.T. 1974. Paper presented at the 9th International Congress on Aeronautical Sciences, Haifa, Israel.

APPENDIX I

THE CRITICAL SPEED AND THE TRANSONIC SIMILARITY PARAMETER

We consider a two-dimensional steady potential flow. The transonic small-disturbance approximation leads in this case to the familiar PDE for the perturbation velocity potential

$$\left[\left(1-M_\infty^2\right) - (\gamma+1) M_\infty^2 \phi_x U^{-1}\right] \phi_{xx} + \phi_{yy} = 0, \qquad (1.1)$$

or, in terms of the variables $\hat{x}$, $\hat{z}$ and $\hat{\phi}$ defined in the text, writing τ for α and $\hat{\eta}$ for $\hat{\epsilon}$,

$$\left(K_s - (\gamma+1)\hat{\phi}_{\hat{x}}\right)\hat{\phi}_{\hat{x}\hat{x}} + \hat{\phi}_{\hat{\eta}\hat{\eta}} = 0, \qquad (1.2)$$

where

$$K_s \equiv \frac{1-M_\infty^2}{M_\infty^{4/3}\tau^{2/3}}, \qquad (1.3)$$

is identified with the similarity parameter of Sprieter (1953), except for a change in the algebraic sign and the omission of the factor $(\gamma+1)^{-2/3}$. As an asymptotic theory, $(\gamma+1)M_\infty^2$ and $M_\infty^{4/3}$ in (1.1) and (1.3) may, of course, be replaced by $(\gamma+1)$ and unity, respectively; similarly, $(1-M_\infty^2)$ by $2(1-M_\infty)$. We also note that, according to (2.1) in the text, $(\gamma+1)M_\infty^2$ in (1.1) could have been written as $(\gamma+1)M_\infty^2\left[1+\frac{\gamma-1}{2}(M_\infty^2-1)\right]$; but the resulting differences are numerically small in the range of M_∞ considered (see below).

The full potential PDE in this case is

$$\left(a^2-u^2\right)\Phi_{xx} + 2uv\Phi_{xy} + \left(a^2-v^2\right)\Phi_{yy} \equiv 0, \qquad (1.4)$$

where a is the sound speed, $u=\Phi_x$, $v=\Phi_y$ and $\Phi = Ux+\phi$. An approximate form of (1.4), valid in the domain $K_s = O(1)$ and τ small, is (with $u'=\phi_x$ $v'=\phi_y$)

$$\left\{1 - M_\infty^2 - M_\infty^2\left[2+(\gamma-1)M_\infty^2\right]\frac{u'}{U} - M_\infty^2\left[\frac{\gamma+1}{2} + (\gamma^2-1)M_\infty^2\right]\left(\frac{u'}{U}\right)^2\right\}\phi_{xx} -$$

$$- 2M_\infty^2\frac{v'}{U}\phi_{xy} + \phi_{yy} = 0 \qquad (1.5)$$

This is one order $\tau^{2/3}$ more accurate than (1.1). The characteristics of (1.4) and (1.5) give the same critical values for (u'/U) up to the second order of $(1-M_\infty^2)$

$$\frac{u'}{U} \sim \frac{1-M_\infty^2}{(\gamma+1)M_\infty^2}\left\{1-\frac{1-M_\infty^2}{2(\gamma+1)}+O[(1-M_\infty)^2]\right\} \tag{1.6}$$

where the leading term $(1-M_\infty^2)/(\gamma+1)M_\infty^2$ is the critical speed based on PDE (1.1).

Comparing (1.1) with (1.5), the small-disturbance equation (1.1) is seen to represent the characteristics system poorly in region near the critical speed, giving erroneous slope dy^c/dx therein. The small-disturbance equation can be written as

$$(\gamma+1)M_\infty^2\left[\frac{1-M_\infty^2}{(\gamma+1)M_\infty^2}-\frac{u'}{U}\right]\phi_{xx}+\phi_{yy}=0, \tag{1.7}$$

over which an improvement in this regard can be gained by writing

$$(\gamma+1)M_\infty^2\left[\left(\frac{u'}{U}\right)_*-\frac{u'}{U}\right]\phi_{xx}+\phi_{yy}=0, \tag{1.8}$$

with $(u'/U)_*$ given by the two-term expansions (1.6). This modification then leads to

$$\left[K_s'-(\gamma+1)\hat{\phi}_{\hat{x}}\right]\hat{\phi}_{\hat{x}\hat{x}}+\hat{\phi}_{\hat{\eta}\hat{\eta}}=0, \tag{1.9}$$

with

$$K_s' \equiv \frac{1-M_\infty^2}{M_\infty^{4/3}\tau^{2/3}}\left[1-\frac{1-M_\infty^2}{2(\gamma+1)}\right]. \tag{1.10}$$

This expression of K_s' is equivalent to

$$K' \equiv \frac{1-M_\infty^2}{\tau^{2/3} M_\infty^{\omega}} , \qquad \omega = \frac{4\gamma+1}{3(\gamma+1)} \tag{1.11}$$

noting that

$$K'/K_s' = 1 + O[(1-M_\infty)^2] .$$

APPENDIX II

APPLICATION OF GREEN'S THEOREM AND THE FAR-FIELD BEHAVIOR

II.1 A relation for the weak solution

Let ϕ denote a function satisfying

$$\left(\frac{\partial^2}{\partial x^2}+\frac{\partial^2}{\partial \eta^2}\right)\phi=\frac{\partial}{\partial x}\Sigma \tag{II.1}$$

in an infinite domain in x and η, $\mathcal{D}_\infty$, where the distribution Σ varies with x and η and may also depend on ϕ and its partial derivatives. Let the inner boundary of $\mathcal{D}_\infty$ be the limiting boundary enclosing, and approaching, the two segments W (wing) and T (trace) on the x-axis, also the segment D (shock discontinuity) as shown in the sketch (Fig. A.1). We assume that across T the function ϕ satisfies

$$[\![\,\phi_x\,]\!]=[\![\,\phi_\eta\,]\!]=0 \tag{II.2}$$

where $[\![\ ]\!]$ stands for the jump, $[\![\ ]\!]=(\ )^+-(\ )^-$, and that, across D, the jump takes on values consistent with weak solutions to (II.1), namely, at $x=x^D(\eta)$,

$$[\![\,\phi_x-\Sigma-\frac{\partial x^D}{\partial \eta}\phi_\eta\,]\!]=0, \qquad [\![\phi]\!]=0. \tag{II.3}$$*

We assume further that $\nabla\phi$ vanishes at the infinity in the mean, i.e.,

$$\overline{\nabla\phi}\equiv\lim_{R\to\infty}\frac{1}{R}\oint\phi(x_1,\eta_1)\,ds_1=0 \tag{II.4}$$

where R is the radius of a circle centered at (x,η) and $ds_1=\sqrt{dx_1^2+d\eta_1^2}$, and that the integral of $\frac{\partial}{\partial x}\Sigma$ over $\mathcal{D}_\infty$ exists. Application of Green's theorem to this system yields a relation

$$\phi(x,\eta)=\frac{1}{2\pi}\int_{W^+T^+D^+}\left\{[\![\frac{\partial\phi}{\partial n_1}]\!]\ln r'-[\![\phi]\!]\,\vec{n}_1\cdot\nabla_1\ln r'\right\}ds_1+$$
$$+\frac{1}{2\pi}\iint_{\mathcal{D}_\infty}\left(\frac{\partial}{\partial x_1}\Sigma\right)\ln r'\,dx_1d\eta_1 \tag{II.5}$$

*This is equivalent to (2.14), for $\Sigma=\frac{\gamma+1}{2K_n}\phi_x^2+2\epsilon\textcircled{M}K_n^{-1}\phi_y+6\textcircled{M}'K_n^{-1}\phi$.

where $r' = \sqrt{(x-x_1)^2 + (\eta - \eta_1)^2}$, and n is the inward normal into $\mathcal{D}_\infty$, the integration is taken only along one side of the boundary segments. The last integral over $\mathcal{D}_\infty$ can be evaluated as

$$\iint_{\mathcal{D}_\infty} \left(\frac{\partial}{\partial x_1}\Sigma\right) \ln r' \, dx_1 d\eta_1 = -\int_{D^+} [\![\Sigma]\!] \ln r' \, d\eta_1 - \iint_{\mathcal{D}_\infty} \Sigma \, \frac{x-x_1}{r'^2} \, dx_1 d\eta_1 ,$$

also,

$$\int_{D^+} [\![\frac{\partial \phi}{\partial n_1}]\!] \ln r' \, ds_1 = \int_{D^+} [\![\phi_x - \phi_\eta \frac{\partial x^D}{\partial \eta}]\!] \ln r' \, d\eta_1 \quad ;$$

Thus, applying the first of (11.3),

$$\frac{1}{2\pi} \int_{D^+} \left\{ [\![\frac{\partial \phi}{\partial n_1}]\!] \ln r' - [\![\phi]\!] \frac{\partial}{\partial n_1} \ln r' \right\} ds + \frac{1}{2\pi} \iint_{\mathcal{D}_\infty} (\Sigma)_{x_1} \cdot \ln r' \, dx_1 d\eta_1$$

$$= -\frac{1}{2\pi} \iint_{\mathcal{D}_\infty} \Sigma \cdot \frac{x_1 - x}{r'^2} \, dx_1 d\eta_1 \qquad (11.6)$$

We now apply (11.6) to the last integral of (11.5), and the second of (11.3) to the line integral over D^+; then, we integrate, by parts (with respect to x_1), the line integral over W^+ and T^+ in (11.5), and finally involk (11.2); we recover the basic relation for the weak solution of (11.1), first given in Murman and Cole's (1971) original paper

$$\phi = \frac{1}{2\pi} \int_{LE}^{TE} [\![\phi_\eta]\!] \ln r' \, dx_1 + \frac{1}{2\pi} \int_{LE}^{TE} [\![\phi_{x_1}]\!] \left\{ \tan^{-1}\left(\frac{x-x_1}{\eta}\right) + \frac{\pi}{2} \operatorname{sgn} \eta \right\} dx_1 -$$

$$- \frac{1}{2\pi} \iint_{\mathcal{D}_\infty} \frac{x_1 - x}{r'^2} \cdot \Sigma \cdot dx_1 d\eta_1 , \qquad (11.7)$$

where the first two integrals are taken along the x-axis. The above result still holds if there are more than one D (shock) boundary. Assuming $\Sigma = 0\ (\frac{1}{r^\sigma})$ at large distance, the existence of the last (double) integral requires

$$\sigma > 1 . \qquad (11.8)$$

+ Is is assumed that $\Sigma \cdot \ln r$ vanishes at the infinity; this is satisfied by (11.8).

II.2 Remarks

We note in passing that for the airfoil problem governed by the 2-D transonic small-disturbance equation, we have $\Sigma = (\gamma+1)\phi_x^2/2K$. In this case, $\phi_x = O(r^{-1})$, unless the circulation is zero; thus; $\Sigma = O(r^{-2})$, $r \to \infty$, and the double integral exists. At large r, this integral can be represented by a doublet

$$\frac{1}{2\pi} \iint_{\mathcal{D}_\infty} \Sigma \, d\xi_1 d\eta_1 \frac{x}{r^2} ,$$

but only if Σ is integrable ($\sigma > 2$), and this requirement can be met only by a zero lift. In general, this integral is proportional to $x r^{-1} \ln r$ at large r (see below).

We may consider two functions ϕ and ϕ_c, satisfying, respectively, (with $\Sigma_c \neq \Sigma$)

$$\nabla^2 \phi = \frac{\partial}{\partial x} \Sigma , \qquad \nabla^2 \phi_c = \frac{\partial}{\partial x} \Sigma_c , \qquad (II.9, II.10)$$

which may not fulfill the requirements for the basic relation (II.7). The latter requirements may be met, however, by the difference $\varphi \equiv \phi - \phi_c$. In the application to be made later in II.3 and also in Appendix III, we will choose a function Σ_c so closely approach Σ at large r that

$$\Sigma - \Sigma_c = O(r^{-\sigma}) , \qquad \sigma > 1 . \qquad (II.11)$$

With this, we construct a ϕ_c, fulfilling (II.2) on T and (II.3) on D, also approaching at large r sufficiently close to ϕ, that

$$\overline{\nabla \varphi} = \overline{\nabla (\phi - \phi_c)} \to 0 , \qquad as \quad r \to \infty . \qquad (II.12)$$

11.3 Capturing the doublet and comparable singularities in the far field of $\hat{\Phi}_0$

The far field behavior of $\hat{\Phi}_0$ (cf. text for governing equations) can be seen from the relation (11.7) to be dominated by a vortex of a strength $\hat{\Gamma}_0 = [\![\hat{\Phi}_0]\!]_{TE}$ (assuming a closed 2-D body). The subsequent terms of orders $r^{-1}\ln r$ and r^{-1} can be captured with the help of $\hat{\Phi}_c$ and $\hat{\varphi} \equiv \hat{\Phi}_0 - \hat{\Phi}_{0c}$, with Σ_{0c} so chosen that $\sigma > 2$.

In order to construct the Σ_c and Φ_c for this case, we employ an analytic function of the complex variable $\zeta = x + i\eta$

$$\left.\begin{aligned} W_c &\equiv \Phi_c + i\Psi_c = \int_a W_c' \, d\zeta \\ W_c' &\equiv \frac{dW_c}{d\zeta} = -4\frac{i\hat{\Gamma}_0}{\pi(b-a)^2}\left[\sqrt{\zeta-a}\sqrt{\zeta-b} - \zeta + \frac{a+b}{2}\right] \end{aligned}\right\} \qquad (11.13)$$

where $\arg.(\zeta - a)$ and $\arg.(\zeta - b)$ are restricted to the range $(0, 2\pi)$, caps "$\wedge$" on $\hat{\Gamma}_0$, $\hat{\zeta}$, $\hat{a}$ and $\hat{b}$ have been omitted for convenience. This function W_c has the desirable properties: (i) $W_c' \to 0$, as $|\zeta| \to \infty$, (ii) W_c' is continuous across the boundary T (T.V. Sheet), (iii) the circulation around the slot W (wing) is Γ_0, and the total source $\int_a^b [\![\Phi_{c\eta}]\!]\, dx$ is zero, hence, $\hat{\Phi}_0 - \Phi_c \to 0$, as $|\zeta| \to \infty$, and (iv) the Kutta condition ($W_c' \neq \infty$) is satisfied not only at the trailing edge (x = b), but also at the leading edge ($x = a$). We then have $\Sigma_0 - \Sigma_{0c} = o(|\zeta|^{-2})$. i.e., σ for $(\Phi_0 - \Phi_c)$ is $\sigma > 2$.

Now construct Φ_{0c} (omitting "$\wedge$" from $\hat{\Phi}_{0c}$) from $\dagger$

$$\nabla^2 \Phi_{0c} = \frac{1+1}{8K_n}\left(\frac{\partial}{\partial\zeta} + \frac{\partial}{\partial\bar{\zeta}}\right)\left(W_c' + \overline{W_c'}\right)^2 \qquad (11.14)$$

which admits a particular integral

$$\begin{aligned} \Phi_{0c}^{(P)} &= \frac{1+1}{16K_n} R.P.\left[\bar{\zeta}(W_c')^2 + 2W_c'\overline{W_c'} - \zeta W_c'^2 - 2W_c' W_c'\right] \\ &= -\frac{1+1}{4K_n} R.P.\left\{ i\frac{\eta}{2}(W_c')^2 + \frac{1}{2}(W_c - \overline{W_c})W_c' \right\} \\ &= -\frac{1+1}{4K_n}\left[\eta(\Phi_c)_x(\Phi_c)_\eta + \Psi_c(\Phi_c)_\eta\right] \end{aligned} \qquad (11.15)$$

$\dagger$ Note that $\bar{\zeta} \equiv x - i\eta$ and that $\partial/\partial\zeta$ is the partial derivative ζ with $\bar{\zeta}$ fixed.

The ϕ_{oc} sought is simply

$$\phi_{oc} \equiv \frac{\gamma+1}{4K_n}\left[\eta(\phi_c)_x(\phi_c)_\eta + \psi_c(\phi_c)_\eta\right] +$$

$$+\frac{\gamma+1}{8\pi K_n}\int_a^b \left[\frac{\partial}{\partial x}\left(\psi_c [\![\phi_c]\!]_x\right) + (\phi_c)_\eta [\![\phi_c]\!]_x\right] \ln r' \, dx_1 \quad (11.16a)$$

which is analytic at, and across, the entire x-axis, i.e.,

$$[\![\phi_{oc}]\!] = [\![\partial\phi_{oc}/\partial\eta]\!] = 0 \qquad \text{at} \quad \eta = 0 \,, \text{ all } x \,. \quad (11.16b)$$

We note that $\phi_{oc}^{(p)}$ is continuous at $\eta = 0$ and that source distribution in (11.16) is introduced to render $\partial\phi_{oc}/\partial\eta$ continuous by cancelling the $\partial\phi_{oc}^{(p)}/\partial\eta$ jump along the x-axis. Thus, we can apply (11.7) to $\phi_o - \phi_{oc}$ to obtain the far-field description for ϕ_o. Interestingly, the last integral in (11.16a) does not give rise to a source in the far field. This is because

$$\int_a^b \left[\frac{\partial}{\partial x}\left(\psi_c [\![\phi_c]\!]_x\right) + (\phi_c)_\eta [\![\phi_c]\!]_x\right] dx_1 = 0 \quad (11.17)$$

on account of

$$[\![\phi_{cx}]\!]_{LE} = [\![\phi_{cx}]\!]_{TE} = 0 \,, \qquad \int_a^b [\![\phi_c]\!]_x (\phi_c)_\eta \, dx = 0 \,.$$

With

$$i\eta(w_c')^2 + (w_c - w_c)w_c' \sim -\left(\frac{\Pi_o}{2\pi}\right)^2 \cdot \left(\frac{i\eta}{\zeta^2} + \frac{2\ln|\zeta|}{\zeta}\right), \quad (11.18)$$

the final result confirming (2.28) in the text is

$$\phi_o \sim \frac{\Pi_o}{2\pi}\left[\tan^{-1}\left(\frac{x}{\eta}\right) + \operatorname{sgn}\eta\right] + \frac{\gamma+1}{16K_n}\left(\frac{\Pi_o}{\pi}\right)^2 \frac{x}{|\zeta|^2}\left[\ln|\zeta| + \frac{\eta^2}{|\zeta|^2}\right] +$$

$$+ D_o^i \frac{\eta}{|\zeta|^2} + D_o^r \frac{x}{|\zeta|^2} + \cdots \quad (11.19a)$$

where the doublet strengths, however, are explicitly related to the solution interior of $\mathcal{D}_\infty$

$$2\pi D_o^i = -\int_a^b [\![\phi_x]\!] x \, dx \ , \tag{11.19b}$$

$$2\pi D_o^r = \int_a^b K_n^{-1/2} [\![Z]\!]_w \, dx - \frac{1+1}{4\pi} \int_a^b [\![x(\phi_c)_x - \phi_c]\!] (\phi_c)_\eta \, dx +$$

$$+ \frac{1+1}{2K_n} \iint_{\mathcal{D}_\infty} \left[(\phi_{ox})^2 - (\phi_{ocx})^2 \right] dx \, d\eta \ . \tag{11.19c}$$

We point out that, in approaching the leading edge, $(\phi_{ox})^2 \sim \text{Const.} \, |x-a|^{-2/3}$ and $(\phi_{cx})^2 \sim \text{Const.} \, |x-a|$, therefore, the last (double) integral of (11.19c) exist. Observe, also, that ϕ_c and its derivatives are continuous across D (the shock), and (11.19) is unaffected by the presence of the (shock) discontinuities.

APPENDIX III

DETERMINATION OF THE SOURCE STRENGTH $\hat{Q}_1$ AND $\tilde{Q}_1$

III.1 Green's Theorem Applied to $\hat{\Phi} = \hat{\Phi}_0 + \epsilon\hat{\Phi}_1$

The solution $\hat{\Phi} = \hat{\Phi}_0 + \epsilon\hat{\Phi}_1$ satisfying PDE (2.6) can be cast formally in a form same as (II.1). In terms of the variables $\hat{\xi} = \hat{x} + i\hat{\eta}$ and $\hat{\xi}_* = \hat{x} - i\hat{\eta}$, and dropping "$\wedge$" from $\hat{\Phi}$, $\hat{x}$, $\hat{y}$, $\hat{\xi}$ and $\hat{\xi}_*$ (also writing $\bar{\xi}$ for $\hat{\xi}_*$). The PDE in question is

$$4\frac{\partial^2}{\partial\xi\,\partial\bar{\xi}}\left(\Phi_0 + \epsilon\Phi_1\right) = \frac{\partial}{\partial x}\left(\Sigma_0 + \epsilon\Sigma_1\right), \tag{III.1}$$

with

$$\Sigma_0 = \frac{\gamma+1}{2K_n}\left(\Phi_{0x}\right)^2,$$

$$\Sigma_1 = \frac{1}{K_n}\left\{\left[2\Theta\frac{\partial}{\partial y} + 2\Theta^2\frac{\Theta'}{K_n}\eta\frac{\partial}{\partial\eta} + \Theta'\right]\Phi_0 + (\gamma+1)\,\Phi_{0x}\,\Phi_{1x}\right\}.$$

The third term of Σ_1 arises from the transformation of (x, z, y) to (x, η, y), with K_n being a function of y in $\eta = \sqrt{K_n}\,z$. In the following, we will apply the result of the Green Theorem, (II.7), to the function

$$\varphi \equiv \left(\Phi_0 + \epsilon\Phi_1\right) - \left(\Phi_{0c} + \epsilon\Phi_{1c}\right) \tag{III.2}$$

with Φ_{0c} given as in (II.16) and Φ_{1c} so constructed to fulfill the requirement for applicability of (II.7). Since the solutions Φ_0 and Φ_1 have only the weak logarithmic dependence on ϵ, the result obtained below for $(\Phi_0 + \epsilon\Phi_1)$ can be equivalently obtained from a separate application of (II.7) to $(\Phi_0 - \Phi_{0c})$ and $\epsilon(\Phi_1 - \Phi_{1c})$. The reason for the consideration of their difference, φ, is for the economy of the theoretical effort, since (II.7) has already been established and shown to be unaffected by the presence of imbedded shocks (for $K_n > 0$). The application of (II.7) to $\epsilon(\Phi_1 - \Phi_{1c})$ for the case in which the shock satisfies the transferred boundary conditions (2.25) - (2.27), does not appear to be straight forward.

Our objective is to capture terms in the far-field description for ϕ_1 up to, and including, the source term. For this purpose, we shall find ϕ_{1c} among the solutions to the Poisson equation

$$4\frac{\partial^2}{\partial\zeta\,\partial\bar{\zeta}}\phi_{1c}=\frac{\partial}{\partial x}\Sigma_{1c} \tag{III.3a}$$

with Σ_{1c} and ϕ_{1c} behaves at large r as

$$\Sigma_1-\Sigma_{1c}=O(|\zeta|^{-\sigma}),\qquad \sigma>1\ , \tag{III.3b}$$

$$\phi_{1c}=O(|\zeta|\cdot\ln|\zeta|)\ . \tag{III.3c}$$

For convenience, ϕ_{1c} and its η-derivative will also be made continuous at the x-axis, i.e.,

$$[\![\,\phi_{1c}\,]\!]=[\![\,\partial\phi_{1c}/\partial\eta\,]\!]=0\ ,\qquad \text{at}\ \ \eta=0\ . \tag{III.3d}$$

The key equation to be arrived at from (II.7) for the present purpose will be therefore,

$$\begin{aligned}(\phi_o-\phi_{oc})+\epsilon(\phi_1-\phi_{1c})=&\frac{1}{2\pi}\int_a^b[\![\,\phi_{o\eta}+\epsilon\phi_{1\eta}\,]\!]\ln r\,dx_1\ -\\ &-\frac{1}{2\pi}\int_a^b[\![\,\phi_{ox}+\epsilon\phi_{1x}\,]\!]\left\{\tan^{-1}\left(\frac{x-x_1}{\eta}\right)+\frac{\pi}{2}\,\mathrm{sgn}\,\eta\right\}\ -\\ &-\frac{1}{2\pi}\iint_{\mathcal{D}_\infty}\frac{x_1-x}{|\zeta|^2}\left[\Sigma_o-\Sigma_{oc}+\epsilon(\Sigma_1-\Sigma_{1c})\right]dx_1d\eta_1\ .\end{aligned} \tag{III.4}$$

For this equation to be valid in the case involving a shock, the distribution of Σ_o must be computed with the discontinuities of ϕ_{ox} and $\phi_{o\eta}$ evaluated (not at $x=x_o^D(\eta)$, but) at the shock boundary

$$x=x_o^D(\eta)+\epsilon\,x_1^D(\eta)\ . \tag{III.5}$$

Therefore, the relation among terms with subscripts "o" in (III.4) is not identical to the corresponding relation for the leading approximation obtained previously in § II.3, Appendix II, as long as $\epsilon\to 0$. In the far field ($|\zeta|\to\infty$), however, since (cf. § II.3),

$$\Sigma_o-\Sigma_{oc}=O(|\zeta|^{-\sigma}),\qquad \sigma>2\ ,$$

and, whether an imbedded shock exists or not,

$$-\frac{1}{2\pi}\iint_{\mathcal{A}_\infty}\frac{x_1-x}{|\zeta|^2}\left(\Sigma_o-\Sigma_{oc}\right)d\xi_1 d\eta_1 \sim \frac{1}{2\pi}\iint_{\mathcal{A}_\infty}\left(\Sigma_o-\Sigma_{oc}\right)d\xi_1 d\eta_1\cdot\frac{x}{|\zeta|^2}, \tag{III.6}$$

Therefore, the presence of an imbedded shock can make an additional contribution, if any, to the relation in the far field

$$\phi_1-\phi_{1c}\sim\frac{M_1}{2\pi}\left[\tan^{-1}\left(\frac{x}{\eta}\right)+\frac{\pi}{2}\operatorname{sgn}\eta\right]-$$

$$-\frac{1}{2\pi}\iint_{\mathcal{A}_\infty}\frac{x_1-x}{|\zeta|^2}\left(\Sigma_1-\Sigma_{1c}\right)d\xi_1 d\eta_1+O(|\zeta|^{-2}), \tag{III.7}$$

only as a doublet, hence, not of great consequence. Since the double integral in (III.7) vanishes in the limit $|\zeta|\to\infty$ when condition (III.3b) is met, the source term in the far-field description of ϕ_{1c} must be the same as in that of ϕ_1. The remaining task is, therefore, to construct Σ_{1c} and ϕ_{1c}.

Having in mind the requirement (III.3b), and the form of Σ_1, we take Σ_{1c} to be

$$\Sigma_{1c}=\frac{1}{K_n}\left\{\left[2\textcircled{M}\frac{\partial}{\partial y}+2\textcircled{M}^2\frac{\textcircled{M}'}{K_n}\eta\frac{\partial}{\partial\eta}+\textcircled{M}'\right]\phi_{0A}+\right.$$

$$\left.+(\gamma+1)\frac{\partial}{\partial x}(\phi_c)\cdot\frac{\partial}{\partial x}(\phi_{1cc})\right\}, \tag{III.8}$$

with ϕ_{0A} and ϕ_{1cc} chosen to yield, at large $|\zeta|$

$$\left.\begin{aligned}\phi_0-\phi_{0A}&=O\left[(\ln|\zeta|)^p|\zeta|^{-2}\right],\\ \phi_1-\phi_{1cc}&=O(1),\end{aligned}\right\} \tag{III.9}$$

where $p\neq\infty$. This choice of Σ_{1c} will make

$$\Sigma_1-\Sigma_{1c}=O\left[(\ln|\zeta|)^2|\zeta|^{-2}\right], \tag{III.10}$$

thus, fulfilling (III.3b).

It suffices to take

$$\phi_{0A}=\phi_c+\phi_{oc}^{(p)}+\phi_d \tag{III.11}$$

where ϕ_c and ϕ_{oc} are the same given earlier in § II.3. The ϕ_d is a Laplace solution (to the thin-airfoil problem) introduced to account for the doublet behaviour in the far-field and can be represented by the vortex and source distribution ϕ_d = R.P. (W_d)

$$W_d = \frac{1}{2\pi} \int_a^b (q + i\gamma_d)[\ln(\zeta - s) - i\pi]\, ds \qquad \text{(III.12)}$$

such that

$$\int_a^b [\![\phi_{dx}]\!]\, dx = [\![\phi_d]\!]_{TE} = 0, \qquad \int_a^b [\![\phi_{d\eta}]\!]\, dx = 0,$$

$$\int_a^b [\![\phi_{d\eta}]\!]\, x\, dx = -\pi D_o^r$$

$$\int_a^b \frac{\partial}{\partial x} \langle \phi_c - \phi_d \rangle\, x\, dx = -\frac{\pi}{2} D_o^i. \qquad \text{(III.13a,b,c,d)}$$

Thus, at large $|\zeta|$, $\phi_{oA} \sim \phi_o + O[(\ln|\zeta|)^p |\zeta|^{-2}]$ and the first of (III.9) is fulfilled. Notice that the "Kutta condition" at the leading and trailing edges are unnecessary for ϕ_d, as long as ϕ_{dx} and $\phi_{d\eta}$ are integrable in x on the wing.

For the ϕ_{1cc} in Σ_{1c}, it suffices to take a particular solution to (III.3a) with the omission of the nonlinear (last) term of Σ_{1c} in (III.8), because the nonlinear contribution is of an order $|\zeta|^{-1}$ higher at large $|\zeta|$. This leads to (with $K_o = K_n - \mathcal{M}^2$)

$$\phi_{1cc} = \frac{\mathcal{M}}{2K_n}\left[\frac{\partial}{\partial y} + \frac{1}{2}\frac{\mathcal{M}'}{\mathcal{M}}\frac{K_o}{K_n}\frac{\bar{\zeta}-\zeta}{2}(W_c - \bar{W}_c) - \right.$$

$$\left. - \frac{\mathcal{M}\mathcal{M}'}{8K_n}(\zeta-\bar{\zeta})^2(W_c' - \bar{W}_c')\right] \qquad \text{(III.14)}$$

With ϕ_{1cc} and ϕ_{oA} so chosen, we see that Σ_{1c} can fulfill the requirement (III.10). We may now proceed to seek a solution to (III.3a) for the ϕ_{1c}. This will be carried out in III.2 below for straight oblique wing only, for which $\mathcal{M}' \equiv 0$.

III.2 The far-field description and determination of $\hat{Q}_1$ for straight oblique wings

With the foregoing choices of ϕ_{0A}, ϕ_{1cc}, and ϕ_c, Σ_{1c} can be expressed in terms of ϕ_c or W_c. For oblique wings with $\Theta' = 0$, we have

$$\Sigma_{1c} = \frac{2\Theta}{K_n}\frac{\partial}{\partial y}\phi_{0A} + \frac{\gamma+1}{K_n}(\phi_c)_x(\phi_{1cc})_x$$

$$= 2\frac{\Theta}{K_n}\left\{\frac{1}{2}\frac{\partial}{\partial y}\left(W_c' + \bar{W}_c' + W_d' + \bar{W}_d'\right) + \frac{\gamma+1}{16K_n}\frac{\partial}{\partial y}\left[(\bar{\varsigma}-\varsigma)\left(W_c'W_c'' - \right.\right.\right.$$

$$\left. - \overline{W'W_c''} - (W_c' - \bar{W}_c')^2 - (W_c - \bar{W}_c)(W_c'' - \bar{W}_c'')\right]\Bigg\} +$$

$$+ \frac{(\gamma+1)}{4K_n^2}\Theta\left\{\frac{\partial}{\partial y}\left[\frac{\bar{\varsigma}}{2}W_c'W_c'' + \frac{\varsigma}{2}\overline{W_c'W_c''} - \frac{\varsigma}{2}W_cW_c'' - \frac{\bar{\varsigma}}{2}\overline{W_cW_c''}\right] + \right.$$

$$\left. + \frac{\varsigma-\bar{\varsigma}}{2}\left(\bar{W}_{cy}'W_c'' - W_{cy}'\bar{W}_c''\right) - \frac{\varsigma-\bar{\varsigma}}{2}\left(\bar{W}_c'W_{cy}'' - W_c'\bar{W}_{cy}''\right)\right. \tag{III.15}$$

where the first and second groups of terms under curly brackets arises from $(2\Theta/K_n)\partial\phi_{0A}/\partial y$ and $[(\gamma+1)/K_n]\cdot(\phi_c)_x\cdot(\phi_{1cc})_x$, respectively. A particular solution $\phi_{1c}^{(P)}$ to the Poisson equation (III.3a) can be obtained by directly integrating with respect to ς and $\bar{\varsigma}$, adding suitable function of ς and $\bar{\varsigma}$ to facilitate fulfillment of conditions (III.3c) and (III.3d) for ϕ_{1c}. The results can be written as

$$\phi_{1c}^{(P)} = -\frac{1}{2K_n}\frac{\partial}{\partial y}\left\{\frac{\varsigma\bar{\varsigma}}{2}\left[(W_c-\bar{W}_c)+(W_d-\bar{W}_d)\right]\right\} +$$

$$+ \frac{(\gamma+1)\Theta}{32K_n^2}\left\{2\left(\frac{\varsigma\bar{\varsigma}}{2}\right)^2\frac{\partial}{\partial y}\left(W_c'^2+\bar{W}_c'^2\right) + (\varsigma+\bar{\varsigma})\frac{\partial}{\partial y}\left(\int_\infty (W_c')^2 d\varsigma + \int_\infty \overline{(W_c')^2 d\varsigma}\right) - \right.$$

$$- \frac{\partial}{\partial y}(W_c-\bar{W}_c)^2 + \frac{\partial}{\partial y}\left[(W_c-\bar{W}_c)(\varsigma\bar{W}_c' - \bar{\varsigma}W_c')\right] +$$

$$+ \varsigma W_c'\bar{W}_{cy} + \bar{\varsigma}\bar{W}_c'W_{cy} - \bar{W}_c(\varsigma W_c')_y - W_c(\overline{\varsigma W_c'})_y -$$

$$\left. - \frac{1}{\pi}\frac{\partial\Gamma}{\partial y}i(\varsigma-\bar{\varsigma})(W_c'+\bar{W}_c') - \frac{2}{\pi}i(W_c'-\bar{W}_c')\int_a^b \frac{\partial}{\partial y}\gamma_c(s;y)\ln|s-s|ds\right\}. \tag{III.16}$$

This function has the following properties:

(i) At large $|\varsigma|$, $\phi_{1c}^{(p)}$ fulfills not only (III.3c), but agrees completely with ϕ_1 of (2.29) after setting $\textcircled{H}' = 0$ therein, except for the absence of the (additive) harmonic functions R.P. $\{-C_1^i\eta + C_1^r x + \frac{1}{2\pi}(Q_1 + i\Gamma_1)(\ln\varsigma - i\pi)\}$.

(ii) The far-field of $\phi_{1c}^{(p)}$ contains no source and vortex terms, to be sure.

(iii) $\phi_{1c}^{(p)}$ is continuous (no jump) across the x-axis (i.e., at $\eta = 0$ for all x), hence, fulfilling requirement $[\![\phi_{1c}]\!]_T = 0$.

We observe in this connection that $(w_c - \bar{w}_c)$ and $(w_c' - \bar{w}_c')$ are symmetric in η, so are

$$\varsigma w_c' \bar{w}_{cy} + \bar{\varsigma} w_c' w_{cy} - \bar{w}_c (\varsigma w_c')_y - w_c (\bar{\varsigma} \bar{w}_c')_y$$

and

$$\frac{\partial}{\partial y}(w_c - \bar{w}_c)(\varsigma \bar{w}_c' - \bar{\varsigma} w_c');$$

and that

$$\int_\infty w_c'^2 d\varsigma + \int_\infty \overline{w_c'^2 d\varsigma}$$

can be represented in terms of $\gamma_c(x) = [\![\phi_{cx}]\!] = 4\frac{M_e}{\pi}|(x-a)(x-b)|^{1/2}(b-a)^{-2}$ as

$$-\frac{1}{2\pi^2}\int_a^b\int_a^b \frac{\gamma_c(s_1)\gamma_c(s_2)}{s_1 - s_2} \ln\left|\frac{\varsigma - s_1}{\varsigma - s_2}\right| ds_1 ds_2 -$$

$$-\frac{1}{2\pi}\frac{dP}{dy} i(\varsigma - \bar{\varsigma})(w_c' - \bar{w}_c') + \frac{i}{\pi}(w_c' - \bar{w}_c')\int_a^b \frac{\partial}{\partial y}(\gamma_c(s;y)) s \ln|\varsigma - s| ds,$$

which again has the symmetry in η. We, thus, may complete the determination of ϕ_{1c} by adding a source distribution so that

$$\phi_{1c} = \phi_{1c}^{(p)} - \frac{1}{2\pi}\int_{-\infty}^{\infty} [\![\partial\phi_{1c}^{(p)}/\partial\eta]\!] \ln|\varsigma - s| ds \qquad (III.17)$$

may fulfill the requirement on the $\partial\phi_{1c}/\partial\eta$ across the x-axis, cf. (III.3d). In approaching the x-axis, $\partial\phi_{1c}^{(p)}/\partial\eta$ can be evaluated from

$$\frac{\partial}{\partial\eta}\left(\phi_{1c}^{(p)}\right) = i\left(\frac{\partial}{\partial\xi}-\frac{\partial}{\partial\bar{\xi}}\right)\phi_{1c}^{(p)} \sim \frac{M}{K_n}\frac{\partial}{\partial y}(\psi_c+\psi_d) +$$

$$+\frac{\gamma+1}{32K_n^2}M\left\{\frac{\partial}{\partial y}\left[\frac{\partial}{\partial x}\left(6x(\phi_c)_x\psi_c - 2x\phi_c(\psi_c)_x\right) - 16x(\phi_c)_x(\psi_c)_x\right] +\right.$$

$$+\frac{4}{\pi}\frac{dP}{dy}(\phi_c)_x + 8x(\phi_c)_x(\psi_c)_{xy} -$$

$$\left.-\frac{4}{\pi}(\phi_c)_{xx}\frac{\partial}{\partial y}\int_a^b \gamma_c(s;y)\, s\ln|x-s|\,ds\right\} \qquad \text{(III.18)}$$

This gives

$$[\![\frac{\partial\phi_{1c}^{(p)}}{\partial\eta}]\!]_{\eta=0} = \frac{M}{K_n}\frac{\partial}{\partial y}[\![\psi_d]\!] + \frac{(\gamma+1)M}{32K_n^2}\left\{\frac{\partial}{\partial y}\left[\frac{\partial}{\partial x}\left(6x\psi_c[\![\psi_{cx}]\!] - 2x\psi_{cx}[\![\phi_c]\!]\right)-\right.\right.$$

$$\left.-16x(\psi_c)_x[\![\phi_{cx}]\!]\right] + \frac{4}{\pi}\frac{dP}{dy}[\![\phi_{cx}]\!] + 8x(\psi_c)_{xy}[\![\phi_{cx}]\!] -$$

$$\left.-\frac{4}{\pi}[\![\phi_{cxx}]\!]\frac{\partial}{\partial y}\int_a^b \gamma_c(s;y)\, s\ln|x-s|\,ds\right\} \qquad \text{(III.19)}$$

We observe that, over the wake portion,

$$[\![\partial\phi_{1c}^{(p)}/\partial\eta]\!]_T = 0\,, \qquad \text{(III.20)}$$

since ψ_d and ϕ_{cx} is continuous across the x-axis downstream of the T.E.

Since ϕ_{1c} does not give rise to a source in the far-field, we have, as $|\xi|\to\infty$, a source strength for ϕ_{1c} as (recalling "$\wedge$" has been omitted from $\hat{\phi}_1$ and $\hat{Q}_1$)

$$Q_1 = Q_{1c} = -\frac{1}{2\pi}\int_a^b [\![\partial\phi_{1c}^{(p)}/\partial\eta]\!]\,dx$$

$$= 2\pi\frac{M}{K_n}\frac{\partial}{\partial y}D_0^r + \frac{\gamma+1}{8\pi K_n^2}M\frac{\partial}{\partial y}\frac{b\Gamma^2}{b-a} +$$

$$+\frac{1+1}{2K_n^2}\,\textcircled{H}\cdot\frac{\partial}{\partial y}\int_a^b x(\psi_c)_x\,[\![\phi_{cx}]\!]\,dx\;+$$

$$-\frac{(1+1)\,\textcircled{H}}{8K_n^2\pi}\,\Gamma\frac{d\Gamma}{dy}-\frac{1+1}{4K_n^2}\,\textcircled{H}\cdot\int_a^b x\,[\![\phi_{cx}]\!]\,\psi_{cxy}\,dx\;+$$

$$+\frac{1+1}{8\pi K_n^2}\,\textcircled{H}\cdot\int_a^b [\![\phi_{cxx}]\!]\frac{\partial}{\partial y}\int_a^b \gamma_c(s;y)\,s\,\ln|x-s|\,ds \qquad (III.21)$$

The above result for straight oblique wings (with $\textcircled{H}' \equiv 0$) does not require the assumption of a local similarity in the 3-D structure. In cases in which the 3-D similitude applies, the far-field source strength $\tilde{Q}_1$ for the similarity solution $\tilde{\phi}_1$, cf. (4.14b), can be determined from (III.2) through (4.16b)

$$\tilde{Q}_1 = \frac{\hat{Q}_1}{\textcircled{H}\,\hat{c}\hat{c}'} + \frac{1+1}{4\pi K_n^2}\,\tilde{\Pi}_0^2\ln\hat{c}\;,$$

noting in this case that $\partial/\partial\hat{y} = -(\hat{c}'/\hat{c})\,[\hat{x}\,\partial/\partial\hat{x} + \hat{z}\,\partial/\partial\hat{z}]$, and using (4.15) to relate $\hat{\Pi}_0$, $\hat{D}_0^r$, and $\hat{D}_0^i$ to $\tilde{\Pi}_0$, $\tilde{D}_0^r$, and $\tilde{D}_0^i$. The final result for the source strength in the far-field $\tilde{\phi}_1$ is (with $\tilde{\beta}-\tilde{\alpha}=2$)

$$\tilde{Q}_1 = \frac{4\pi}{K_n}\,\tilde{D}_0^r + \frac{1+1}{8\pi K_n^2}\,\tilde{\Pi}_0^2\,[3+\hat{\alpha}+4(1+\hat{\alpha})^2]. \qquad (III.22)$$

FIGURE CAPTIONS

Figure 1 Illustration of the reference chord, the span and the aspect ratio used for a straight oblique wing(a), a more general curved oblique wing(b), and symmetric swept wings(c); the shaded areas in (c) indicates regions of breakdown. Breakdown (nonuniformity) of the theory may also occur in the tip region (cf. text).

Figure 2 Illustration of the Cartesian and the orthogonal curvilinear coordinate systems in the wing plane ($z = z' = 0$).

Figure 3 Examples of $\tilde{\phi}_{0\tilde{x}}$, $\tilde{\phi}_{1\tilde{x}}$, and $\tilde{\phi}_{2\tilde{x}}$ on the upper and lower surfaces of a straight oblique wing at $K_n = 3.6$. The airfoil section is NASA 3612-02, 40 rescaled to an arbitrary thickness.(Refer to text for results shown in dots); wing has no twist and bend; local incidence is zero.

Figure 4(a) Results for a straight oblique wing at $K_n = 3.45$ at two incidences: $\Delta\alpha = 0$ (in solid curve) and $\Delta\alpha = 0.582\tau$ (in dash curve). Distribution of $\tilde{\phi}_{0\tilde{x}}$.

Figure 4(b) (Continued) Distribution of $\tilde{\phi}_{1\tilde{x}}$.

Figure 4(c) (Continued) Distribution of $\tilde{\phi}_{2\tilde{x}}$.

Figure 5(a) Comparison with a major to minor axes ratio of 20 at 22.5° sweep and a free-stream Mach number 0.8242. The present result is shown in solid curve. This graph gives C_p distrubution at the span station $\tilde{y} = -0.69$.

Figure 5(b) (Continued) Span station $\tilde{y} = 0$.

Figure 5(c) (Continued) Span station $\tilde{y} = .69$.

Figure 6(a) Comparison for a 12% thick elliptic oblique wing with major to-minor axes ratio of 14 at 30° yaw and $M_\infty = 0.7549$. This graph gives surface C_p at span station $\tilde{y} = -0.89$.

Figure 6(b) (Continued) Span station $\tilde{y} = -0.69$.

Figure 6(c) (Continued) Span station $\tilde{y} = 0$.

Figure 6(d) (Continued) Span station $\tilde{y} = 0.69$.

Figure 6(e) (Continued) Span station $\tilde{y} = 0.89$

Figure 7(a) Comparison for a 12% thick, elliptic oblique wing with an axes ratio 14 at 30° yaw and $M_\infty = 0.7677$ This graph gives surface C_p at span station $\tilde{y} = -0.79$.

Figure 7(b) (Continued) Span station $\tilde{y} = -0.59$.

Figure 7(c) (Continued) Span station $\tilde{y} = -0.20$.

Figure 7(d) (Continued) Span station $\tilde{y} = 0$.

Figure 7(e) (Continued) Span station $\tilde{y} = 0.20$.

Figure 7(f) (Continued) Span station $\tilde{y} = 0.59$.

Figure 7(g) (Continued) Span station $\tilde{y} = 0.79$.

Figure 8 Surface distributions of $\tilde{\phi}_{1\tilde{x}}$ on a nonlifting oblique wing with an airfoil section NACA 64006 for a component similarity parameter of $K_n = 2.50$. The surface value of $\tilde{\phi}_{0\tilde{x}}$ can be recovered from the $C_{p'(0)}$ distribution shown (cf. text).

Figure 9 Comparison of surface $C_{p'}$ on a nonlifting elliptic oblique wing obtained from local-similarity solutions (in discrete symbols) with corresponding numerical data via the unsteady analogy (in solid curves). The airfoil section and K_n value are the same as in Figure 8, and $\epsilon(M)$ is taken to be 0.10, using $\tilde{\phi}_{1\tilde{x}}$ for case (A) of Figure 8. The $C_{p'}$ is computed for a 6% thickness ratio and $M_n = 0.827$. The latter conditions together with $\epsilon(M) = 0.10$, gives $M_\infty = 0.895$ and $R_1 = 22.6$ for a sweep angle of $\Lambda = 22.5°$.

Figure 10(a) Comparison of surface $C_{p'}$ on a nonlifting obique wing of lenticular planform from the local-similarity solution's (in discrete symbols) with the corresponding numerical data via the unsteady analogy (in solid curves). The airfoil section and K_n value are the same as in Figure 8, and $\epsilon(M) = 0.10$, using $\tilde{\phi}_{1\tilde{x}}$ for case(A) of Figure 8. This graph shows results for three span stations on the aft panel, $\tilde{y} = 0$, 0.5 and 0.8.

Figure 10(b) (Continued) Span stations on the fore panel, $\tilde{y} = -0.2$ and -0.5.

Figure 11(a) Comparison of surface $C_{p'}$ on a nonlifting oblique wing of half-lenticular planform, with the straight axis at the leading edge. The $\tilde{\phi}_{1\tilde{x}}$ for case (B) is used for computing $C_{p'}$ which is computed otherwise in the same manner as in Figure 10. This graph shows results for span station $\tilde{y} = 0$, 0.50 and 0.80 on the aft panel.

Figure 11(b) (Continued) Span stations $\tilde{y} = -0.2$, and -0.50 on the fore panel.

Figure 12(a) Comparison of surface $C_{p'}$ on a nonlifting oblique wing of half-lenticular planform, with the straight axis at the trailing edge. This pertains to case (C) in Figure 10. The graph shows results for span stations $\tilde{y} = 0$, 0.50, and 0.80.

Figure 12(b) (Continued) Span stations $\tilde{y} = -0.2$ and -0.5 on the fore panel.

Figure II.1 Illustration of the wing boundary (W), the trace boundary (T), and the shock-discontinuity boundary (D).

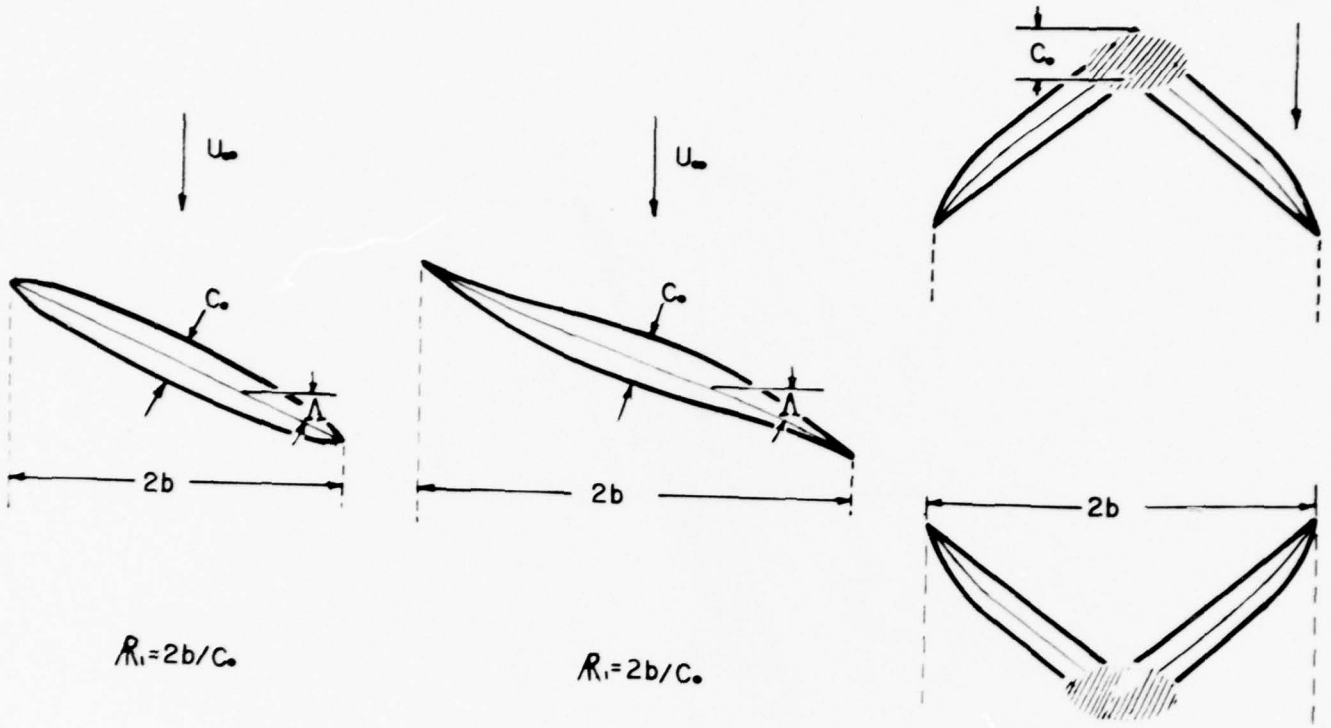

$AR_1 = 2b/C_\infty$

$AR_1 = 2b/C_\infty$

$AR_1 = 2b/C_\infty$

(a)

(b)

(c)

Figure 1

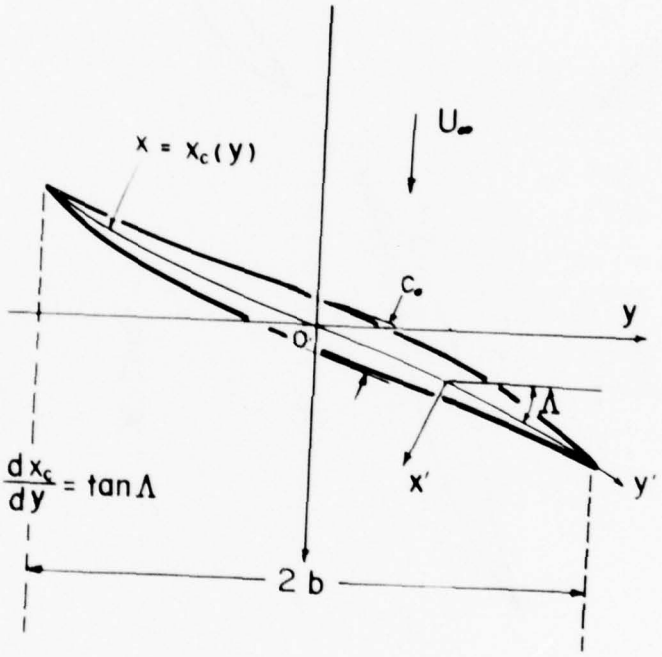

Figure 2

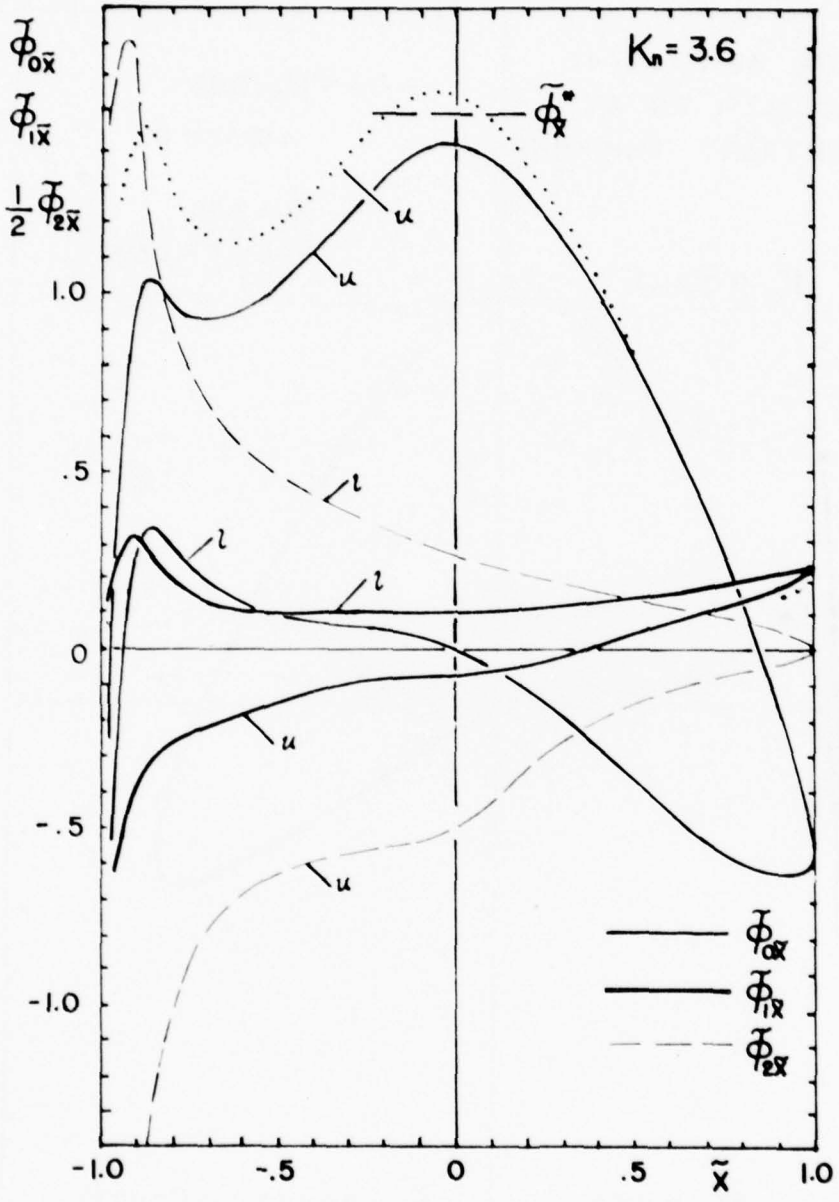
$K_n = 3.6$
$\tilde{\Phi}^*_{\tilde{x}}$
$\Phi_{0\tilde{x}}$
$\Phi_{1\tilde{x}}$
$\frac{1}{2}\Phi_{2\tilde{x}}$
u
l
1.0
.5
0
-.5
-1.0
-1.0
-.5
0
.5
1.0
$\tilde{x}$

Figure 3

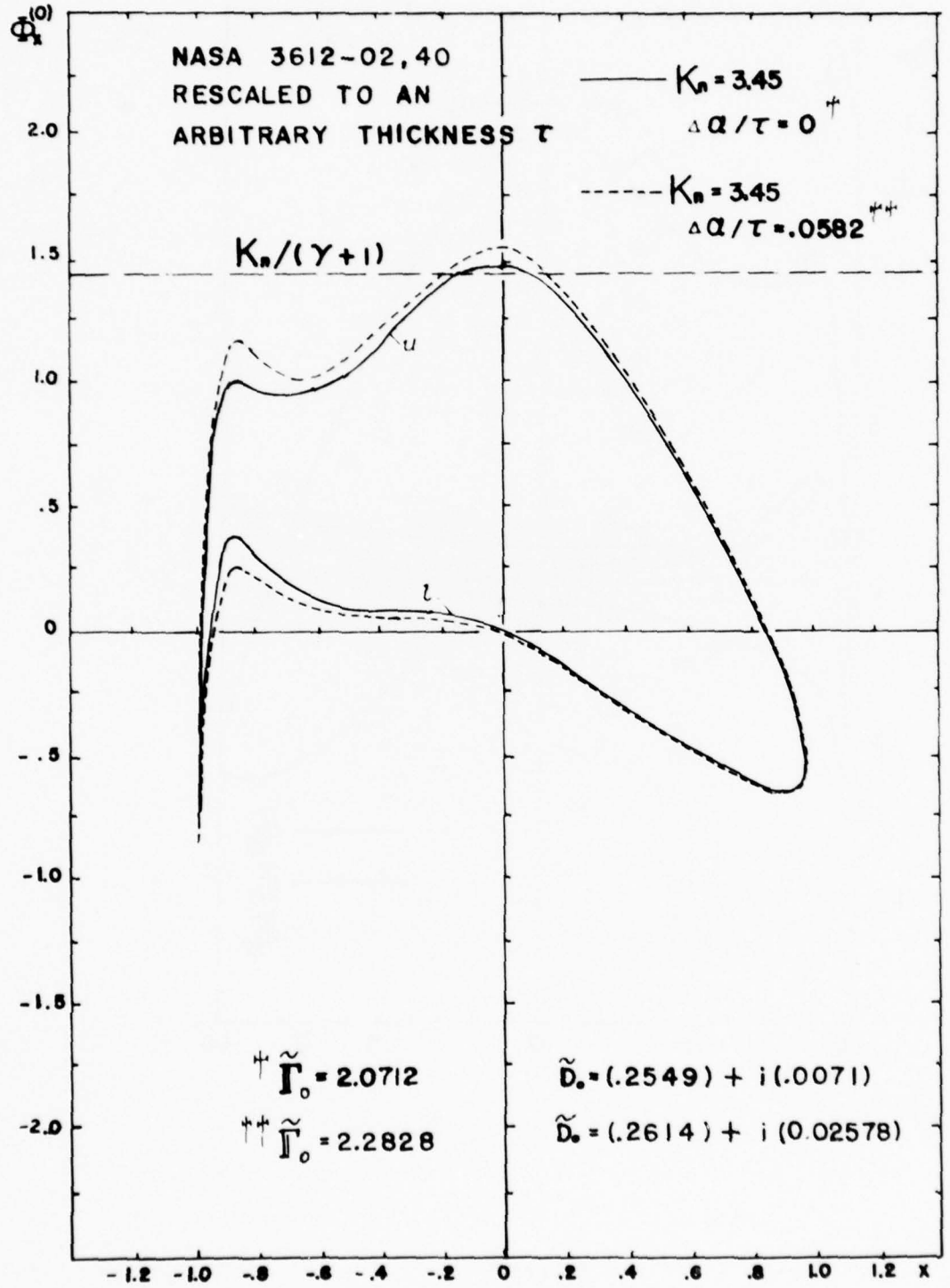
NASA 3612-02,40
RESCALED TO AN
ARBITRARY THICKNESS τ
$K_n = 3.45$
$\Delta\alpha/\tau = 0$ †
$K_n = 3.45$
$\Delta\alpha/\tau = .0582$ ††
$K_n/(\gamma+1)$
u
l
$\Phi_x^{(0)}$
† $\tilde{\Gamma}_0 = 2.0712$
†† $\tilde{\Gamma}_0 = 2.2828$
$\tilde{D}_0 = (.2549) + i(.0071)$
$\tilde{D}_0 = (.2614) + i(0.02578)$
2.0
1.5
1.0
.5
0
-.5
-1.0
-1.5
-2.0
-1.2 -1.0 -.8 -.6 -.4 -.2 0 .2 .4 .6 .8 1.0 1.2 x

Figure 4(a)

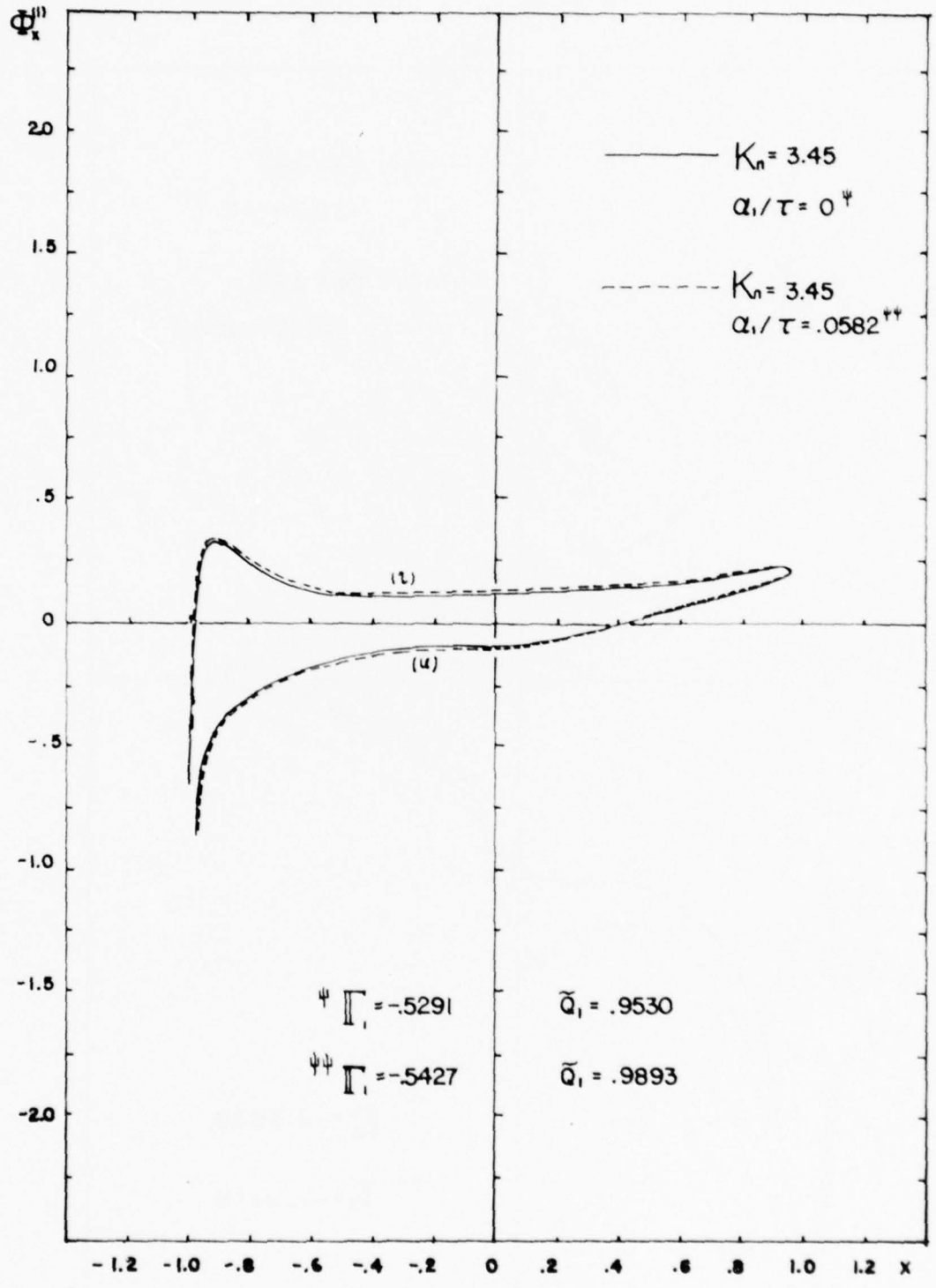
$\Phi_x^{(1)}$
2.0
1.5
1.0
.5
0
-.5
-1.0
-1.5
-2.0
$K_n = 3.45$
$a_1/\tau = 0^{\psi}$
$K_n = 3.45$
$a_1/\tau = .0582^{\psi\psi}$
(l)
(u)
$^{\psi}\Gamma_1 = -.5291$
$\tilde{Q}_1 = .9530$
$^{\psi\psi}\Gamma_1 = -.5427$
$\tilde{Q}_1 = .9893$
-1.2 -1.0 -.8 -.6 -.4 -.2 0 .2 .4 .6 .8 1.0 1.2 X

Figure 4(b)

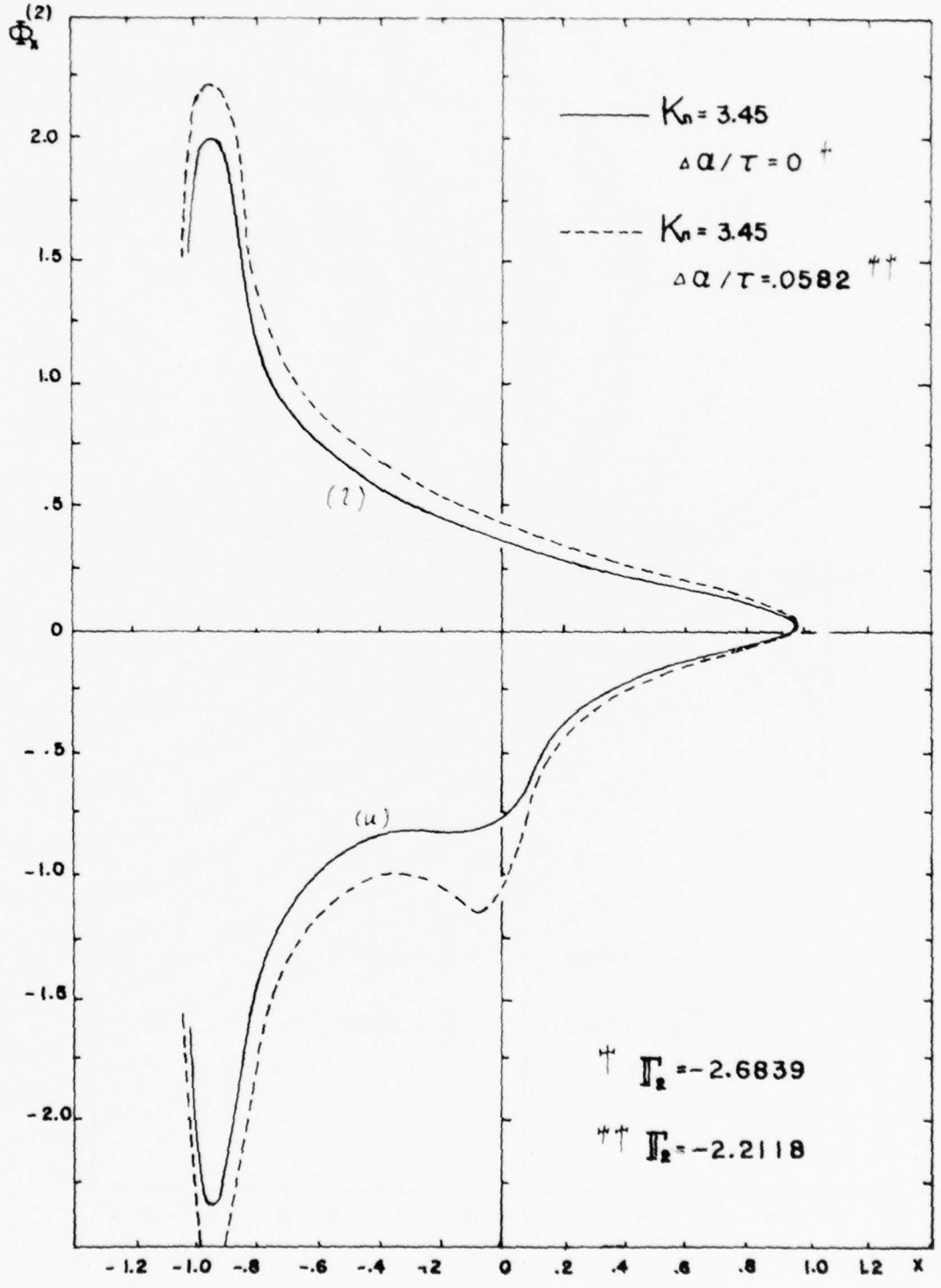
$\Phi_R^{(2)}$
$K_n = 3.45$
$\Delta\alpha/\tau = 0$ †
$K_n = 3.45$
$\Delta\alpha/\tau = .0582$ ††
(l)
(u)
† $\Gamma_R = -2.6839$
†† $\Gamma_R = -2.2118$
2.0
1.5
1.0
.5
0
-.5
-1.0
-1.5
-2.0
-1.2
-1.0
-.8
-.6
-.4
-.2
0
.2
.4
.6
.8
1.0
1.2
X

Figure 4(c)

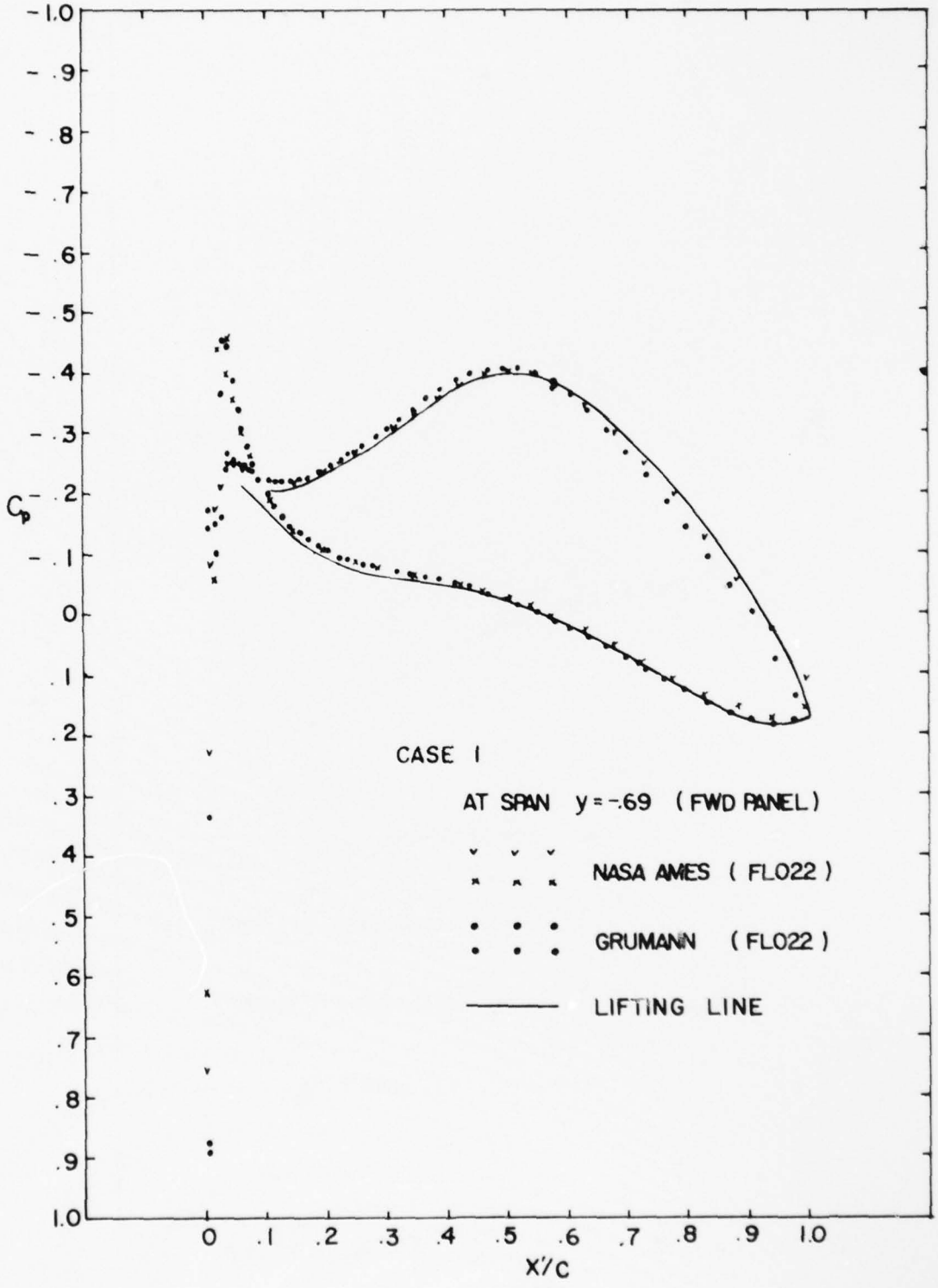
-1.0
-.9
-.8
-.7
-.6
-.5
-.4
-.3
-.2
-.1
0
.1
.2
.3
.4
.5
.6
.7
.8
.9
1.0
C_p
0
.1
.2
.3
.4
.5
.6
.7
.8
.9
1.0
X'/C
CASE 1
AT SPAN y = -.69 (FWD PANEL)
NASA AMES (FL022)
GRUMANN (FL022)
LIFTING LINE

Figure 5(a)

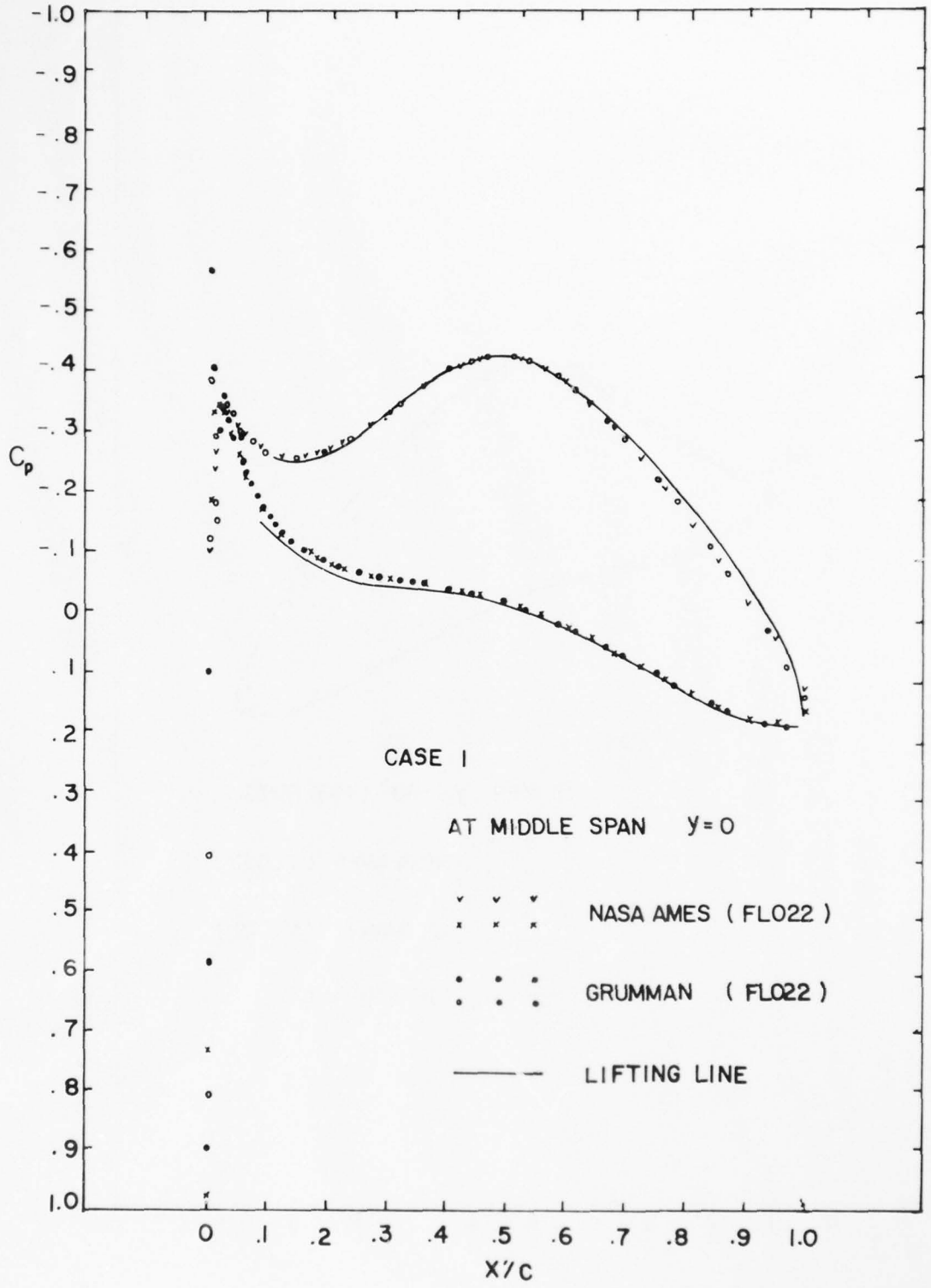
-1.0
-.9
-.8
-.7
-.6
-.5
-.4
-.3
-.2
-.1
0
.1
.2
.3
.4
.5
.6
.7
.8
.9
1.0
C_p
0
.1
.2
.3
.4
.5
.6
.7
.8
.9
1.0
X/C
CASE 1
AT MIDDLE SPAN y=0
NASA AMES (FL022)
GRUMMAN (FL022)
LIFTING LINE

Figure 5(b)

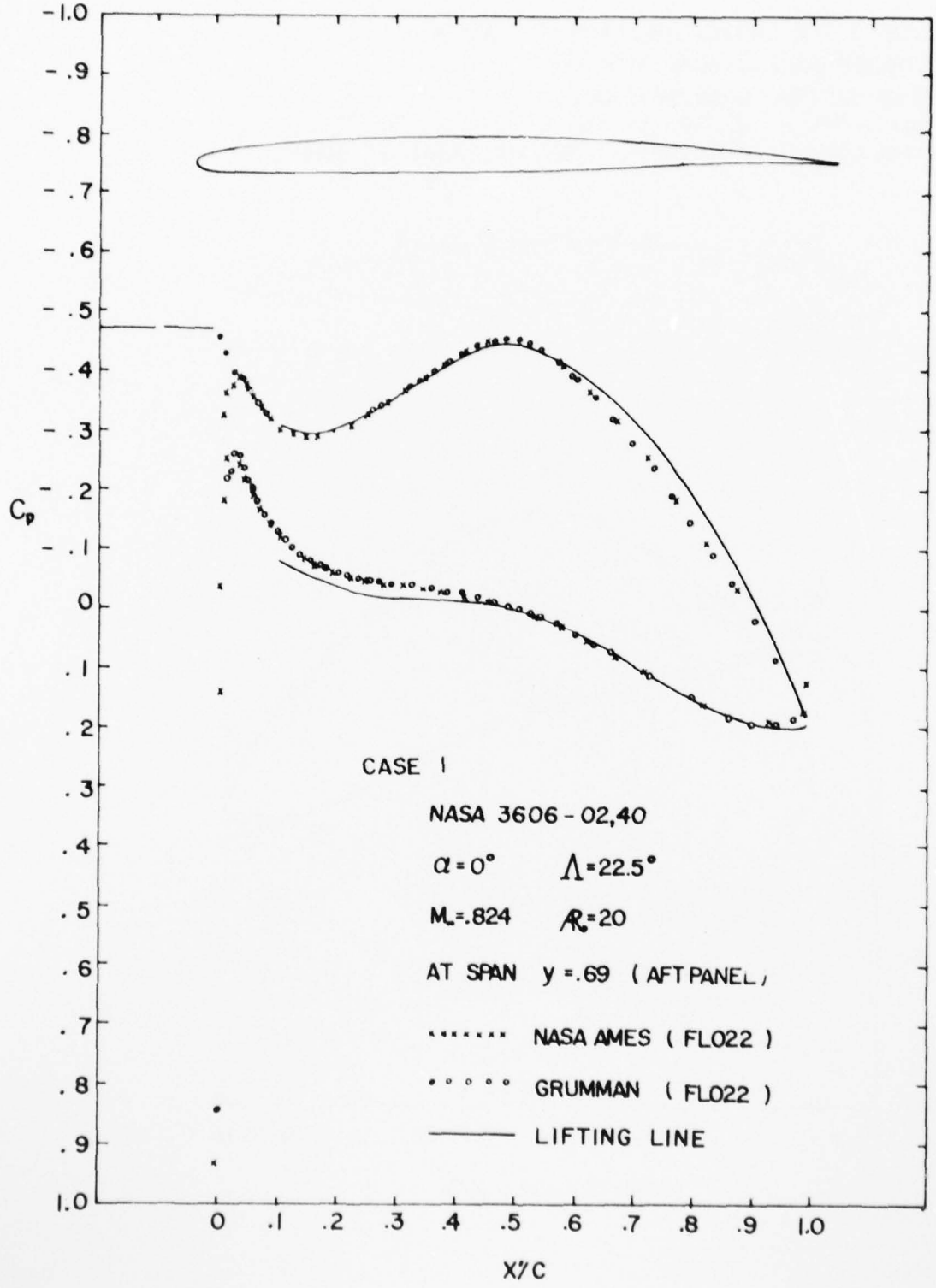
-1.0
-.9
-.8
-.7
-.6
-.5
-.4
-.3
-.2
-.1
0
.1
.2
.3
.4
.5
.6
.7
.8
.9
1.0
C_p
CASE 1
NASA 3606-02,40
$\alpha = 0°$ $\Lambda = 22.5°$
$M_\infty = .824$ $R_e = 20$
AT SPAN y = .69 (AFT PANEL)
NASA AMES (FL022)
GRUMMAN (FL022)
LIFTING LINE
0 .1 .2 .3 .4 .5 .6 .7 .8 .9 1.0
X/C

Figure 5(c)

CASE 3 ELLIPTICAL PLANFORM $AR_o = 14$
STRAIGHT AXIS AT 50% CHORD
WING SECTION NASA 36 12-02, 40
$M_\infty = 0.755$ $\Lambda = 30^\circ$ $\alpha = 0^\circ$
SPAN STATION $y'/b' = -0.89$ SEC. LIFT COEFF. $C_L = 0.2671$

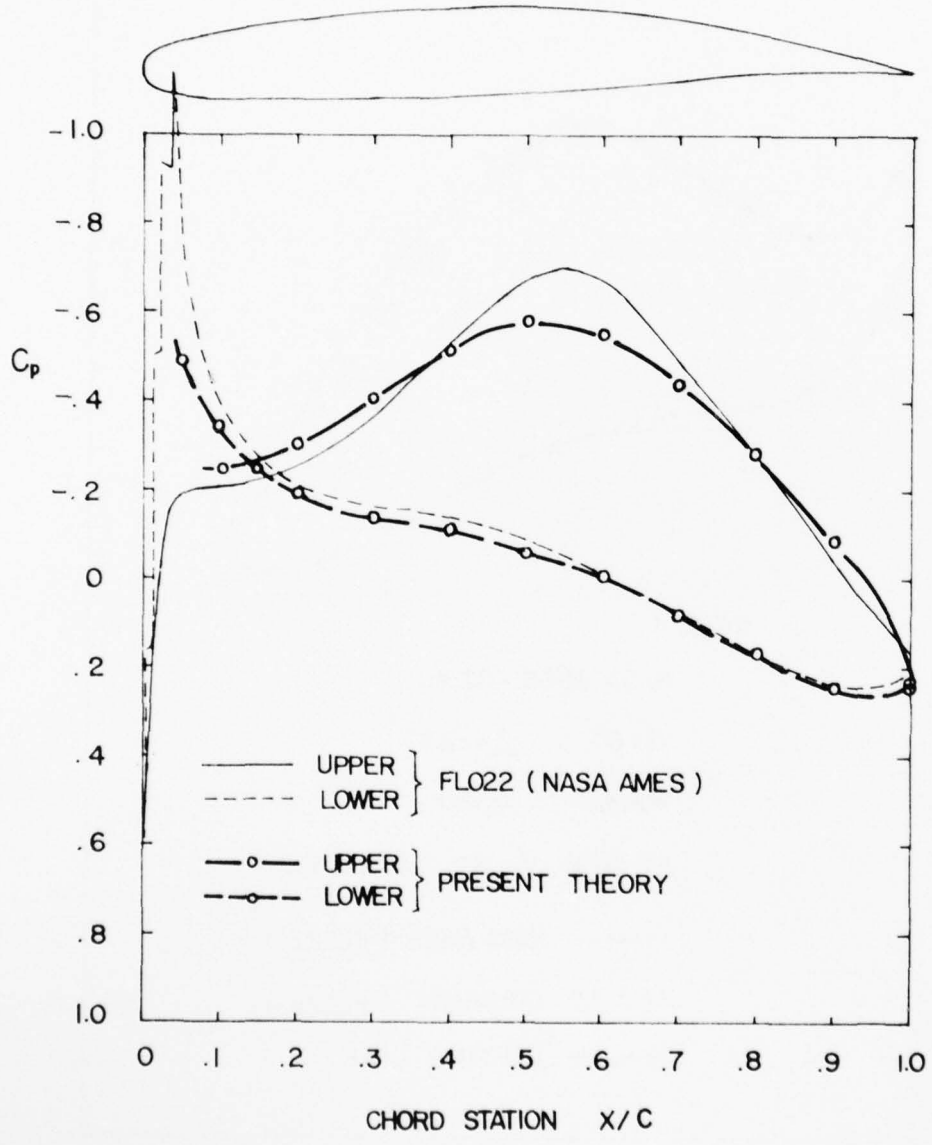

Figure 6(a)

CASE 3 $R_e = 14$

SPAN STATION $y/b = -0.69$ SEC. LIFT COEFF. $C_L = 0.3024$

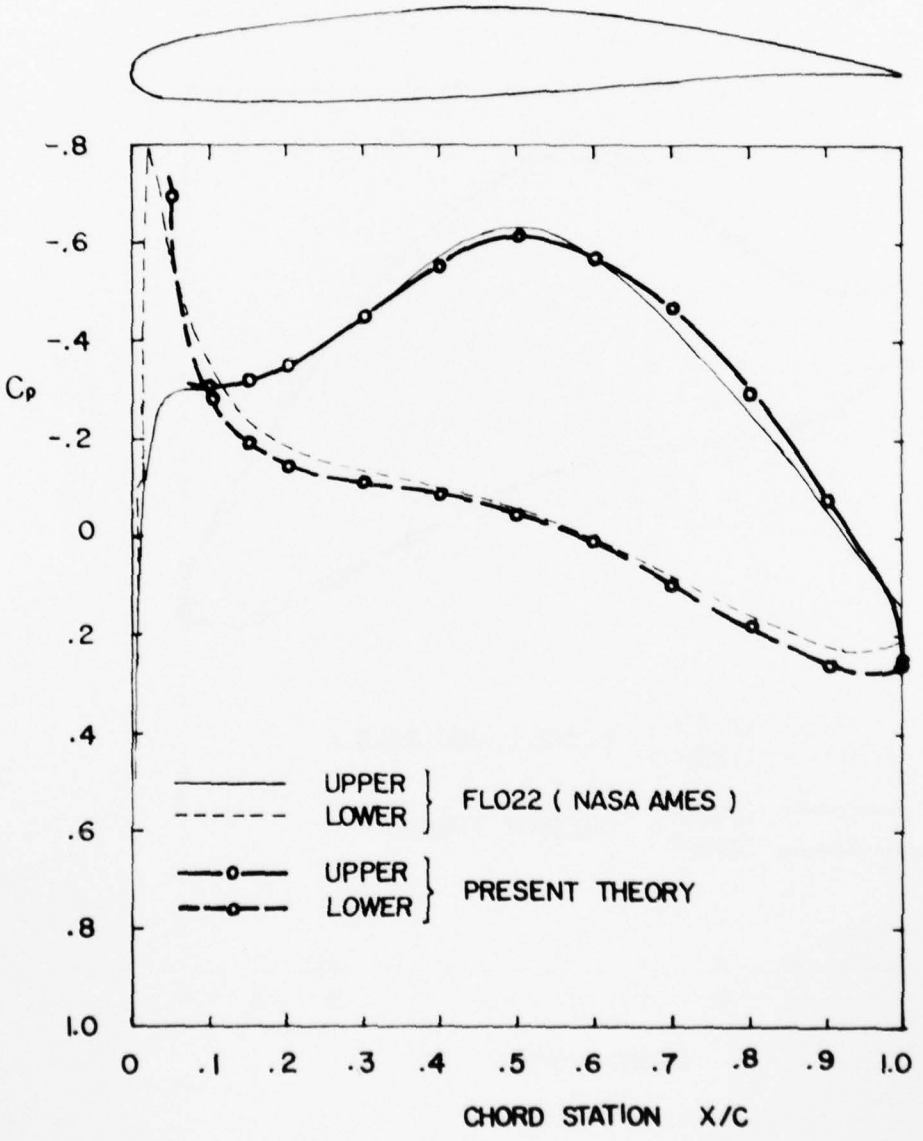

Figure 6(b)

CASE 3 $A_R = 14$

SPAN STATION $y'/b' = 0.00$ SEC. LIFT COEFF. $C_L = 0.3871$

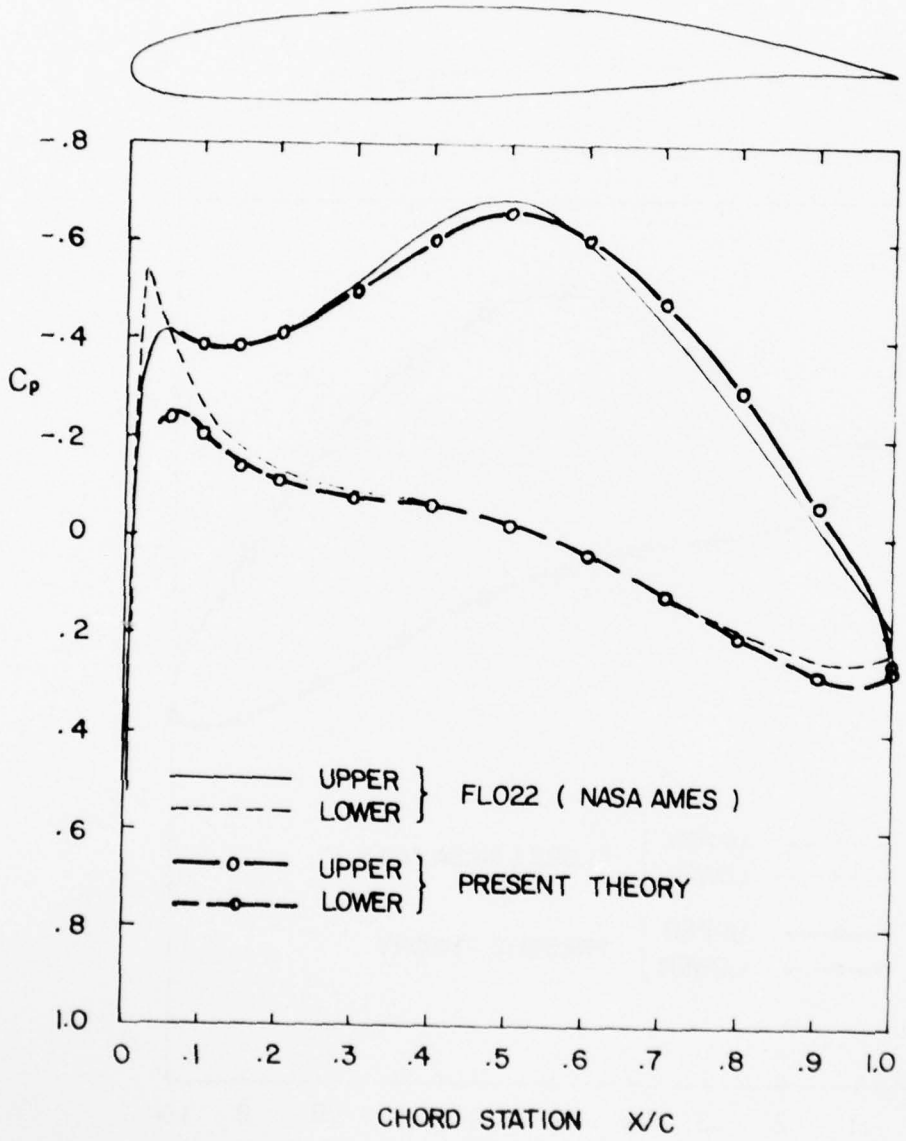

Figure 6(c)

CASE 3 $AR. = 14$

SPAN STATION $y'/b' = 0.69$ SEC. LIFT COEFF. $C_L = 0.4690$

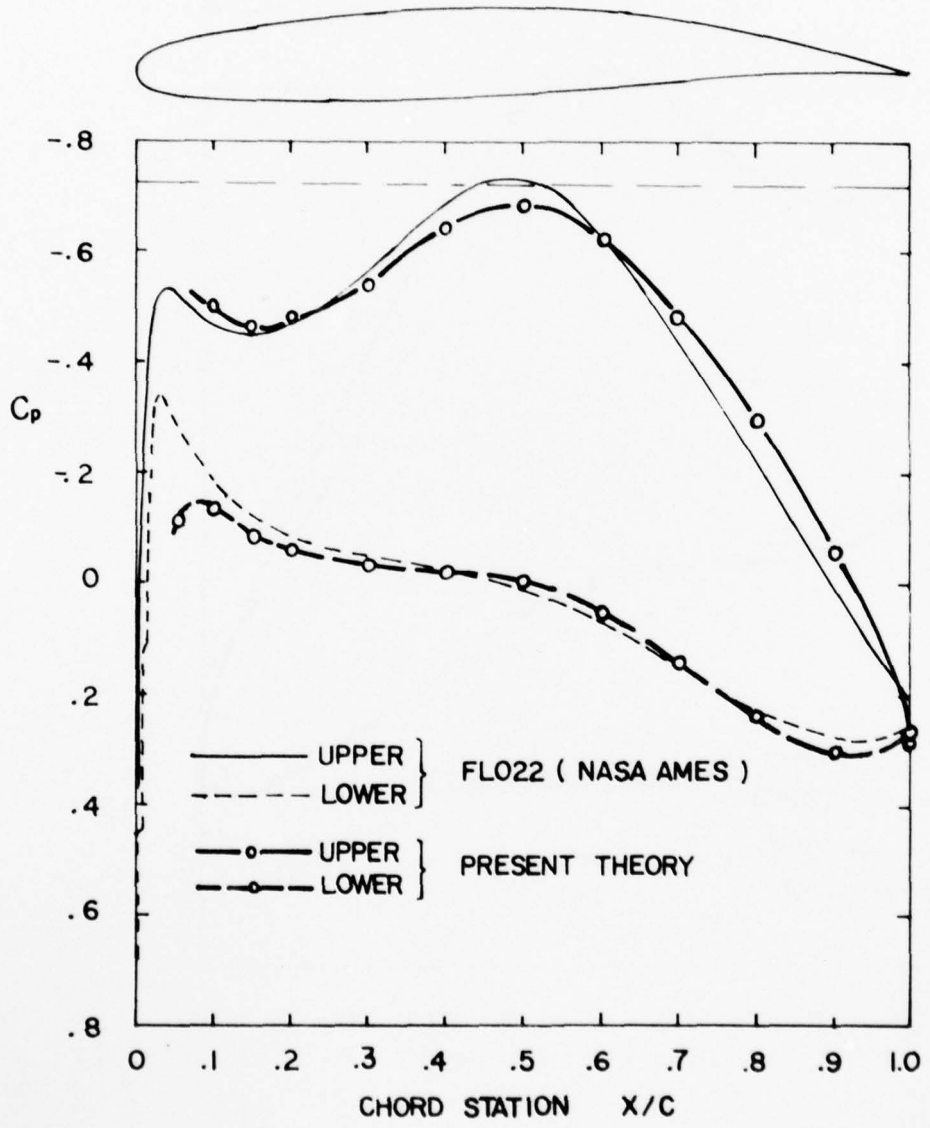

Figure 6(d)

CASE 3 $AR. = 14$

SPAN STATION $y/b = 0.89$ SEC. LIFT COEFF. $C_L = 0.4805$

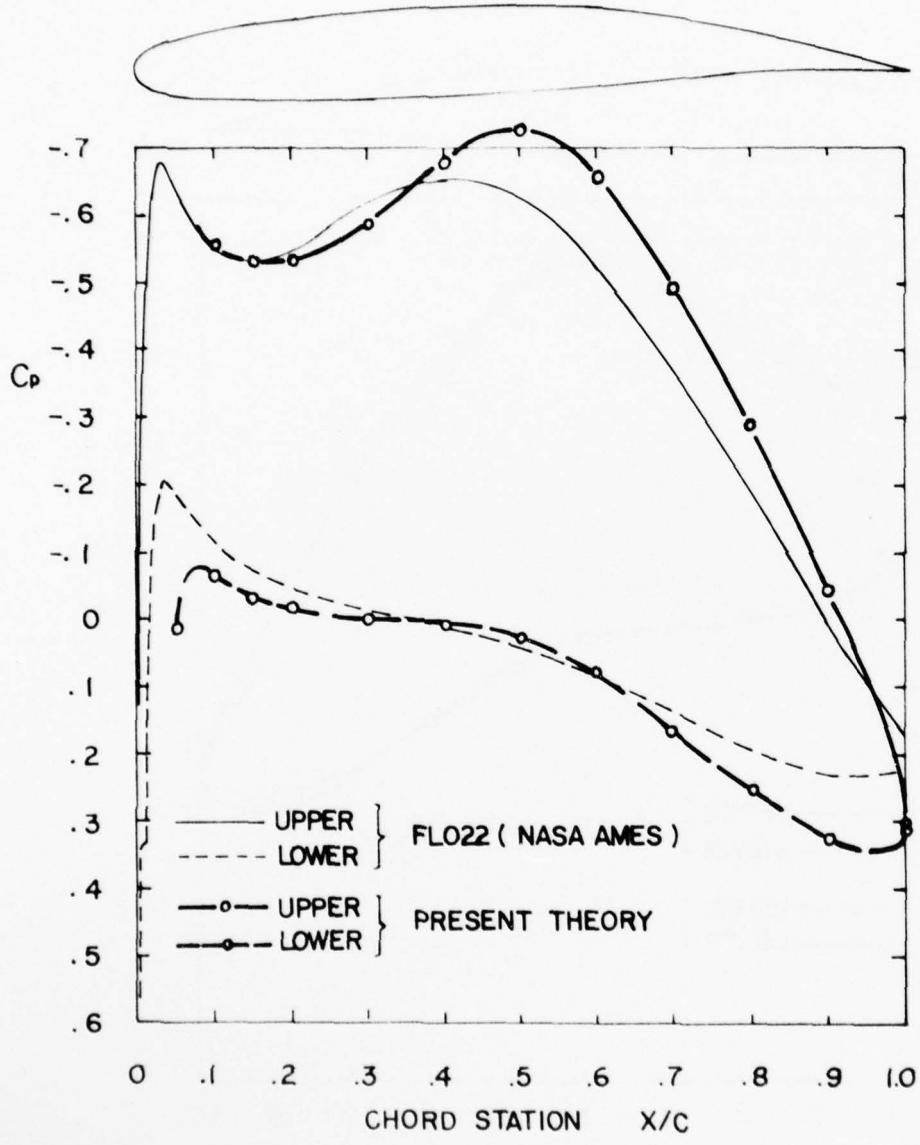

Figure 6(e)

CASE 5 ELLIPTICAL PLANFORM $R_e = 14$
STRAIGHT AXIS AT 50% CHORD
WING SECTION NASA 36 12-02, 40
$M_\infty = 0.768$ $\Lambda = 30°$ $\alpha = 0°$
SPAN STATION $y/b = -0.79$ SEC. LIFT COEFF. $C_L = 0.2883$

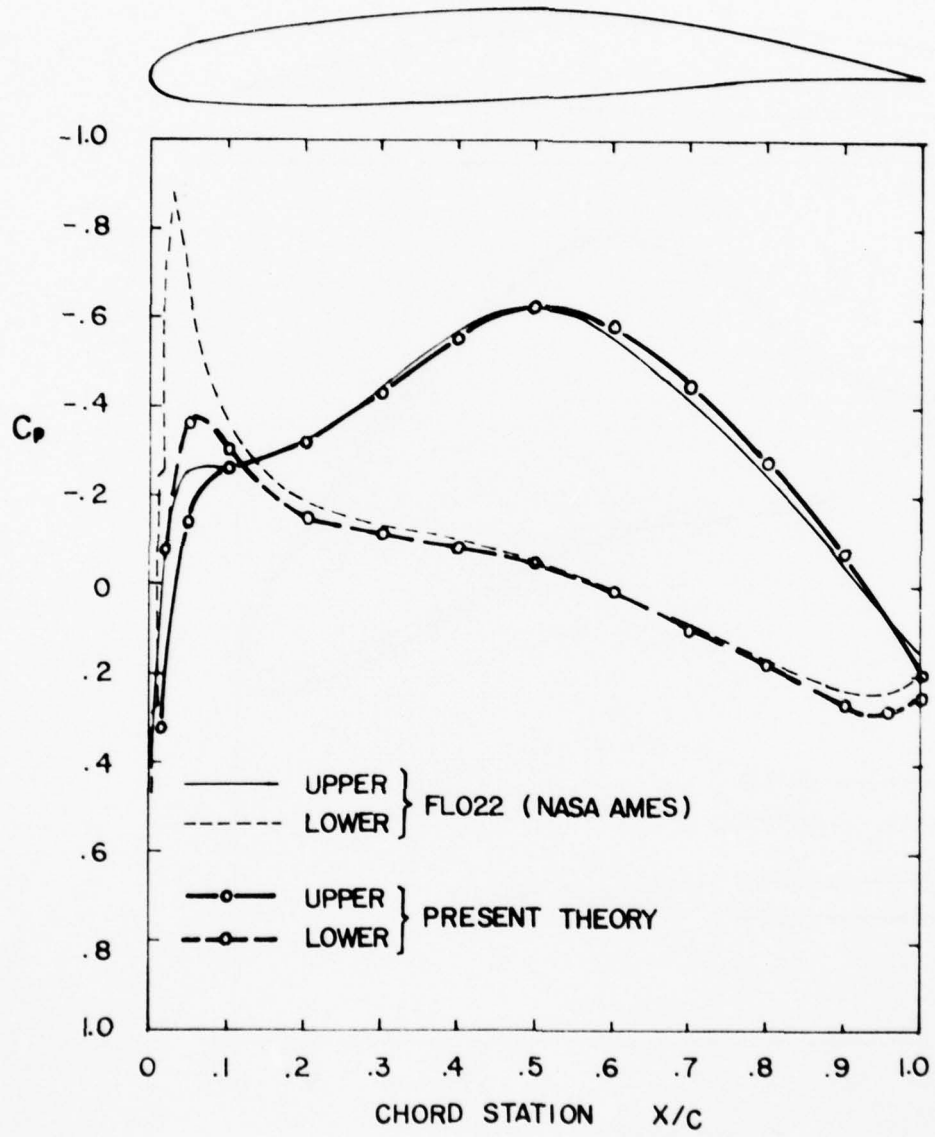

Figure 7(a)

CASE 5 $R_n = 14$

SPAN STATION $y'/b' = -0.59$ SEC. LIFT COEFF. $C_L = 0.3263$

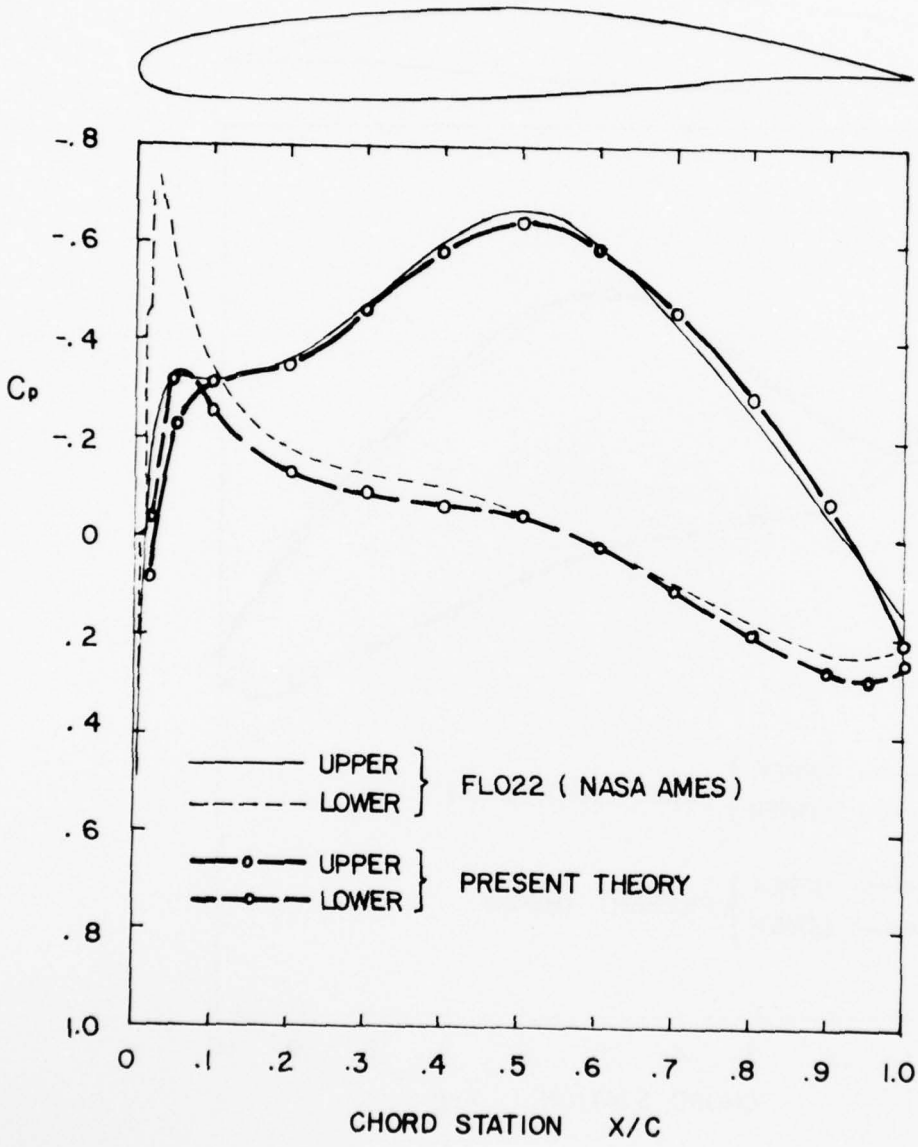

Figure 7(b)

CASE 5

SPAN STATION $y'/b' = -0.20$ SEC. LIFT COEFF. $C_\ell = 0.3795$

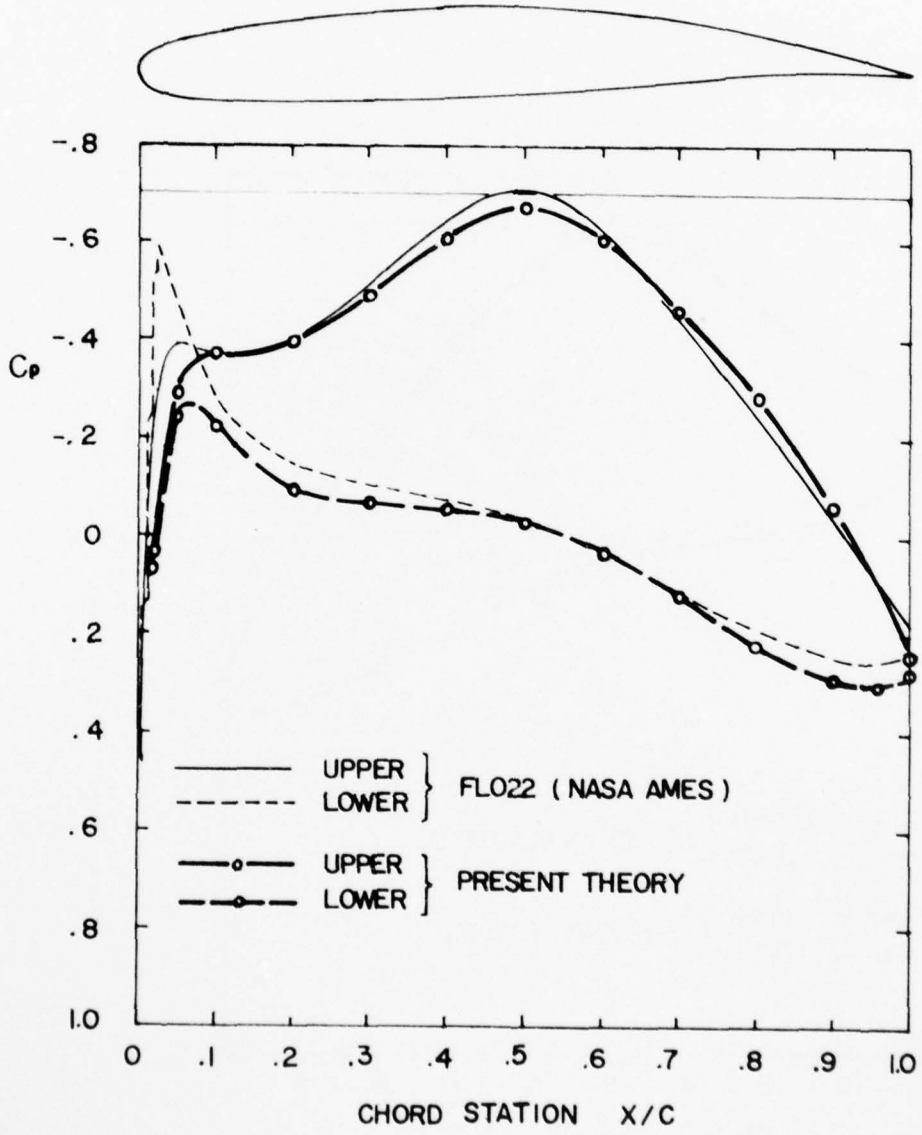

Figure 7(c)

CASE 5

SPAN STATION $y'/b' = 0.00$ SEC. LIFT COEFF. $C_L = 0.3937$

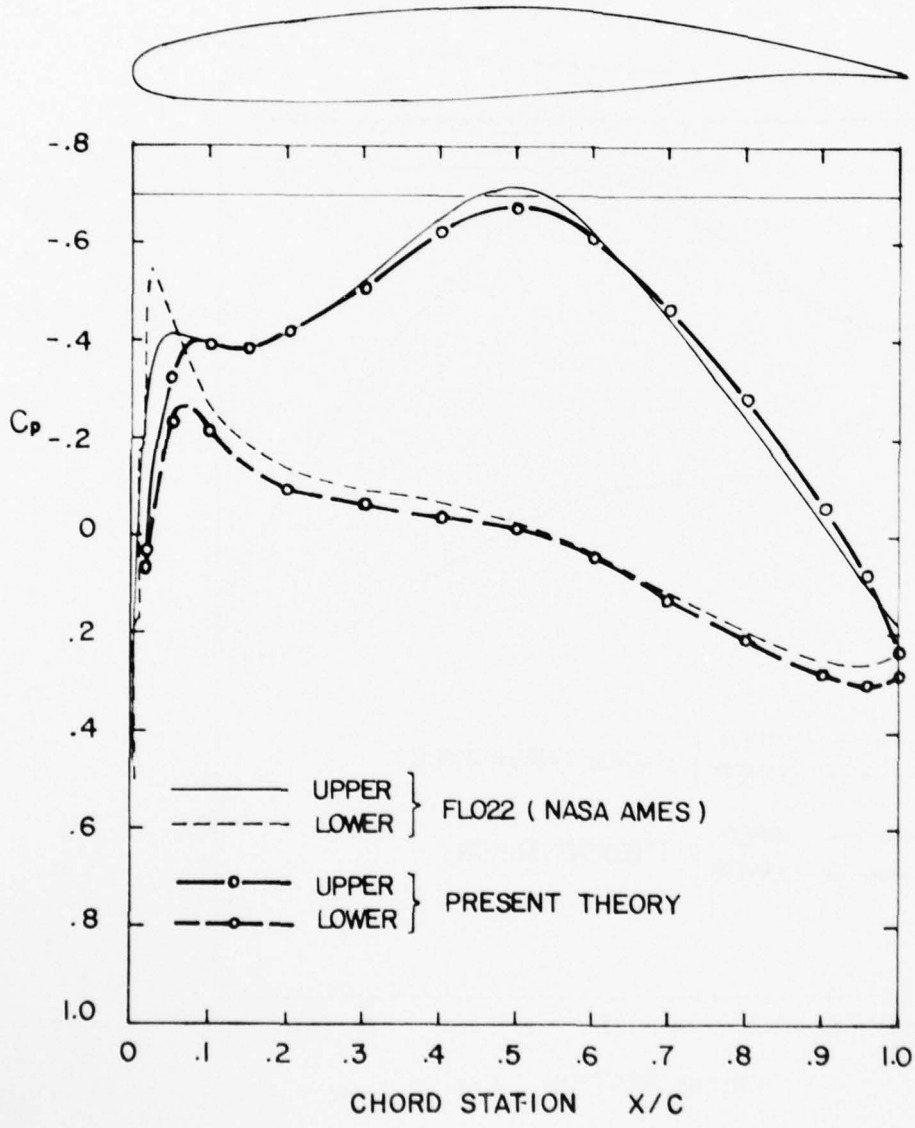

Figure 7(d)

CASE 5

SPAN STATION $y'/b' = 0.20$ SEC. LIFT COEFF. $C_L = 0.4223$

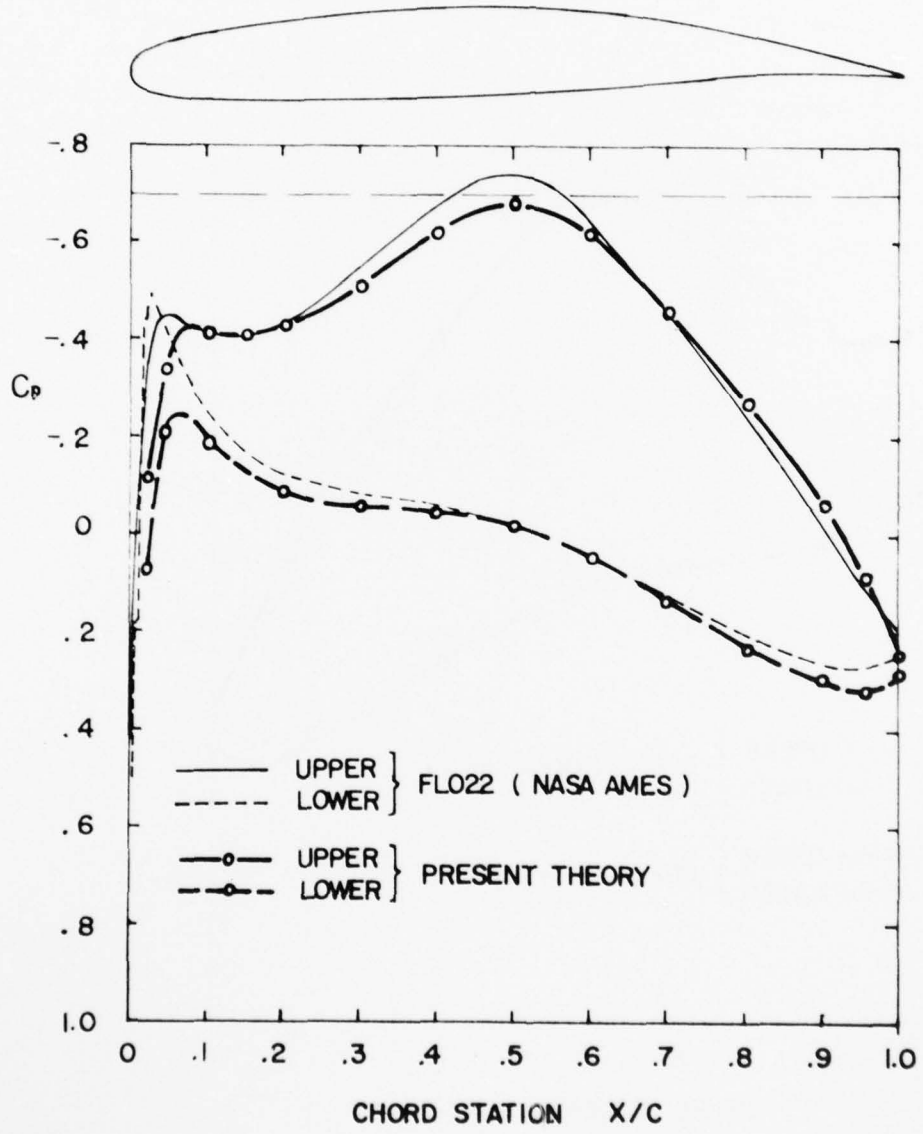

Figure 7(e)

CASE 5

SPAN STATION $y'/b' = 0.59$ SEC. LIFT COEFF. $C_L = 0.4601$

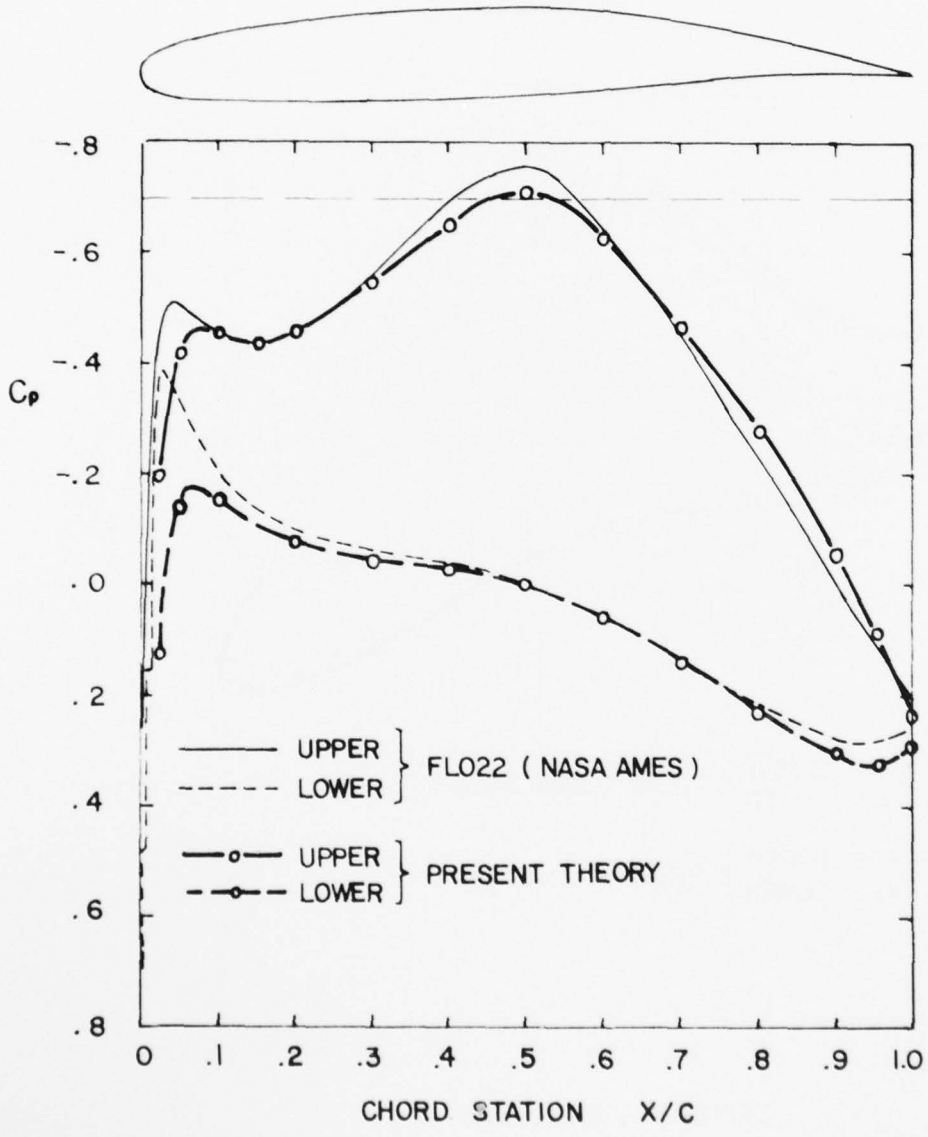

Figure 7(f)

CASE 5

SPAN STATION $y'/b' = 0.79$ SEC. LIFT COEFF. $C_L = 0.5034$

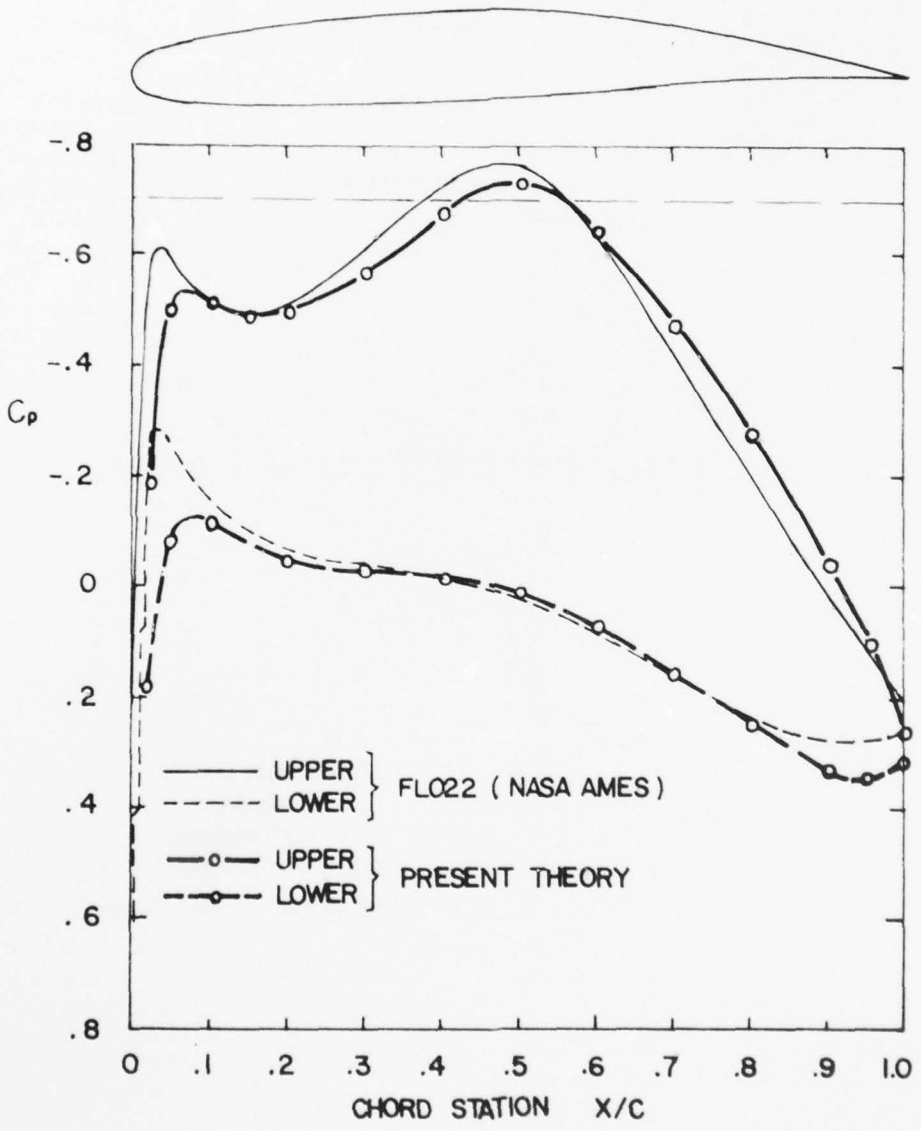

Figure 7(g)

AD-A070 232 UNIVERSITY OF SOUTHERN CALIFORNIA LOS ANGELES DEPT O--ETC F/G 20/4
THE OBLIQUE WING AS A LIFTING-LINE PROBLEM IN TRANSONIC FLOW.(U)
MAY 79 H K CHENG, S Y MENG N00014-75-C-0520
UNCLASSIFIED USCAE-53-4514-1541 NL

2 OF 2
AD A070232

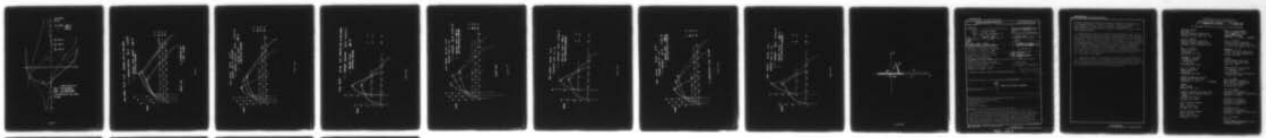

END
DATE FILMED
7-79
DDC

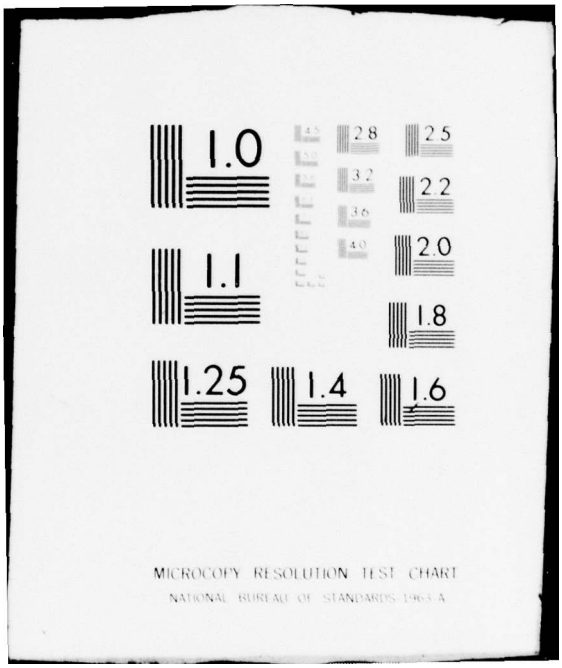
1.0
1.1
1.25
1.4
1.6
2.8
3.2
3.6
4.0
2.5
2.2
2.0
1.8
MICROCOPY RESOLUTION TEST CHART
NATIONAL BUREAU OF STANDARDS-1963-A

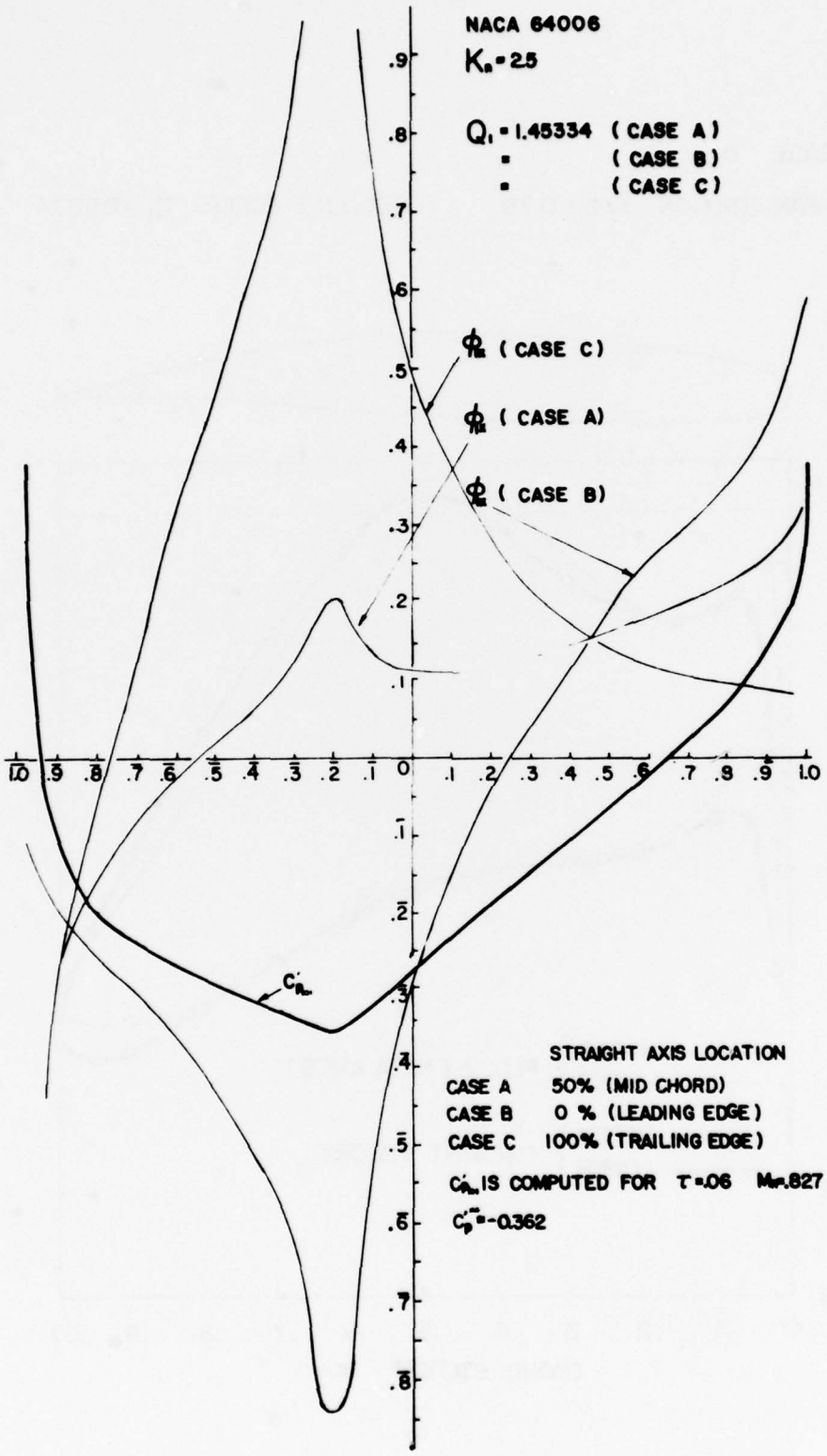
NACA 64006
$K_n = 2.5$
$Q_1 = 1.45334$ (CASE A)
= (CASE B)
= (CASE C)
Φ_{nL} (CASE C)
Φ_{nL} (CASE A)
Φ_{nL} (CASE B)
$C'_{n_{M_\infty}}$
STRAIGHT AXIS LOCATION
CASE A 50% (MID CHORD)
CASE B 0 % (LEADING EDGE)
CASE C 100% (TRAILING EDGE)
$C'_{n_{M_\infty}}$ IS COMPUTED FOR $\tau = .06$ $M_\infty = .827$
$C'^{**}_p = -0.362$

Figure 8

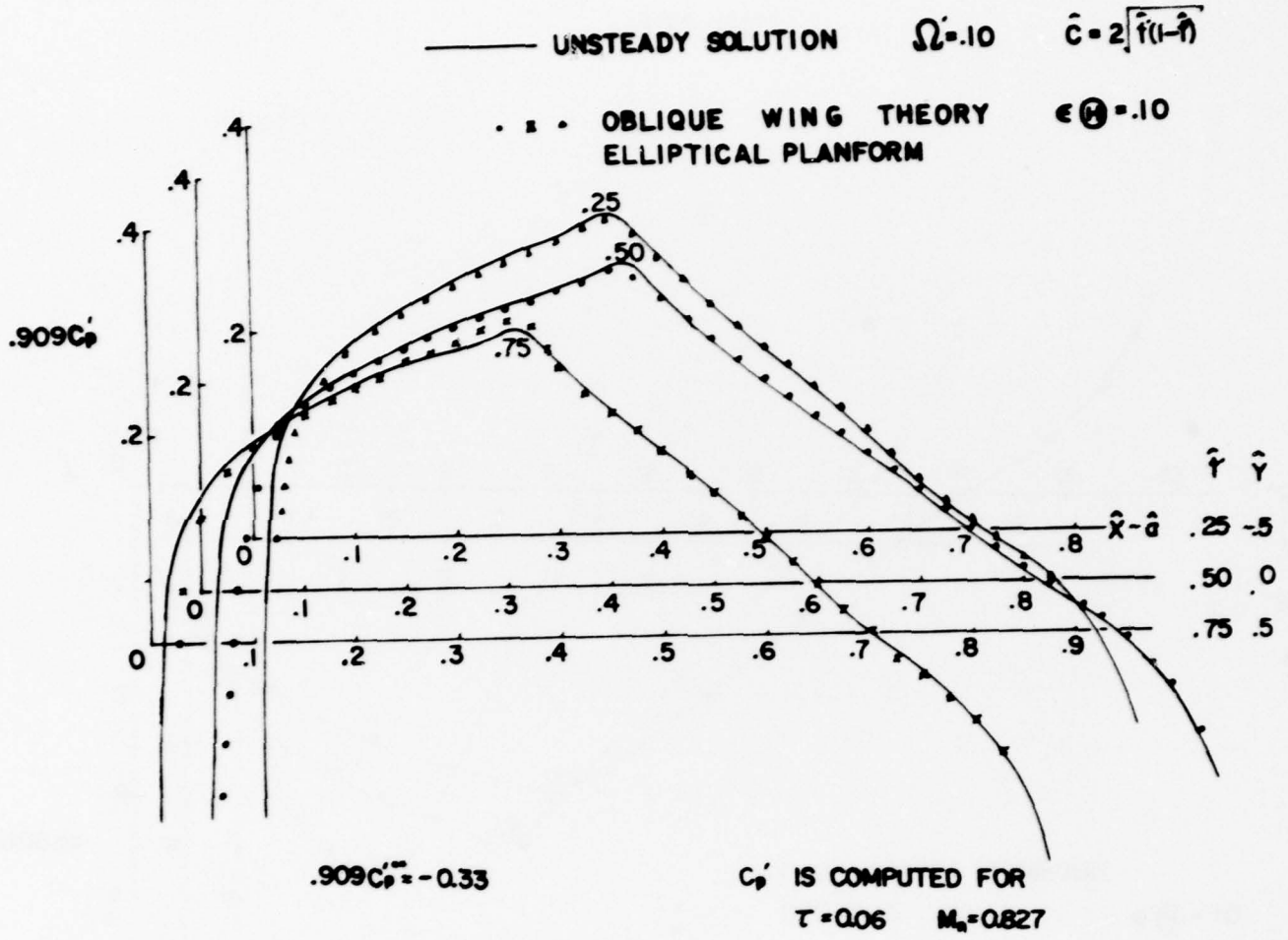
NACA 64006 K_M=2.5 α=0° STRAIGHT AXIS AT MID-CHORD
UNSTEADY SOLUTION Ω'=.10 $\hat{c}=2\sqrt{\hat{f}(1-\hat{f})}$
OBLIQUE WING THEORY $\epsilon_{(M)}$=.10
ELLIPTICAL PLANFORM
.909C_p'
.25
.50
.75
$\hat{f}$ $\hat{Y}$
$\hat{x}-\hat{a}$ .25 -.5
.50 0
.75 .5
.909$C_p'^{im}$=-0.33
C_p' IS COMPUTED FOR
τ=0.06 M_∞=0.827

Figure 9

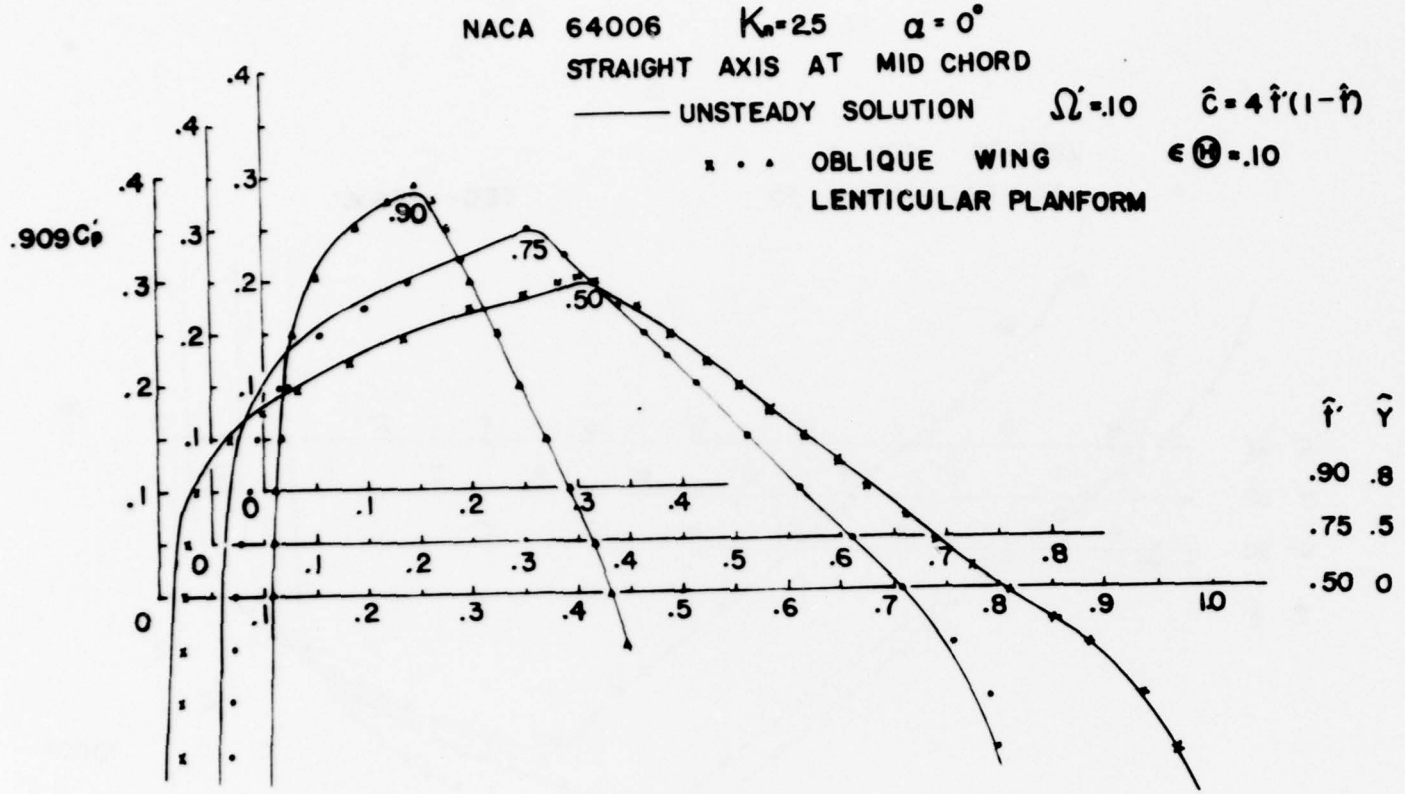
NACA 64006 K_m=2.5 $\alpha = 0^\circ$
STRAIGHT AXIS AT MID CHORD
—— UNSTEADY SOLUTION Ω'=.10 $\hat{c} = 4\hat{f}'(1-\hat{f}')$
x • • OBLIQUE WING ϵ Ⓗ=.10
LENTICULAR PLANFORM
.909 C_p'
$\hat{f}'$ $\hat{Y}$
.90 .8
.75 .5
.50 0

Figure 10(a)

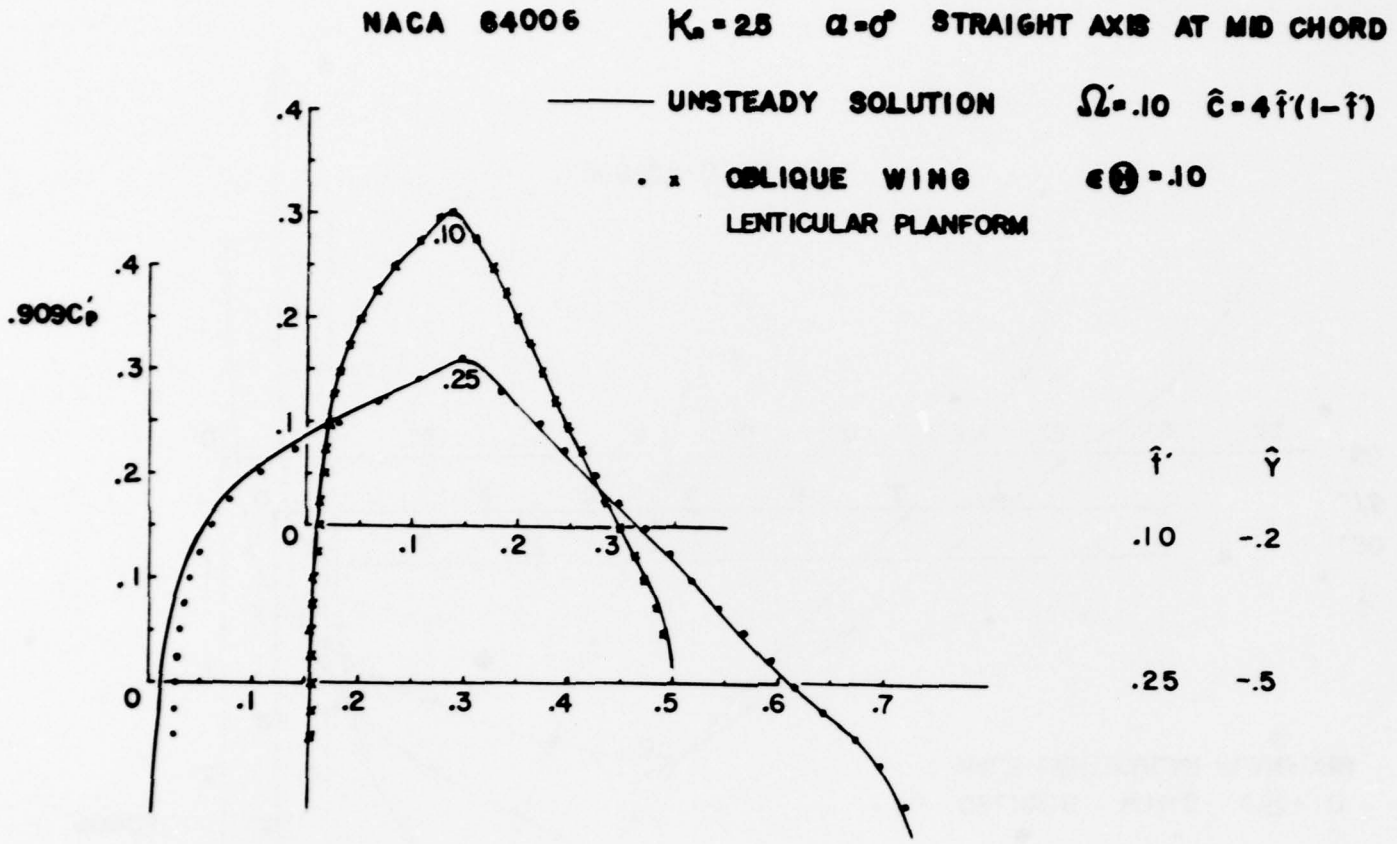
NACA 64006 $K_n = 2.5$ $\alpha = 0°$ STRAIGHT AXIS AT MID CHORD
UNSTEADY SOLUTION $\Omega' = .10$ $\hat{c} = 4\hat{f}'(1-\hat{f}')$
OBLIQUE WING $\epsilon(\hat{Y}) = .10$
LENTICULAR PLANFORM
$.909C_p'$
.10
.25
$\hat{f}'$ $\hat{Y}$
.10 -.2
.25 -.5

Figure 10(b)

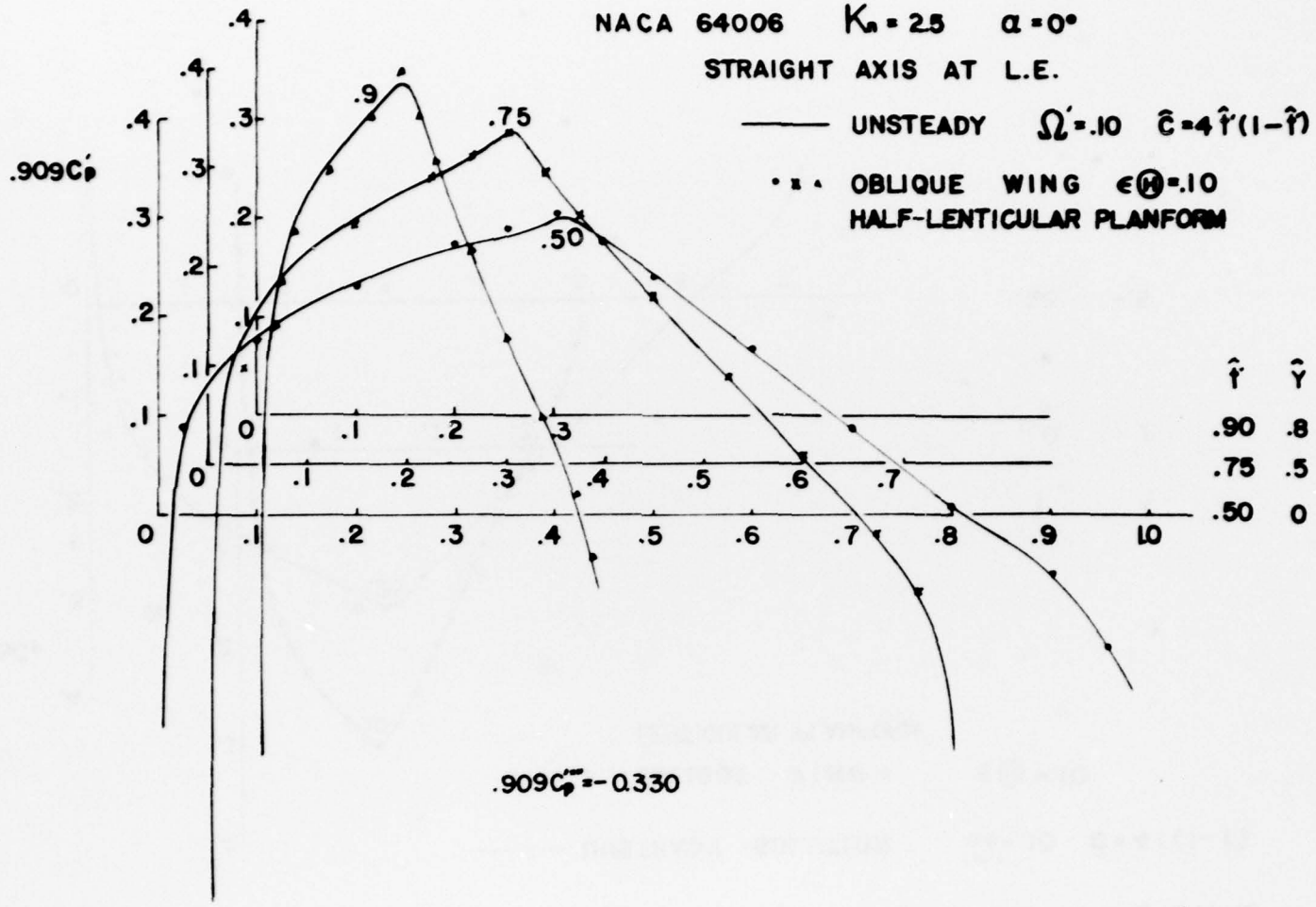
NACA 64006 $K_n = 2.5$ $\alpha = 0°$
STRAIGHT AXIS AT L.E.
UNSTEADY $\Omega' = .10$ $\hat{c} = 4\hat{r}(1-\hat{r})$
OBLIQUE WING $\epsilon_{(M)} = .10$
HALF-LENTICULAR PLANFORM
$.909C_p'$
.9
.75
.50
$\hat{r}$ $\hat{Y}$
.90 .8
.75 .5
.50 0
$.909C_{p_{max}}' = -0.330$

Figure 11(a)

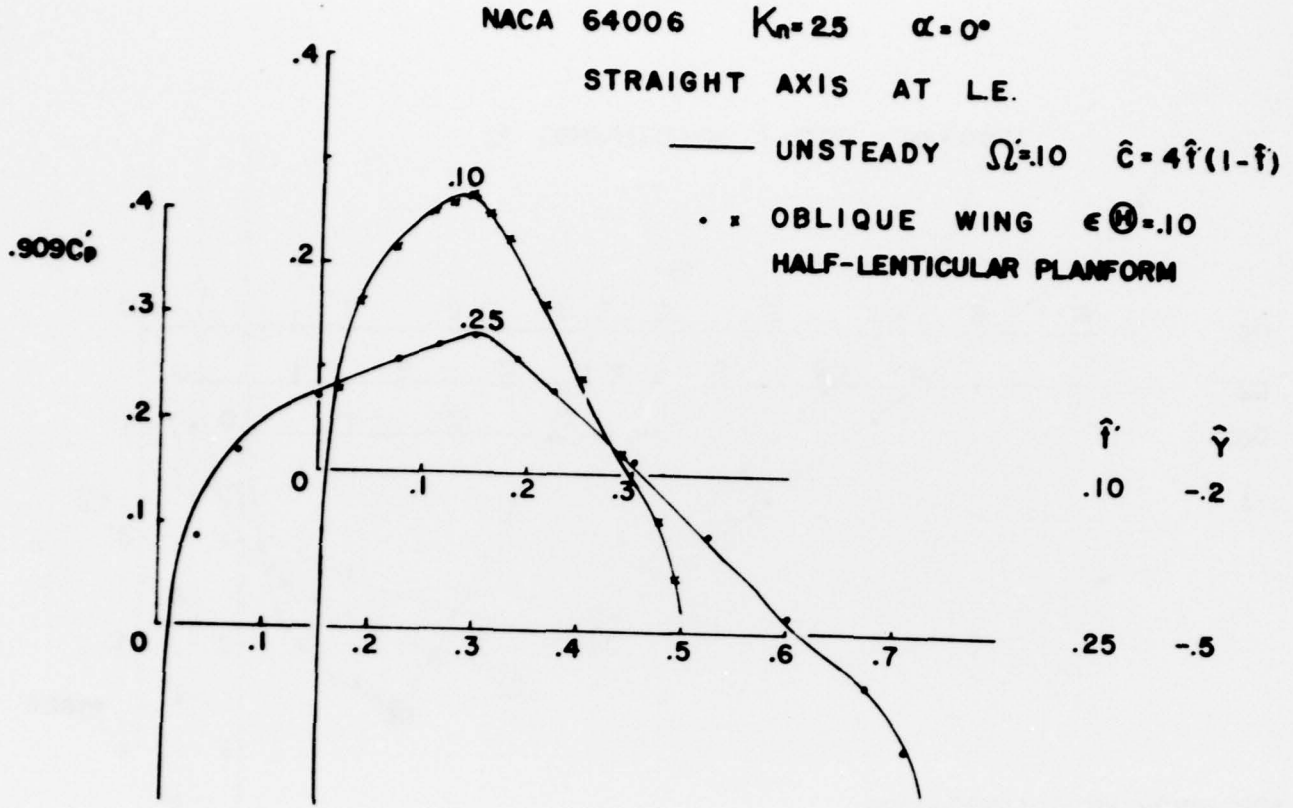
NACA 64006 K_n=.25 α=0°
STRAIGHT AXIS AT L.E.
UNSTEADY Ω'=.10 $\hat{c}=4\hat{f}'(1-\hat{f}')$
• x OBLIQUE WING ε⊛=.10
HALF-LENTICULAR PLANFORM
.909C_p'
.10
.25
$\hat{f}'$ $\hat{Y}$
.10 -.2
.25 -.5

Figure 11(b)

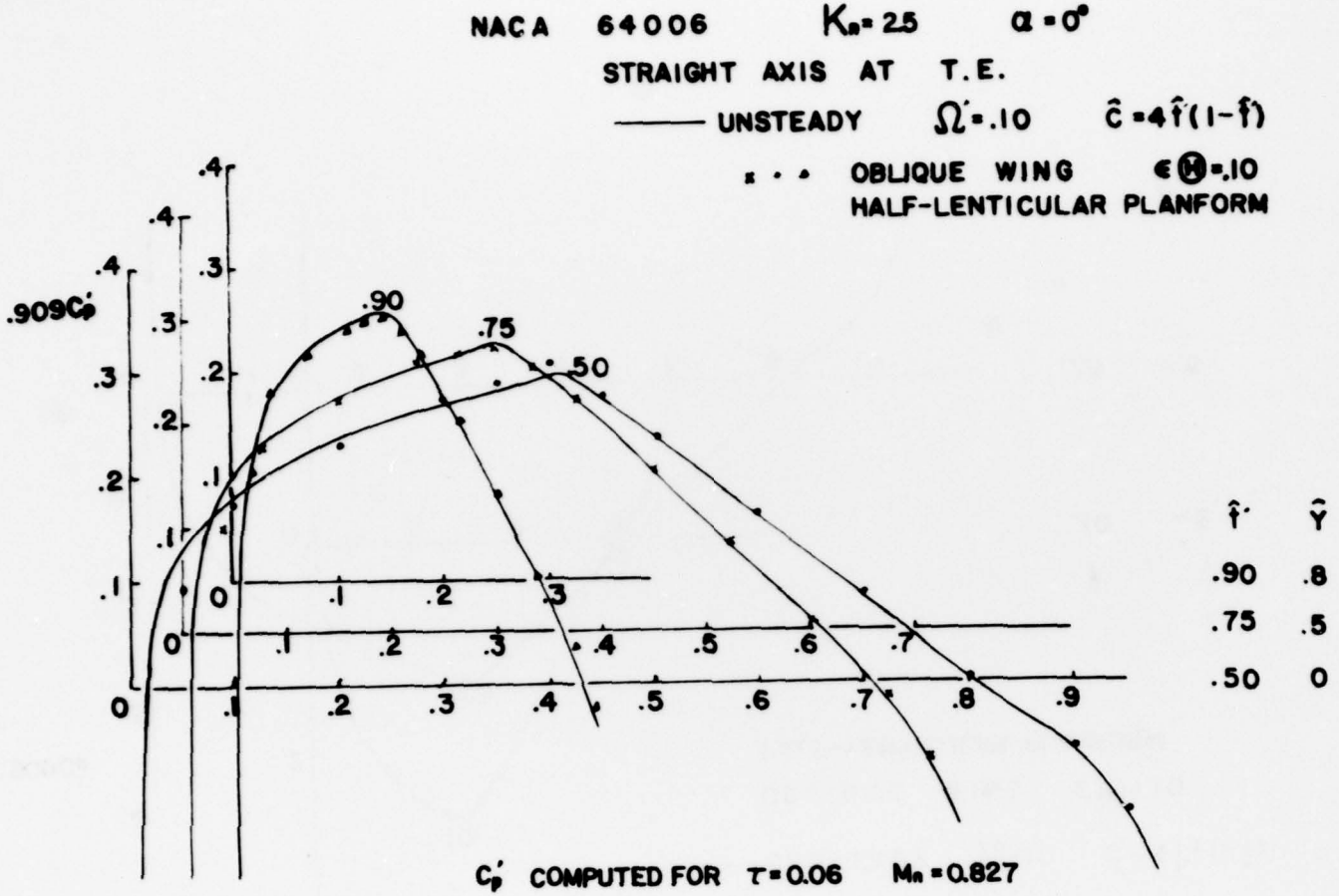
NACA 64006 $K_n = 25$ $\alpha = 0°$
STRAIGHT AXIS AT T.E.
—— UNSTEADY $\Omega' = .10$ $\hat{c} = 4\hat{f}'(1-\hat{f}')$
x · · · OBLIQUE WING $\epsilon_{(M)} = .10$
HALF-LENTICULAR PLANFORM
$.909C_p'$
.90
.75
.50
$\hat{f}'$ $\hat{Y}$
.90 .8
.75 .5
.50 0
C_p' COMPUTED FOR $\tau = 0.06$ $M_n = 0.827$

Figure 12(a)

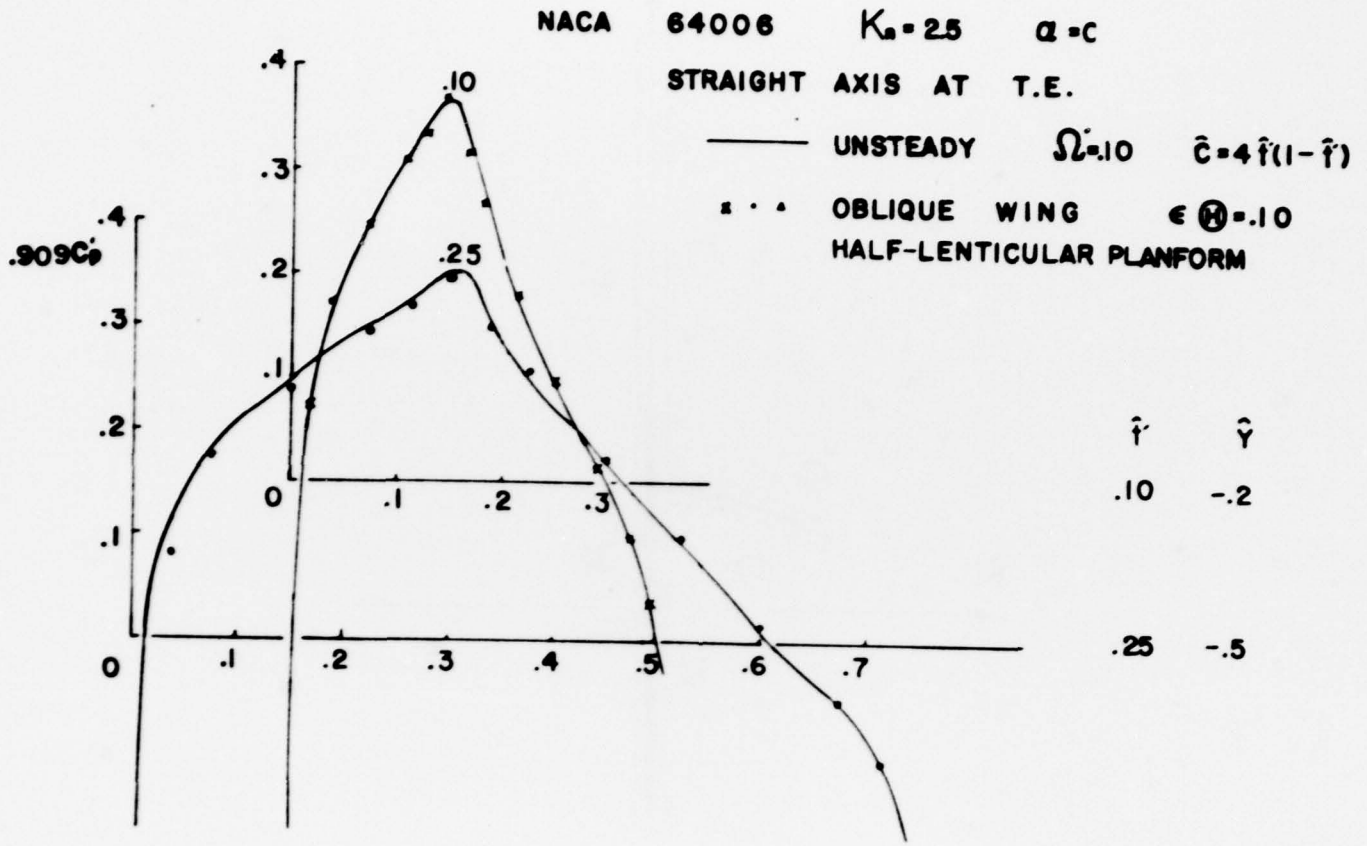
NACA 64006 $K_o = .25$ $\alpha = 0$
STRAIGHT AXIS AT T.E.
UNSTEADY $\Omega = .10$ $\hat{C} = 4\hat{f}'(1-\hat{f}')$
OBLIQUE WING $\epsilon_{(M)} = .10$
HALF-LENTICULAR PLANFORM
$.909C_p$
.10
.25
$\hat{f}'$ $\hat{Y}$
.10 -.2
.25 -.5

Figure 12(b)

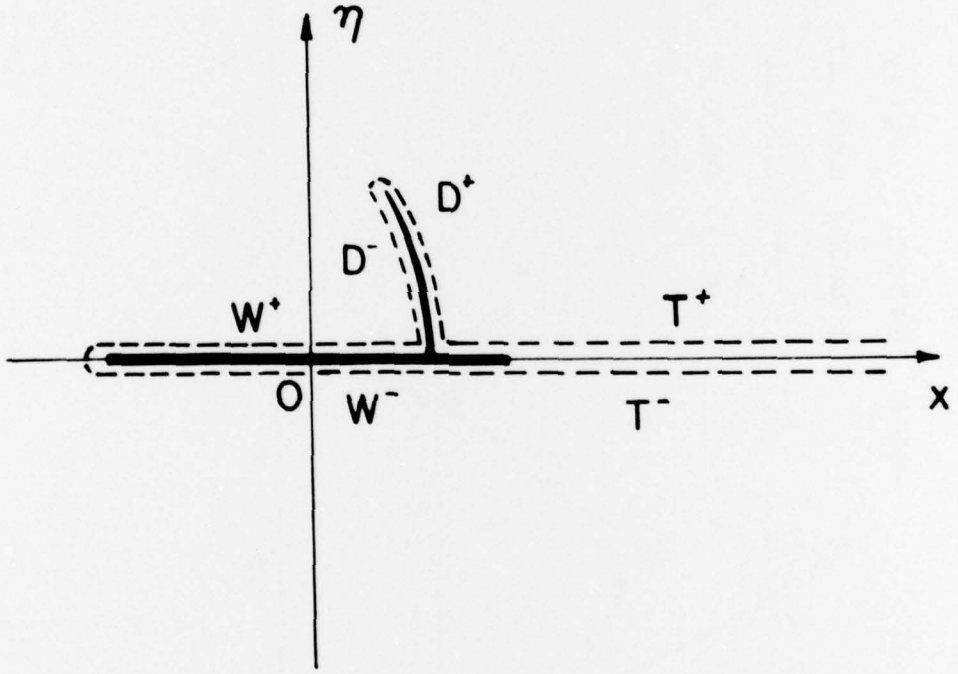

Figure II.1

UNCLASSIFIED

SECURITY CLASSIFICATION OF THIS PAGE (When Data Entered)

REPORT DOCUMENTATION PAGE

READ INSTRUCTIONS BEFORE COMPLETING FORM

1. REPORT NUMBER: USCAE 136
2. GOVT ACCESSION NO.
3. RECIPIENT'S CATALOG NUMBER

4. TITLE (and Subtitle): (6) THE OBLIQUE WING AS A LIFTING-LINE PROBLEM IN TRANSONIC FLOW
5. TYPE OF REPORT & PERIOD COVERED: (9) Technical Report
6. PERFORMING ORG. REPORT NUMBER: 53-4514-1541

7. AUTHOR(s): (10) H.K. Cheng and S.Y. Meng
8. CONTRACT OR GRANT NUMBER(s): (15) N00014-75-C-0520

9. PERFORMING ORGANIZATION NAME AND ADDRESS:
University of Southern California
Department of Aerospace Engineering
Los Angeles, California 90007

10. PROGRAM ELEMENT, PROJECT, TASK AREA & WORK UNIT NUMBERS: Task NR 061-192

11. CONTROLLING OFFICE NAME AND ADDRESS: (11)
Department of the Navy, Code 438
Office of Naval Research
Arlington, Virginia 22217

12. REPORT DATE: May 1979
13. NUMBER OF PAGES: 104

14. MONITORING AGENCY NAME & ADDRESS (if different from Controlling Office):
Department of the Navy, Code 603
Office of Naval Research, Branch Office
1030 East Green Street
Pasadena, California 91106

15. SECURITY CLASS. (of this report): UNCLASSIFIED
15a. DECLASSIFICATION DOWNGRADING SCHEDULE

16. DISTRIBUTION STATEMENT (of this Report):
"APPROVED FOR PUBLIC RELEASE: DISTRIBUTION UNLIMITED".

(12) 113 p.

17. DISTRIBUTION STATEMENT (of the abstract entered in Block 20, if different from Report):
(14) USCAE-53-4514-1541, USCAE-136

18. SUPPLEMENTARY NOTES

19. KEY WORDS (Continue on reverse side if necessary and identify by block number)
Three-dimensional transonic flow
Lifting-line theory
Oblique wing
Similarity solutions

20. ABSTRACT (Continue on reverse side if necessary and identify by block number)

A transonic-flow theory of thin oblique wing of high aspect ratio is presented, which permits a delineation of the influence of wing sweep, center-line curvature, and other three-dimensional (3-D) effects on the nonlinear mixed flow in the framework of an asymptotic theory. The component flow near the wing section is basically plane (two-dimensional) but nonlinear and mixed, being governed by equations consistent with the transonic small-disturbance approximation. The work analyzes 3-D corrections to this

(continued)

DD FORM 1 JAN 73 1473 EDITION OF 1 NOV 65 IS OBSOLETE

UNCLASSIFIED

SECURITY CLASSIFICATION OF THIS PAGE (When Data Entered)

402 029

nonlinear problem and matching its solutions to that of an outer flow. In the (parameter) domain of interest, the outer solutions correspond to a high subsonic, or a linear sonic, outer flow, representable by a Prandtl-Glauert solution involving a swept (or curved) lifting line in the leading approximation.

Among the 3-D effects is one arising from the compressibility correction to the velocity divergence, absent in classical works. More important are the upwash corrections which include the influence of both the near and far wakes, as well as the local curvature of the center line. For straight oblique wings, local similarities exist in the 3-D flow structure, permitting the reduced equations to be solved once for all stations. An analogy also exists between the oblique-wing problem and that of a 2-D transonic flow which is weakly time-dependent; this provides an alternative method of solving numerically the inner airfoil problem. Of theoretical interest is the uncovering of a compressibility correction to the outer flow in the form of a line source and a nonuniformity of the perturbation solutions at a shock root (and its treatment).

A procedure based on a line relaxation method for solving numerically the reduced inner problem is described; solutions with high subcritical, as well as slightly supercritical, component flows are demonstrated. Comparison with corresponding numerical solutions based on full-potential equations for oblique elliptic wing shows encouraging agreement.

DISTRIBUTION LIST FOR UNCLASSIFIED
TECHNICAL REPORTS AND REPRINTS ISSUED UNDER
CONTRACT N00014-75-C-0520 TASK NR 061-192

All addresses receive one copy unless otherwise specified

Technical Library
Building 313
Ballistic Research Laboratories
Aberdeen Proving Ground, MD 21005

Dr. F. D. Bennett
External Ballistic Laboratory
Ballistic Research Laboratories
Aberdeen Proving Ground, MD 21005

Mr. C. C. Hudson
Sandia Corporation
Sandia Base
Albuquerque, NM 81115

Professor P. J. Roache
Ecodynamics Research
Associates, Inc.
P. O. Box 8172
Albuquerque, NM 87108

Dr. J. D. Shreve, Jr.
Sandia Corporation
Sandia Base
Albuquerque, NM 81115

Defense Documentation Center
Cameron Station, Building 5
Alexandria, VA 22314 12 copies

Library
Naval Academy
Annapolis, MD 21402

Director, Tactical Technology Office
Defense Advanced Research Projects
Agency
1400 Wilson Boulevard
Arlington, VA 22209

Office of Naval Research
Attn: Code 211
800 N. Quincy Street
Arlington, VA 22217

Office of Naval Research
Attn: Code 438
800 N. Quincy Street
Arlington, VA 22217

Office of Naval Research
Attn: Code 1021P (ONRL)
800 N. Quincy Street
Arlington, VA 22217 6 copies

Dr. J. L. Potter
Deputy Director, Technology
von Karman Gas Dynamics Facility
Arnold Air Force Station, TN 37389

Professor J. C. Wu
Georgia Institute of Technology
School of Aerospace Engineering
Atlanta, GA 30332

Library
Aerojet-General Corporation
6352 North Irwindale Avenue
Azusa, CA 91702

NASA Scientific and Technical
Information Facility
P. O. Box 8757
Baltimore/Washington International
Airport, MD 21240

Dr. K. C. Wang
Martin Marietta Corporation
Martin Marietta Laboratories
1450 South Rolling Road
Baltimore, MD 21227

Dr. S. A. Berger
University of California
Department of Mechanical Engineering
Berkeley, CA 94720

Professor A. J. Chorin
University of California
Department of Mathematics
Berkeley, CA 94720

Professor M. Holt
University of California
Department of Mechanical Engineering
Berkeley, CA 94720

Dr. H. R. Chaplin
Code 1600
David W. Taylor Naval Ship Research
and Development Center
Bethesda, MD 20084

Dr. Hans Lugt
Code 184
David W. Taylor Naval Ship Research
and Development Center
Bethesda, MD 20084

Dr. Francois Frenkiel
Code 1802.2
David W. Taylor Naval Ship Research
and Development Center
Bethesda, MD 20084

Dr. G. R. Inger
Department of Aerospace Engineering
Virginia Polytechnic Institute and
State University
Blacksburg, VA 24061

Professor A. H. Nayfeh
Department of Engineering Science
Virginia Polytechnic Institute and
State University
Blacksburg, VA 24061

Mr. A. Rubel
Research Department
Grumman Aerospace Corporation
Bethpage, NY 11714

Commanding Officer
Office of Naval Research Branch Office
666 Summer Street, Bldg. 114, Section D
Boston, MA 02210

Dr. G. Hall
State University of New York at Buffalo
Faculty of Engineering and Applied
Sciences
Fluid and Thermal Sciences Laboratory
Buffalo, NY 14214

Dr. R. J. Vidal
CALSPAN Corporation
Aerodynamics Research Department
P. O. Box 235
Buffalo, NY 14221

Professor R. F. Probstein
Department of Mechanical Engineering
Massachusetts Institute of Technology
Cambridge, MA 02139

Commanding Officer
Office of Naval Research Branch Office
536 South Clark Street
Chicago, IL 60605

Code 753
Naval Weapons Center
China Lake, CA 93555

Mr. J. Marshall
Code 4063
Naval Weapons Center
China Lake, CA 93555

Professor R. T. Davis
Department of Aerospace Engineering
University of Cincinnati
Cincinnati, OH 45221

Library MS 60-3
NASA Lewis Research Center
21000 Brookpark Road
Cleveland, OH 44135

Dr. J. D. Anderson, Jr.
Chairman, Department of Aerospace
Engineering
College of Engineering
University of Maryland
College Park, MD 20742

Professor W. L. Melnik
Department of Aerospace Engineering
University of Maryland
College Park, MD 20742

Professor O. Burggraf
Department of Aeronautical and
Astronautical Engineering
Ohio State University
1314 Kinnear Road
Columbus, OH 43212

Technical Library
Naval Surface Weapons Center
Dahlgren Laboratory
Dahlgren, VA 22448

Dr. F. Moore
Naval Surface Weapons Center
Dahlgren Laboratory
Dahlgren, VA 22448

Technical Library 2-51131
LTV Aerospace Corporation
P. O. Box 5907
Dallas, TX 75222

Library, United Aircraft Corporation
Research Laboratories
Silver Lane
East Hartford, CT 06108

Technical Library
AVCO-Everett Research Laboratory
2385 Revere Beach Parkway
Everett, MA 02149

Professor G. Moretti
Polytechnic Institute of New York
Long Island Center
Department of Aerospace Engineering
and Applied Mechanics
Route 110
Farmingdale, NY 11735

Professor S. G. Rubin
Polytechnic Institute of New York
Long Island Center
Department of Aerospace Engineering
and Applied Mechanics
Route 110
Farmingdale, NY 11735

Dr. W. R. Briley
Scientific Research Associates, Inc.
P. O. Box 498
Glastonbury, CT 06033

Professor P. Gordon
Calumet Campus
Department of Mathematics
Purdue University
Hammond, IN 46323

Library (MS 185)
NASA Langley Research Center
Langley Station
Hampton, VA 23665

Professor A. Chapmann
Chairman, Mechanical Engineering
Department
William M. Rice Institute
Box 1892
Houston, TX 77001

Technical Library
Naval Ordnance Station
Indian Head, MD 20640

Professor D. A. Caughey
Sibley School of Mechanical and
Aerospace Engineering
Cornell University
Ithaca, NY 14850

Professor E. L. Resler
Sibley School of Mechanical and
Aerospace Engineering
Cornell University
Ithaca, NY 14850

Professor S. F. Shen
Sibley School of Mechanical and
Aerospace Engineering
Ithaca, NY 14850

Library
Midwest Research Institute
425 Volker Boulevard
Kansas City, MO 64110

Dr. M. M. Hafez
Flow Research, Inc.
P. O. Box 5040
Kent, WA 98031

Dr. E. M. Murman
Flow Research, Inc.
P. O. Box 5040
Kent, WA 98031

Dr. S. A. Orszag
Cambridge Hydrodynamics, Inc.
54 Baskin Road
Lexington, MA 02173

Dr. P. Bradshaw
Imperial College of Science and
Technology
Department of Aeronautics
Prince Consort Road
London SW7 2BY, England

Professor T. Cebeci
California State University,
LongBeach
Mechanical Engineering Department
Long Beach, CA 90840

Mr. J. L. Hess
Douglas Aircraft Company
3855 Lakewood Boulevard
Long Beach, CA 90808

Dr. H. K. Cheng
University of Southern California,
University Park
Department of Aerospace Engineering
Los Angeles, CA 90007

Professor J. D. Cole
Mechanics and Structures Department
School of Engineering and Applied
Science
University of California
Los Angeles, CA 90024

Engineering Library
University of Southern California
Box 77929
Los Angeles, CA 90007

Dr. C. -M. Ho
Department of Aerospace Engineering
University of Southern California,
University Park
Los Angeles, CA 90007

Dr. T. D. Taylor
The Aerospace Corporation
P. O. Box 92957
Los Angeles, CA 90009

Commanding Officer
Naval Ordnance Station
Louisville, KY 40214

Mr. B. H. Little, Jr.
Lockheed-Georgia Company
Department 72-74, Zone 369
Marietta, GA 30061

Professor E. R. G. Eckert
University of Minnesota
241 Mechanical Engineering Building
Minneapolis, MN 55455

Library
Naval Postgraduate School
Monterey, CA 93940

Supersonic-Gas Dynamics Research
Laboratory
Department of Mechanical Engineering
McGill University
Montreal 12, Quebec, Canada

Dr. S. S. Stahara
Nielsen Engineering & Research, Inc.
510Clyde Avenue
Mountain View, CA 94043

Engineering Societies Library
345 East 47th Street
New York, NY 10017

Professor A. Jameson
New York University
Courant Institute of Mathematical
Sciences
251 Mercer Street
New York, NY 10012

Professor G. Miller
Department of Applied Science
New York University
26-36 Stuyvesant Street
New York, NY 10003

Office of Naval Research
New York Area Office
715 Broadway - 5th Floor
New York, NY 10003

Dr. A. Vaglio-Laurin
Department of Applied Science
26-36 Stuyvesant Street
New York University
New York, NY 10003

Professor H. E. Rauch
Ph.D. Program in Mathematics
The Graduate School and University
Center of the City University of
New York
33 West 42nd Street
New York, NY 10036

Librarian, Aeronautical Library
National Research Council
Montreal Road
Ottawa 7, Canada

Lockheed Missiles and Space Company
Technical Information Center
3251 Hanover Street
Palo Alto, CA 94304

Commanding Officer
Office of Naval Research Branch Office
1030 East Green Street
Pasadena, CA 91106

California Institute of Technology
Engineering Division
Pasadena, CA 91109

Library
Jet Propulsion Laboratory
4800 Oak Grove Drive
Pasadena, CA 91103

Professor H. Liepmann
Department of Aeronautics
California Institute of Technology
Pasadena, CA 91109

Mr. L. I. Chasen, MGR-MSD Lib.
General Electric Company
Missile and Space Division
P. O. Box 8555
Philadelphia, PA 19101

Mr. P. Dodge
Airesearch Manufacturing Company
of Arizona
Division of Garrett Corporation
402 South 36th Street
Phoenix, AZ 85010

Technical Library
Naval Missile Center
Point Mugu, CA 93042

Professor S. Bogdonoff
Gas Dynamics Laboratory
Department of Aerospace and
Mechanical Sciences
Princeton University
Princeton, NJ 08540

Professor S. I. Cheng
Department of Aerospace and
Mechanical Sciences
Princeton University
Princeton, NJ 08540

Dr. J. E. Yates
Aeronautical Research Associates
of Princeton, Inc.
50 Washington Road
Princeton, NJ 08540

Professor L. Sirovich
Division of Applied Mathematics
Brown University
Providence, RI 02912

Dr. P. K. Dai (RI/2178)
TRW Systems Group, Inc.
One Space Park
Redondo Beach, CA 90278

Redstone Scientific Information Center
Chief, Document Section
Army Missile Command
Redstone Arsenal, AL 35809

U.S. Army Research Office
P. O. Box 12211
Research Triangle, NC 27709

Editor, Applied Mechanics Review
Southwest Research Institute
8500 Culebra Road
San Antonio, TX 78228

Library and Information Services
General Dynamics-CONVAIR
P. O. Box 1128
San Diego, CA 92112

Dr. R. Magnus
General Dynamics-CONVAIR
Kearny Mesa Plant
P. O. Box 80847
San Diego, CA 92138

Mr. T. Brundage
Defense Advanced Research Projects
Agency
Research and Development Field Unit
APO 146, Box 271
San Francisco, CA 96246

Office of Naval Research
San Francisco Area Office
One Hallidie Plaza, Suite 601
San Francisco, CA 94102

Library
The RAND Corporation
1700 Main Street
Santa Monica, CA 90401

Dr. P. E. Rubbert
Boeing Aerospace Company
Boeing Military Airplane Development
Organization
P. O. Box 3707
Seattle, WA 98124

Dr. H. Yoshihara
Boeing Aerospace Company
P. O. Box3999
Mail Stop 41-18
Seattle, WA 98124

Mr. R. Feldhuhn
Naval Surface Weapons Center
White Oak Laboratory
Silver Spring, MD 20910

Librarian
Naval Surface Weapons Center
White Oak Laboratory
Silver Spring, MD 20910

Dr. J. M. Solomon
Naval Surface Weapons Center
White Oak Laboratory
Silver Spring, MD 20910

Professor J. H. Ferziger
Department of Mechanical Engineering
Stanford University
Stanford, CA 94305

Professor K. Karamcheti
Department of Aeronautics and
Astronautics
Stanford University
Stanford, CA 94305

Professor M. van Dyke
Department of Aeronautics and
Astronautics
Stanford University
Stanford, CA 94305

Professor O. Bunemann
Institute for Plasma Research
Stanford University
Stanford, CA 94305

Engineering Library
McDonnell Douglas Corporation
Department 218, Building 101
P. O. Box 516
St. Louis, MO 63166

Dr. R. J. Hakkinen
McDonnell Douglas Corporation
Department 222
P. O. Box 516
St. Louis, MO 63166

Dr. R. P. Heinisch
Honeywell, Inc.
Systems and Research Division -
Aerospace Defense Group
2345 Walnut Street
St. Paul, MN 55113

Dr. N. Malmuth
Rockwell International Science Center
1049 Camino Dos Rios
P. O. Box 1085
Thousand Oaks, CA 91360

Library
Institute of Aerospace Studies
University of Toronto
Toronto 5, Canada

Professor W. R. Sears
Aerospace and Mechanical Engineering
University of Arizona
Tucson, AZ 85721

Professor A. R. Seebass
Department of Aerospace and Mechanical
Engineering
University of Arizona
Tucson, AZ 85721

Dr. K. T. Yen
Code 3015
Naval Air Development Center
Warminster, PA 18974

Air Force Office of Scientific Research
(SREM)
Building 1410, Bolling AFB
Washington, DC 20332

Chief of Research and Development
Office of Chief of Staff
Department of the Army
Washington, DC 20310

Library of Congress
Science and Technology Division
Washington, DC 20540

Director of Research (Code RR)
National Aeronautics and Space
Administration
600 Independence Avenue, SW
Washington, DC 20546

Library
National Bureau of Standards
Washington, DC 20234

National Science Foundation
Engineering Division
1800 G Street, NW
Washington, DC 20550

Mr. W. Koven
AIR 03E
Naval Air Systems Command
Washington, DC 20361

Mr. R. Siewert
AIR 320D
Naval Air Systems Command
Washington, DC 20361

Technical Library Division
AIR 604
Naval Air Systems Command
Washington, DC 20361

Code 2627
Naval Research Laboratory
Washington, DC 20375

SEA 03512
Naval Sea Systems Command
Washington, DC 20362

SEA 09G3
Naval Sea Systems Command
Washington, DC 20362

Dr. A. L. Slafkosky
Scientific Advisor
Commandant of the Marine Corps
(Code AX)
Washington, DC 20380

Director
Weapons Systems Evaluation Group
Washington, DC 20305

Chief of Aerodynamics
AVCO Corporation
Missile Systems Division
201 Lowell Street
Wilmington, MA 01887

Research Library
AVCO Corporation
Missile Systems Division
201 Lowell Street
Wilmington, MA 01887

AFAPL (APRC)
AB
Wright Patterson, AFB, OH 45433

Dr. Donald J. Harney
AFFDL/FX
Wright Patterson AFB, OH 45433